ADDIS ABABA UNIVERSITY

ADDIS ABABA INSTITUTE OF TECHNOLOGY

SCHOOL OF CIVIL AND ENVIRONMENTAL ENGINEERING

SEISMIC PERFORMANCE EVALUATION OF REINFORCED CONCRETE FRAME –WALL SYSTEM USING FRAGILITY CURVE

(A case study on the structural performance assessment of existing 40/60 condominium building in Addis Ababa)

A thesis submitted to the school of Graduate Studies in Partial fulfillment of the Requirements for the Degree of Master of Science in Civil Engineering (Structures)

by

Dagne Daba

Adviser Dr. Shifferaw Taye

(June 2020)

A Thesis Submitted in Partial Fulfillment of the Requirements for the Degree of Master of Science The undersigned have examined the thesis entitled '**Seismic Performance Evaluation of Reinforced Concrete Frame –Wall System Using Fragility Curve'** presented by **Dagne Daba**, a candidate for the degree of **Master of Science** and hereby certify that it is worthy of acceptance.

Dr. Shifferaw Taye		
Advisor	Signature	Date
Dr. Esayas G/Yohanes		
Internal Examiner	Signature	Date
Dr. Ing. Adil Zekaria		
External Examiner	Signature	Date
Dr. Ing. Mebruk Mohammed		
Chair person	Signature	Date

UNDERTAKING

I certify that research work titled "**Seismic Performance Evaluation of Reinforced Concrete Frame –Wall System Using Fragility Curve**" is my own work. The work has not been presented elsewhere for assessment. Where material has been used from other sources it has been properly acknowledged / referred.

_____

Dagne Daba

DEDICATION

"In loving memory to my beloved father"

ABSTRACT

According to the new Ethiopian building code ES EN 1998-1:2015, there is an adjustment in peak ground acceleration of Addis Ababa. The peak ground acceleration is updated to 0.1g which, were 0.05g in previsions EBCS8-1995. The variation will significantly affect the seismic performance of structure due to this, need to check buildings performance level and status against the new code predominant issue. Besides, building seismic performance and vulnerability analyses are probabilistic and vulnerability can be evaluated by developing fragility function which is expressed in the fragility curve.

Works of literature provide a different technique to evaluate the fragility of structure: Empirical, Expert opinion, Analytical and Hybrid. Each of those methods is subjected to their on limitation, subjectivity in expert opinion, time-demanding in analytical and particularity in the empirical approach. With all its constraint, analytical fragility is the most dominate approaches employed in the research community and a simplified structural model which resembles the real structure behaviour can further reduce the time demand resulted from extensive nonlinear analysis. This research aspires to find a simplified analytical solution which minimizes time demand required under previous analytical fragility analyses. The resulted fragility curves are used to evaluate the performance of case study building in line with conventional pushover analysis.

Before implementing fragility analysis, conventional pushover analysis of the case study building is performed in SAP 2000® and the effect of confinement is considered in determining the material nonlinearity of structural elements. The global level performance points of the building determined with Capacity spectrum method of FEMA 440 under different seismic demand and the selected capacity curve are used to generate Incremental Dynamic Analysis curves of the building. The conversion of the capacity curve to generate Incremental dynamic analysis curves was conducted by utilizing Static Pushover to Incremental Dynamic Analysis algorithm. The generated Incremental Dynamic Analysis curves were calibrated for its elastic stiffness by using statistical results of elastic stiffness computed from time history analysis. Further adjustment to Incremental Dynamic Analysis curves is also introduced to calibrate record to record variability at near collapse limit state with FEMA P695 requirement. At last, the uncertainty related to record-to-record variability of ground motion is extracted from calibrated Incremental Dynamic Analysis curves and combined modelling uncertainty of FEMA P695 recommendations.

Finally, the seismic fragility curve of case study building developed for seismic hazard zones expressed in ES EN 1998-1:2015 and its probability damage states evaluated by considering SYNER-G damage limit state. Considering the lack of data regarding least allowable damage probability, the study adopts FEMA P695 requirement link with near collapse damage states.

Key Words: Dual system, Pushover analysis, Capacity curve, Damage state, Uncertainties, Fragility analysis, Static Pushover to Incremental Dynamic Analysis ,

ACKNOWLEDGMENTS

First and for most, I would like to give glory to the Almighty God and St. Mary for every success in my life and their continuous blessings. They have enriched me courage and strength as well as precious health throughout my life.

The completion of this study was made possible with the genuine guidance, continuous support and endless patience of my supervisor, Dr. Shifferaw Taye. I have felt privileged to be his student and immensely enjoyed working with him and I would like to deeply acknowledge him for all of his support. I am also grateful to thank Dr. Atalay Ayele for his support and comment.

I would like to extend my special appreciation to my wife for her persistent urging also being with me in all ups and downs. I would like to express my profound heartfelt thanks to my relatives, friends and to those people who have collaborated with me.

TABLE OF CONTENTS

LIST OF TABLES

LIST OF FIGURES

LIST OF SYMBOLS AND ACRONYMS

IM Intensity Measure

DM Damage measurement

PGA Peak Ground Acceleration

PGV Peak Ground Velocity

RC Reinforced concrete

T_1 Fundamental period of the structure

S_a Spectral Acceleration

NSP Nonlinear static procedures

NDP Nonlinear Dynamic procedures

MDOF Multi degree of freedom

SDOF Single degree of freedom

ESDOF Equivalent single degree of freedom

CSM Capacity Spectrum Method

IO Immediate occupancy

LS Life safety

CP Collapse Prevention

g gravitational acceleration

SPO2IDA Static Pushover to Incremental Dynamic Analysis

IDA Incremental Dynamic Analysis

IDR Interstory drift ratio

RDR Roof drift ratio

V_b Base shear

Vstory Story Shear

Δ_{roof} roof displacement

Φ standard normal cumulative distribution function

β_m dispersion associated to modeling

β_{RTR} dispersion associated to record to record uncertainty

β_{tot} total dispersion associated in given damage state

K_{50} Elastic stiffness related to 50% fractile

K_{16} Elastic stiffness related to 16% fractile

K_{84} Elastic stiffness related to 84% fractile

θ_{max} Maximum interstory drift

θ_{Roof} Roof Drift ratio

Sa(T1) Spectral acceleration in g unit at fundamental period

PEER Pacific Earthquake Engineering Research

V_{30} Shear wave velocity at top 30m.

MER Main Ethiopian Rift

CHAPTER 1: INTRODUCTION

1.1 Background

As urbanization develops in the city, the values of land become expensive and then the building gets longer and slender. The rises in height introduce question whether the structural forms enough to bear dynamic loads like earthquake and wind load for this, structural forms have shifted from classical moment-resisting frame systems to tubular systems which made it possible to reach the heights that are present today. Using a shear wall dual frame system is economical and satisfactory for lateral resistance for moderate height, which is common in today's Addis Ababa. The apartment buildings being under construction by the Addis Ababa city administration saving housing development enterprise are among a representative feature.

Analysis of structure subjected to earthquake involves either linear or nonlinear depending on the complexity of structure and its importance. Building codes also provide a minimum expected reference load and analysis methods. With increasing knowledge and understanding of mankind towards seismic actions gets better, there will be better modelling. Accordingly, the number of building codes in the world undergoes continuous revision. Whenever there are changes in code provision, there will be a need to conduct performance evaluation structure as per the new code especially. Performance evaluation involves using nonlinear analysis and development of computation technology also provides the required support. Meanwhile, the need for change in seismic code in Ethiopian was well recognized and the code is updated in 2015 by Ethiopian Standard Authority.

In the new Ethiopian building code, ES EN 1998-1:2015, Addis Ababa zones on earthquake hazard map are changed, peak ground acceleration updated to 0.1g, which were 0.05g in the previous EBCS8-1995. The change in value significantly affects the seismic performance of structure due to this, need to assess building performance level and status against the new code predominant issue.

1.2 Problem Statement

The structural design practice for the earthquake in Ethiopia was previously based on EBCS 8-1995 as a reference. However, the proposed seismic data to Addis Ababa was very low as compared to various researches which depict the need for code revision. The

current building code ES EN 1998:2015 provision takes the difference into account and improves it, Peak Ground Acceleration of Addis Ababa is raised from 0.05g to 0.1g. The change will considerably affect the seismic performance of structures design by using former code and demands checking structures performance level. Whereas building seismic performance and vulnerability analyses are probabilistic, vulnerability is evaluated by developing fragility function and expressed in the fragility curve.

1.3 Objectives

1.3.1 General objective

This study intends to propose a way for structural performance assessment and vulnerability analysis of existing reinforced concrete shear wall-frame buildings. A case study building in Addis Ababa on 40/60 housing project is taken to assess its performance for the expected earthquake as per the new provision. The paper also aspires to find a simplified analytical solution which minimizes time demand required under previous analytical fragility analyses.

1.3.2 Specific objective

- Develop seismic fragility curve using SYNER-G damage measurement and estimate performance level of the building under specific hazard level, using PGA as intensity measurement.
- To evaluate the global level structural performance according to the performance level set by FEMA 356.

1.4 Limitations

Though the structural performance assessment of the case study building applying nonlinear analysis bases on the working drawing data; the following considerations were not taken in to account: existing damages, soil structure interaction and bond slip.

1.5 Research Strategy

This section describes methods adopted in assessing the seismic performance of 40/60 condominium building that is being constructed in large scale and expected to continue for the coming few years. Structural and geometric properties of the building will be collected from existing working drawing. These data will be applied in nonlinear static pushover analysis of the building on SAP2000. To overview of its probabilistic aspect, the worst

capacity curve from pushover analysis will be used to generate fragility curves. Lastly, the results will be discussed and recommendation will be drawn for a similar building, detail steps to be followed in the study are also indicated in Figure 1-1

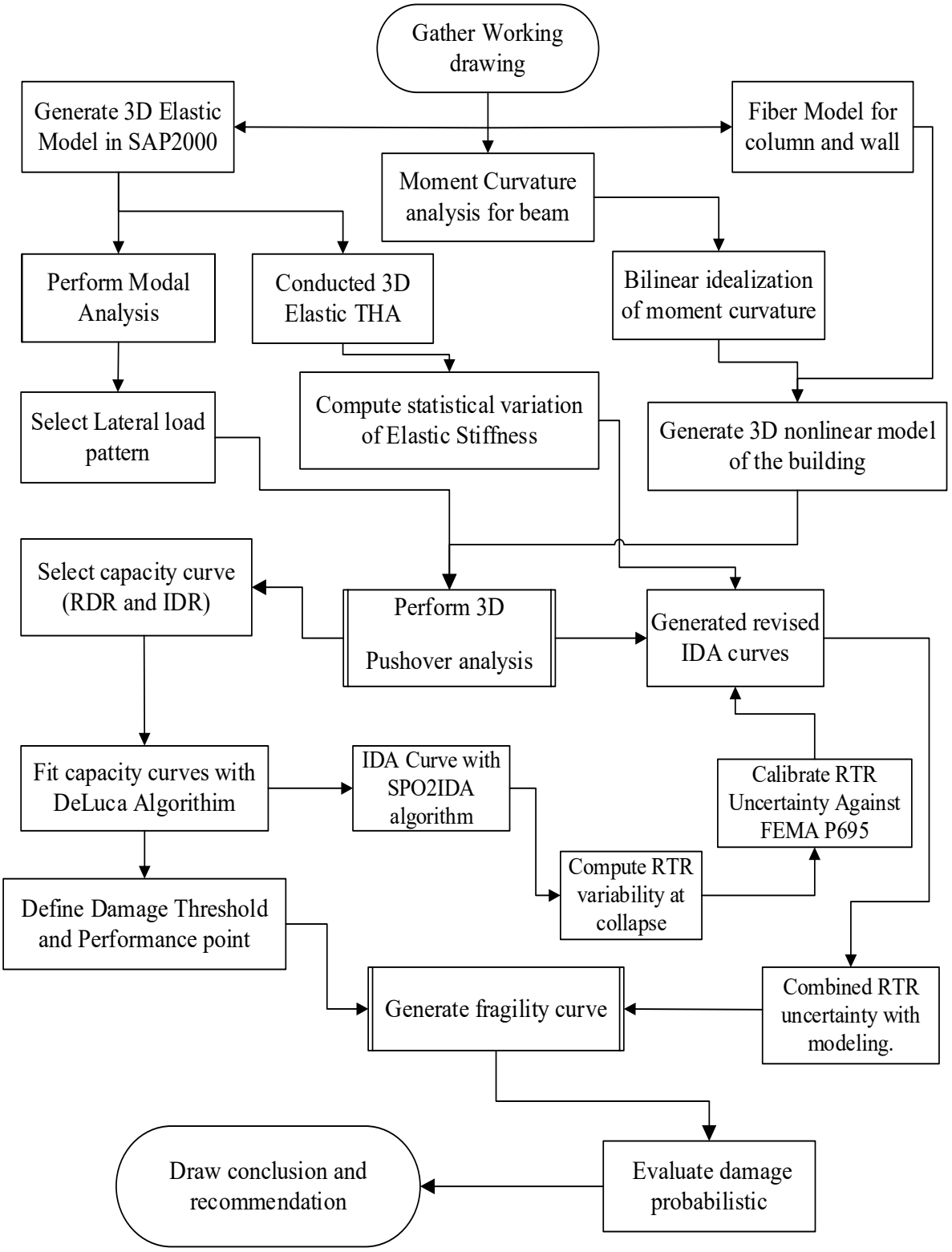

Figure 1-1: Research Strategy

1.6 Significance of the research

- Results can be used as input for seismic rehabilitation and vulnerability analysis of housing project in the municipality.
- The findings can also applied in emergency response and disaster planning by national agencies and insurance companies for estimating the overall loss after an earthquake event.

1.7 Content and Organization of the thesis

A brief review of the content of each chapter will be presented as follows:

In chapter 1 an introduction of the thesis is presented, pointing out the main objectives of the work developed.

Chapter 2 review existing state of the art in seismic fragility analysis which includes available method to perform fragility analysis with involved uncertainties. Pervious research works are also reviewed in this section.

Chapter 3 describes the case study building and in detail discuss on its existing structural system.

Chapter 4 review source of nonlinearity in structural analysis and discus methodology used to incorporate each nonlinearity. The conducted pushover analysis and performance point of the building under three PGA level is reported in this section

Chapter 5 discuss state of the art in selection and matching of time histories and utilized parameters to select the accelerograms from PEER strong ground motion database.

The adopted methodology form generating fragility curve from capacity cure are discussed in conjunction with available methods for determining uncertainty parameters is discussed in Chapter 6. Moreover IDA curves and fragility curves are summarized in graphical from in this section.

Finally, the conclusions drawn from this thesis work and the recommendations for the future work are presented in Chapter 7.

CHAPTER 2: LITERATURE REVIEW

The first section of this chapter overviews the state of the art on nonlinear pushover analysis and predominate nonlinear modelling techniques adopted for frame and shear wall element

In the second part of the chapter, review on seismic fragility analysis, intensity measurement, damage measurement, associated uncertainties and methods used to estimate uncertainty parameter depicted in detail. Moreover, previous studies on seismic fragility analysis are also described in this section.

2.1 Pushover Analysis and Nonlinear Modeling Techniques

2.1.1 Background

After recent major earthquake (M6.7 Northridge 1994, M7.2 Kobe 1995 and M7.4 Kocaeli 1999), seismic analysis and design is in the process of fundamental changes. Even though structure design by current code service their life safety purpose, the level of damage to structures, economic loss due to loss of use, and cost of repair were unexpectedly high. Hence, the necessity for using ever more accurate methods, which explicitly account for geometrical nonlinearities and material inelasticity, for evaluating seismic demand on structures, became evident. Within this framework, two analysis tools are currently offered with different levels of complexity and of required computational effort; nonlinear static pushover analysis and nonlinear dynamic analysis (Pinho 2007). Those procedures are fundamental analysis tool provided by different building codes like; FEMA-356/440, ATC-40, Eurocode 8 and ASCE-41 for seismic design and retrofitting (rehabilitation) of structures. Furthermore, there are a lot of undergoing researches to provide simplified and time efficient nonlinear analysis procedures.

Despite the advancement of computer technology and availability of commercial software, Non-linear analysis still demands significantly efforts and it should be carried out with specific objectives. Some of instance where nonlinear analysis implemented with respect to performance evaluation of existing building are to (NIST,2013):

1. Assess and design seismic retrofit solutions for existing buildings;
2. Design new buildings that employ structural materials, systems, or other features that do not conform to current building code requirements;

3. Assess the performance of buildings for specific owner requirements;
4. Improve and calibration of existing Design standards;
5. Evaluate Seismic risk.

2.1.2 Source of Nonlinearity in Structures

In mechanics, nonlinear behavior refers to the condition of a structure where the response to realistic loading cannot be linearly extrapolated from the response to small loads, without incurring significant inaccuracies. Nonlinearity are caused by different ways, but the three main cause are: geometric, material and contact nonlinearity.

Geometric nonlinearity is usually referred as kinematic nonlinearity and it is the effect of change in geometry due to applied load on the overall response of structure. Common engineering stress and strain equation becomes insufficient to capture the response of the structure thus, equilibrium equation need to be formulated on bases of deformed geometry.

Material nonlinearity occurs when ductile materials are strained beyond their elastic limit and their structural response against the loading becomes nonlinear, turn down Hooks' law.

Contact nonlinearity arise from presences of nonlinear boundary conditions, nonlinear spring support and partial contact slipping in supports.

2.1.3 Nonlinear Static Pushover Analysis

The static pushover analysis method has no rigorous theoretical base rather it is based on assumption that the response of structure is controlled by the first mode of vibration and the mode shape remains constant throughout its time history. This provides the fundamental and theoretical tool to transformation dynamic problem to static problem(Krawinkler and Seneviratna 1998). That is why nonlinear static analysis are usually refereed as extension of equivalent static analysis in to nonlinear regime. The commonly used method to perform pushover analysis are: Conventional and Adaptive methods. In adaptive pushover analysis the lateral load pattern is update in each analysis step in order to consider stiffness degradation on its inelastic range. While conventional pushover analysis is conducted under predefined constant load pattern and its detail review is conducted in the subsequent section.

As aforementioned, conventional or classical static pushover analysis is carried out under constant gravity loads and monotonically increasing lateral loading applied on the masses of the structural model. While the applied lateral forces increase in the course of the analysis, the engineer can follow the gradual emergence of plastic hinges, the evolution of the plastic mechanism and damage, as a function of the magnitude of the imposed lateral loads and of the resulting displacements the lateral load could be applied under predefined invariant load patter. The outcome of the pushover analysis is the so-called pushover curve (capacity curve), which represents the variation of the base shear (V_b) with respect to the roof displacement (Δ_{roof}) in a selected controlled node as indicated in Figure 2-1 and this curve gives important information about the global strength and deformation capacity of the structure under analysis. Capacity spectrum and Displacement coefficient methods provides means to determination of performance point of the structure under pushover analysis, those procedure can be also used to emulate Equivalent single degree of freedom (ESDOF) of Multi degree of freedom (MDOF).

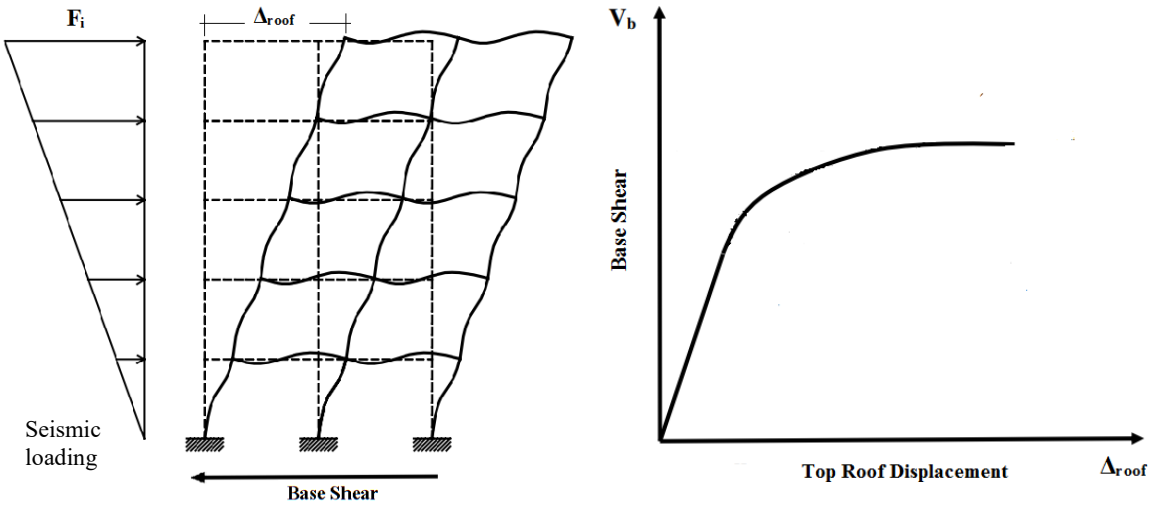

Figure 2-1: Illustration of pushover analysis

Capacity Spectrum Method

Capacity spectrum method provides a graphical representation of the expected seismic performance of the existing or retrofitted structure by the intersection of the structure's capacity spectrum with a response spectrum (demand spectrum) representation of the earthquake's displacement demand on the structure with equivalent damping. The basic assumption in this technique is that the maximum inelastic deformation of a nonlinear SDOF system can be approximated from the maximum deformation of a linear elastic

SDOF system that has a period and a damping ratio that are larger than the initial values of those for the nonlinear system as show in Figure 2-2. Hence, the equivalent period and damping are both a function of structure performance point, the solution is obtained in iteration.

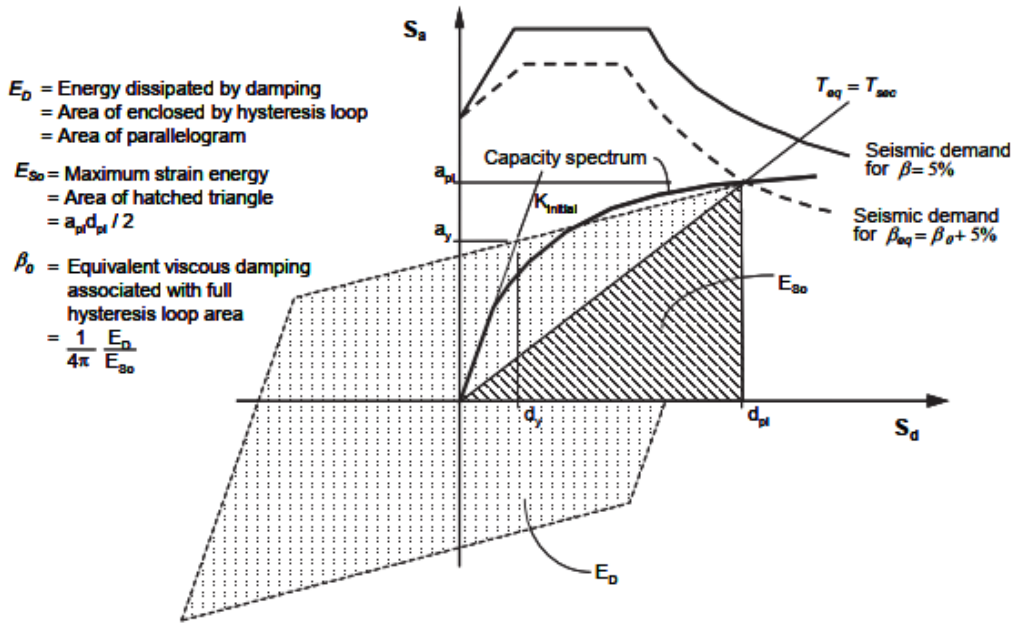

Figure 2-2: Graphical representation of the Capacity Spectrum Method as per FEMA-440

2.1.4 Limitation of Pushover Analysis

Nonlinear Static analysis is purely mathematical, which does not directly include structures dynamic behavior and despite of this limitation, the use of nonlinear static analysis for performance evaluation and rating is getting popular amongst structural engineering community. The main reason for their success lies in the possibility of gaining an important insight into the nonlinear seismic behaviour of structures in a simple and practical way.

2.1.5 Nonlinear Modeling Techniques for Frame Elements

Nonlinearity modeling of structure ambits from simple nonlinear springs which lump the behavior of the whole structure into a single degree of freedom system to three-dimensional finite element formulations which return the structural behavior by integrating the stress-strain relationships of the constituent materials. While, the component level nonlinearity can be idealized as distributed plasticity or concentrated plasticity.

Concentrated plasticity is the simplest techniques where the inelastic deformations are concentrated at node of the element, principally at the end node of element. For regions in a framed member away from the plastic hinge, elastic behavior is assumed and Inelastic spring (Figure 2-3 b) or rigid-plastic hinge (Figure 2-3 a) are tuned to fit backbone and cyclic detrition properties of selected nodes. When the section reaches its plastic capacity, a plastic hinge is formed and element stiffness is adjusted lumping the plasticity in zero-length hinges with moment-rotation model parameters, these elements have relatively condensed numerically efficient formulations. However, it does not accurately represent the distributed plasticity and associated geometric nonlinearity NIST (2013).

Distributed plasticity analysis models (Figure 2-3 c-e) the spread of inelasticity through the cross-sections and along the length of the members in this analysis, a member needs to be subdivided into several elements along its length to model the inelastic behavior more accurately. Distribution plasticity are dealt by using concentrated plasticity with defined hinge length or discretized nonlinear finite element. Integration of deformations along the hinge length captures the spread of yielding more realistically than the concentrated hinges, while the finite hinge length facilitates calculation of hinge rotations.

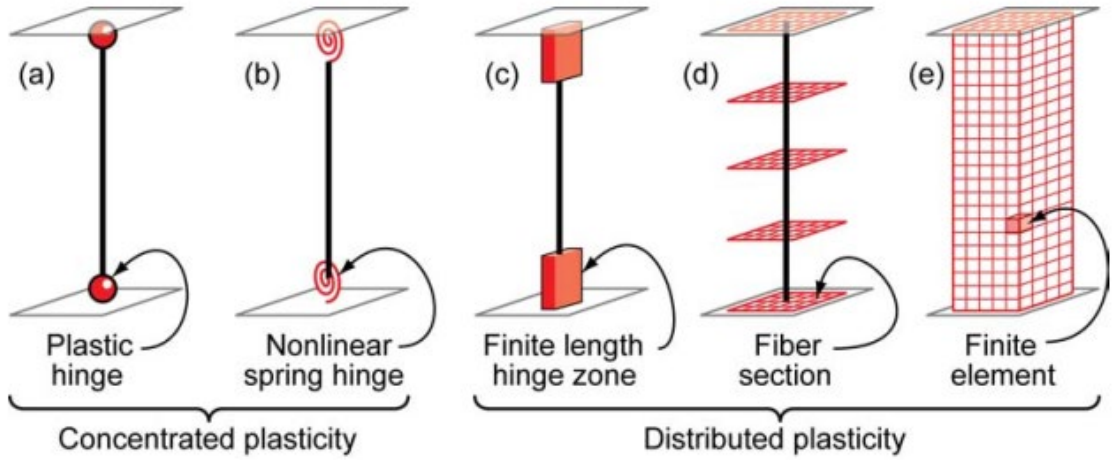

Figure 2-3: Idealized plasticity for beam-column element adopted from NIST (2013)

The fiber formulation models distribute plasticity by numerical integrations through the member cross sections and along the member length. Uniaxial material models are defined to capture the nonlinear hysteretic axial stress-strain characteristics in the cross sections. The plane-sections-remain-plane assumption is enforced, where uniaxial material "fibers" are numerically integrated over the cross section to obtain stress resultants (axial force and moments) and incremental moment-curvature and axial force-strain relations. The cross-

section parameters are then integrated numerically at discrete sections along the member length, using displacement or force interpolation functions. Figure 2-4 shows typical subdivision in fibers for RC column sections that is utilized in this paper to their respective material nonlinearity.

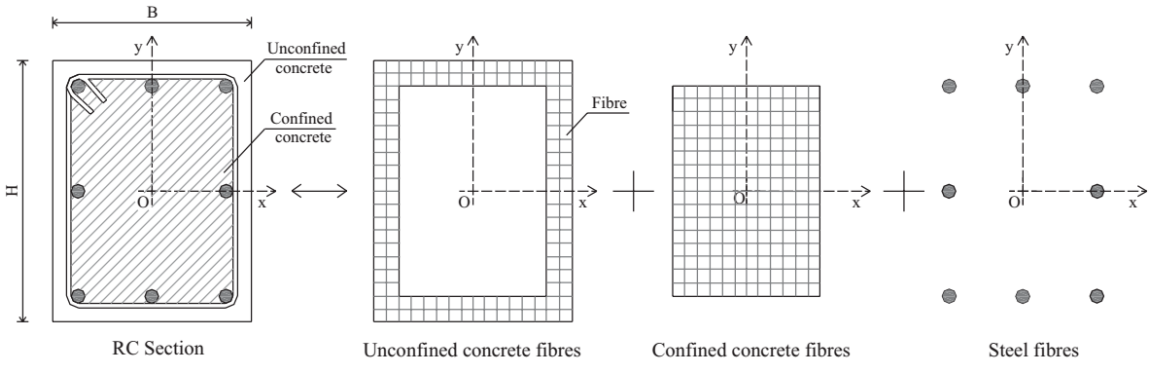

Figure 2-4: Typical Fiber model of a reinforce concrete column section

Finite element method (Figure 2-3 e) is the most complex and versatile type of material inelasticity modeling procedure where the member is discretized into small finite element with well-defined nonlinear hysteretic properties. This method possess challenge in terms of model parameter calibration and computational resources.

2.1.6 Nonlinear Modelling Techniques for RC Shear Walls

A robust analytical shear wall model for nonlinear analysis of multi-story buildings is essential for reliable seismic performance assessment. These models must be capable of estimating the global seismic demands with acceptable accuracy and within a reasonable computational time. Further, they must be applicable in three-dimensional analyses of multi-story buildings. Some of the available models approached typically used in building analysis and in the subsequent section.

Beam-Column Element model

The simplest of all available model where the shear wall is represented by an equivalent column at the center line of the wall section. Non-linear axial-flexural hinges are located at the bottom and top of the column, whereas optional shear hinges can be located at the mid height as indicated in Figure 2-5. Further, the connecting beams and slabs within the wall are replaced by rigid links to make the deformation compatible with the actual wall width. The moment rotation of the entire wall section is assigned to the column line and offering rigid plastic hinges at the member ends are computationally efficient. Although

the model requires predefined hinge length, it is reasonable and suitable for walls of small proportions and it can also be used as preliminary model to quickly assessment of performance of wall. For very wide and complex cellular wall arrangement, this may not be able to correctly model the 3D response. (PEER 2010)

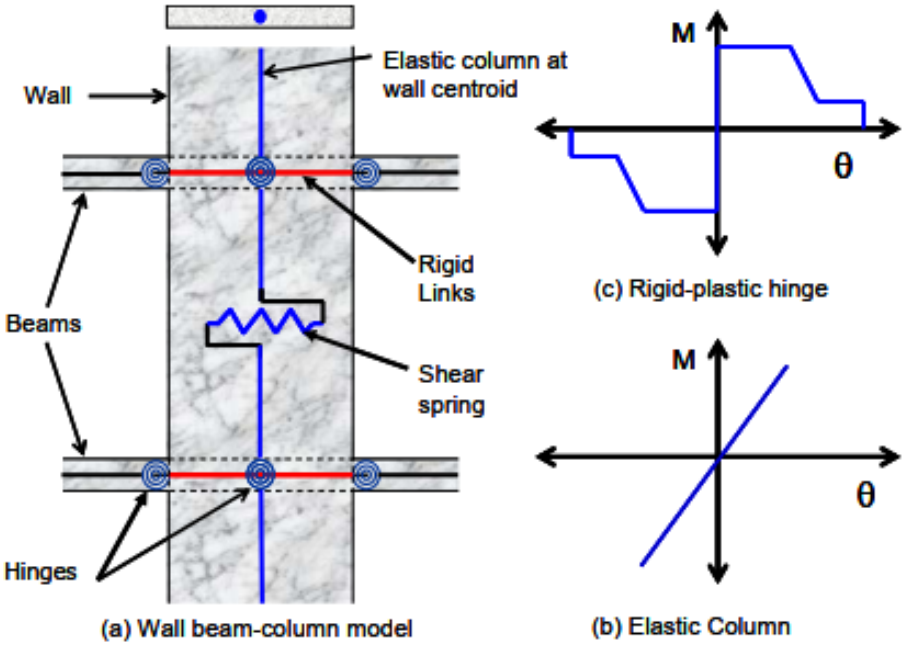

Figure 2-5: Equivalent beam-column element idealization of RC shear wall(PEER 2010)

Multi-Layer Shell Element

The multi-layer shell element constituted on the principles of composite material mechanics and it can simulate the coupled in-plane/out-of-plane bending and the coupled in-plane bending-shear nonlinear behaviors of RC shear walls. Here, the shear wall is represented using fine meshed fiber or smeared layers of composite material and it is also referred as Fiber beam-column model in PEER (2010). Finite element formulation created to obtain strain and curvature of middle layer and the remaining layers' response quantities are determined using assumption that plane section will remain plane. Finally, the corresponding stress will be calculated through the constitutive relations of the material assigned to the layer.

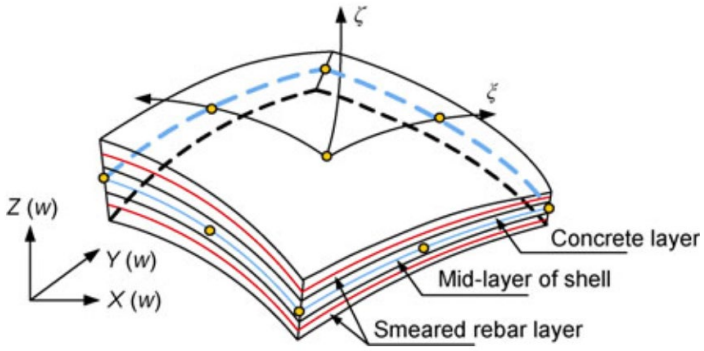

Figure 2-6: multilayer shell element

2.2 Seismic Fragility Analysis

2.2.1 Definition and Background

The vulnerable conditions of a building can be described using vulnerability functions or fragility functions. Vulnerability functions describe the probability of losses (such as social losses or economic losses) given a level of ground shaking, whereas fragility functions describe the probability of exceeding different limit states (physical damage levels) given a level of ground shaking hence, Fragility curves constitute one of the key elements of probabilistic seismic risk analysis. Fragility function also provides a probabilistic measure of safety margin with respect to design-basis or other events specified by a stakeholder. Such a margin can be used to evaluate system weaknesses or deficiencies identified during an inspection or condition assessment and can provide a means to assess if the observed weaknesses or deficiencies might be expected to have a significant impact on system risk (Wen et al. 2004). Furthermore, fragility functions can be used to design retrofitting schemes by carrying out cost/benefit studies for different types of structural intervention schemes.

Fragility curves are usually expressed in form of lognormal distribution. There is nothing fundamental about the lognormal distribution that makes universal thought to represent fragility function. Porter (2017) justifies the following four reasons to its use:

1. *Simplicity*. It has a simple, parametric form for approximating an uncertainty quantity that must take on a positive value, using only an estimate of central value and uncertainty;
2. *Precedent*. It has been widely used for several decades in earthquake engineering.
3. *Information-theory reasons*. It is the distribution that assumes the least knowledge (more precisely, the maximum entropy—a term of art from information theory that

will not be explained here) if one only knows that the variable is positively valued with specified median and logarithmic standard deviation.

4. *Often fits data*. It often reasonably fits observed distributions of quantities of interest here, such as ground motion conditioned on magnitude and distance, the collapse capacity of structures, and the marginal distribution of loss conditioned on shaking.

2.2.2 Intensity Measurement

An Intensity Measure (IM) is the ground motion parameter that is being used in order to relate the ground motion to the damage of the structures. Several measures of the strength of ground motion (IMs) have been developed. Each intensity measure may describe different characteristics of the motion. The use of a particular IM in seismic risk analysis should be guided by the extent needed to the measure corresponding damage to the components of a system or the system of systems. The selection of intensity measurement also depends on method of deriving fragility function. Optimum intensity measures are defined in terms of practicality, effectiveness, efficiency, sufficiency, robustness and computability (Pitilakis et al. 2014). Intensity Measures are classified into two groups: Empirical (Non-instrumental) intensity measures and Instrumental intensity measures.

Non-instrumental IMs are expressed in terms of macroseismic intensity scales that perceptibility measures of damage to structures, ground surface effects and human reactions to earthquake shaking. Macroseismic intensity scale is a qualitative scale expressed in terms of Roman numerals representing different intensity levels. An advantage of this type of intensity measure is that it is directly related to the vulnerability of the buildings and there is no requirement to take instrumental measurements. The gathered data depends on the area where it is collected and how far away this area is from the epicenter. Some of most common macroseismic intensity are Mercalli – Cancani – Seiberg (MCS), Modified Mercalli (MM), Medvedev – Sponheuer – Karnik (MSK), European Macroseismic Scale (EMS)[1] and Japanese Meteorological Agency (JMA)[2] (Elnashai and Sarno 2008).

In instrumental intensity measures, instruments are used in order to record the ground motion and then recorded accelerograms are processed to get the appropriate

[1] MCS, MM, MSK and EMS are 12- level scale measurement used in America and Europe
[2] JMA is 7-level scale measurement used in Japan.

measurement. The instrumental intensity measures include the Peak ground Velocity (PGV), Peak Ground Acceleration (PGA), Peak Ground Displacement (PGD), Spectral Acceleration at the first mode of vibration S_a(T1,5%) , spectral displacement S_d, root mean square of the acceleration(RMS) and Roof Drift Ratio(RDR). Spectral acceleration and/or spectral displacement are suitable IM, for regular buildings whose mode of vibration is dominated by first mode(SYNER-G 2011).

2.2.3 Damage Measurement

In prediction of seismic vulnerability several damage measurements may be used, which express damage of members (element level) and/or global damage of structure. Damage measurement (DM) is a scalar quantity that characterize structural response of the system due to seismic load. Selecting DM depends on the level of assessment required. Common DMs for members that were used in previous studies include: The peak chord rotation demand at member end, the peak shear force demand, the local Park and Ang Damage Index, The node rotations and Displacement ductility. In addition, the following DM can be used to evaluate global seismic performance of building includes: The residual deformation, the global Park and Ang Damage Index, Maximum base shear, the peak roof drifts, Inter-Story Drift , the peak inter-story drift angle and Peak floor accelerations.

Selecting a suitable DM depends on the application and the structure itself; it may be desirable to use two or more DMs (all resulting from the same nonlinear analyses) to assess different response characteristics, limit-states, or modes of failure of interest in a Performance based Earthquake Engineering (PBEE) assessment. If the damage to non-structural contents in a multi-story frame needs to be assessed, the peak floor accelerations are the obvious choice. On the other hand, for structural damage of frame buildings, Maximum Inter-Story drift (θ_{max}) relates well to joint rotations and both global and local story collapse, thus becoming a strong DM candidate. The latter, expressed in terms of the total drift, instead of the effective drift which would take into account the building tilt, will be our choice of DM for most illustrative cases here, where foundation rotation and column shortening are not severe (Vamvatsikos 2002). The peak inter-story drift angle is used for structural damage of buildings and relates well to joint rotations. The peak floor accelerations are used for damage to non-structural components in multi-story buildings. The Inter-story drift is the ratio of the maximum story displacement over the story height. It gives significant information on the structural and non-structural damage.

2.2.4 Limit states and Damage states

In seismic risk assessment, the performance levels of a building can be defined through damage thresholds called limit states. A limit state defines the threshold between different damage conditions, whereas the damage state defines the damage conditions themselves. Methods for deriving fragility curves generally model the damage on a discrete damage scale. In empirical procedures, the scale is used in reconnaissance efforts to produce post-earthquake damage statistics, whereas in analytical procedures the scale is related to limit state mechanical properties of the buildings, such as displacement capacity. The number of the damage states depends on the damage scale used. Some of the most frequently damage scales used are: HCR, HAZUS, Vision2000, EMS98, ATC-13 (SYNER-G 2011).

2.2.5 Different Approaches for Seismic Fragility

There are several methods available and used in the literature to derive fragility functions for different elements/structures exposed to seismic hazard. There are four main approaches to generate the seismic fragility of a structural system or component: empirical, expert opinion based, analytical and hybrid (Pitilakis et al. 2014; SYNER-G 2011).

Empirical approaches

Empirical approaches are based on post-earthquake surveys and observations of actual damage. They are specific to particular sites and seismic-tectonic, geological and geotechnical conditions, as well as the properties of the damaged structures. Empirical methods have the advantage of being based on real observed data, thus successfully account for various effects such as soil-structure interaction, site effects, and variability in the structural capacity of a group of buildings and the mechanisms, which govern the failure modes. However, this may also provide a drawback, as empirically derived fragility curves remain specific to a given area with specific site conditions, earthquake parameters (magnitude, depth, etc.) and structural capacity of buildings. Moreover, available data are often based on low-magnitude events with limited damage, which lead to fragility curves that may be unreliable for greater magnitude events (i.e. the portions of the curves corresponding to high seismic levels). It has also been noted that undamaged buildings after an event are not properly accounted for in the survey(Pitilakis et al. 2014). Other downside of empirical fragility curve rises from the fact that it requires extensive field data of many earthquakes with different magnitudes. For instance, Rossetto and Elnashai (2003) gathered a huge database that is composed of 340,000 buildings inspected after 19

different earthquakes and locations in order to construct the empirical fragility curves for European-type reinforced concrete frame buildings.

Expert opinion-based approaches

Expert opinion-based fragility curves depend on the judgment and the information of the experts. These experts are asked to provide an estimate of the probability of damage for different types of structures and several levels of ground shaking. Since expert judgment fragility curves are based on expert opinion and experience, they are versatile and relatively fast to establish, but their reliability is questionable because of their dependence on the experiences of the experts consulted. Examples of this method are: The introduction of Damage Probability Matrices (DMPs) based on expert judgement and opinion using the MMIs in the Applied Technology Council (Report ATC-13, 1985) and the study of Kostov et al. (2007)who produced DPMs of buildings of different periods in Sofia, according to EMS-98, and then converted them to vulnerability curves. The Damage Probability Matrices (DPM) express the conditional probability of obtaining a damage level j, due to a ground motion of intensity i, P[D = j/i] in a discrete form.

Analytical approaches

This method features a more detailed vulnerability assessment with direct physical meaning. The analytical fragility curves are computed by constructing appropriate structural models which express the probability of damage computed under increasing seismic intensity. Figure 2-7 summarizes the basic procedures that are being followed to calculate the analytical vulnerability curves or damage probability matrices. The advantage of this method is that it provides results that are very close to reality. One of the main disadvantages of analytical vulnerability curves is that they are computationally demanding and time consuming. Also, the capability of modelling the structure significantly affects the reliability of the results. Moreover, this may cause the deviation of the response of the analytical model from the actual behavior of the structure under concern. As a result, analytical approach to quantify seismic fragility always possesses a trade-off between accuracy and computational effort.

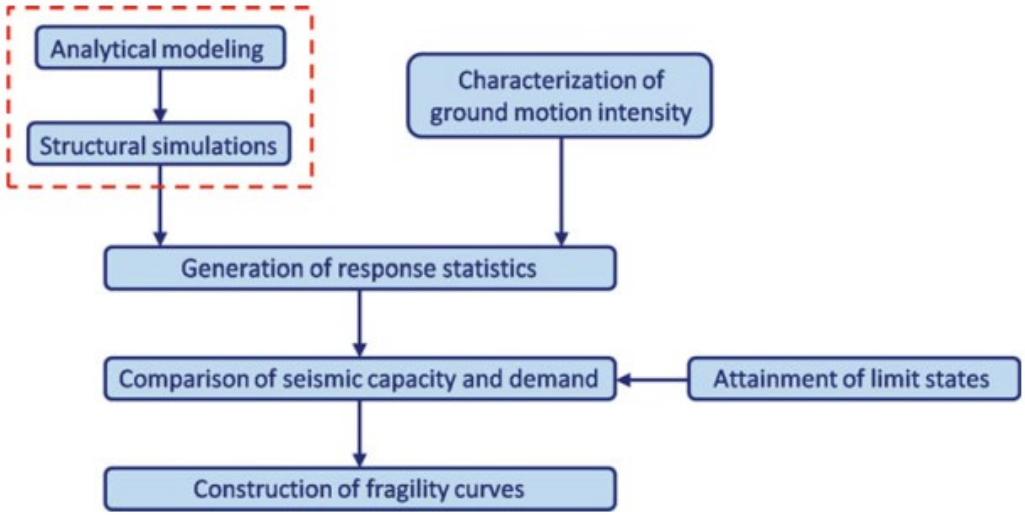

Figure 2-7: Generalized framework of seismic fragility analysis(Erberik 2015).

In general, for Specific limit state, analytical fragility curves are derived in form cumulative distribution function with respect to spectral displacement (any damage measurement) at the performance point. Equation 2-1 and

Figure 2-8 describe mathematical form and graphical representation of fragility curves given for given damage state respectively.

$$P[D > C \mid IM] = \Phi\left(\frac{1}{\beta tot}\ln\left(\frac{S_d}{\bar{S}_{d,DS}}\right)\right) \tag{2-1}$$

Where:

P[--]: probability of reaching or exceedance of a give limit state;

Φ: standard normal cumulative distribution function;

β_{tot}: is the standard deviation of the natural logarithm of spectral displacement for damage state, ds;

$\bar{S}_{d,ds}$ is the median value of spectral displacement at which the building reaches the threshold of damage state, ds;

S_d: is Spectral displacement used to measure seismic intensity.

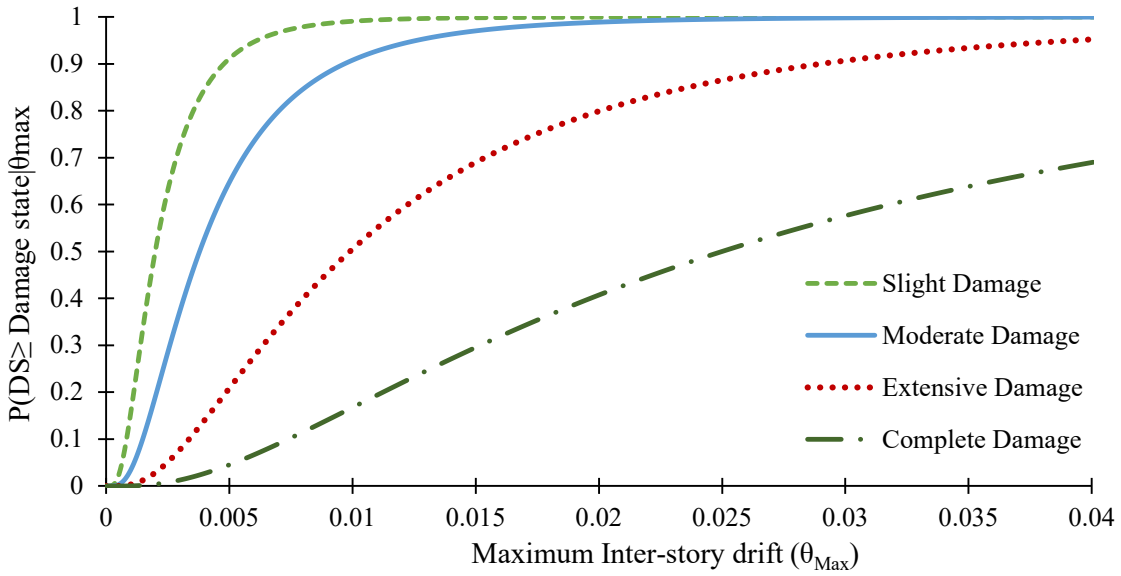

Figure 2-8: Typical fragility curves of damage limit state specified in HAZUS

Hybrid approaches

Hybrid fragility curves are based on the combination of different methods for damage prediction. Often, the aim is to compensate for the lack of observational data, the deficiencies of the structural models and the subjectivity in expert opinion data.

2.2.6 Uncertainty Associated with Fragility Analysis

Several uncertainties are introduced in the process of constructing a set of fragility curves of a specific element at risk. They are associated to the parameters of fragility curves, and to the derivation methodology, as well as in the relationship between physical damage state and the performance of the element at risk. The uncertainties are usually categorized in aleatory and epistemic. Aleatory uncertainty is one that is presumed to be due to the intrinsic randomness of a phenomenon. An epistemic uncertainty is one that consider uncertainty caused by lack of knowledge, which is usually related to the method or the available data. A systematic framework on uncertainties within earthquake engineering is performed by (Wen et al. 2004) including the aleatory and epistemic uncertainty models that considered system demand and capacity. The uncertainties associated with demand and capacity could be illustrated in Figure 2-9.

In general, the uncertainty of the fragility parameters is estimated through the standard deviation, $\beta_{tot,}$ describes the total variability associated with each fragility curve. Three primary sources of uncertainty are usually considered, namely, the definition of damage

states, β_{DS}, the response and resistance (capacity) of the element, β_C, and the earthquake input motion (demand), β_D. Damage state definition uncertainties are engaged because the thresholds of the damage indexes or parameters used to define damage states are not known. The total variability is modelled by the combination of the three contributors, with assumption that they are stochastically independent and log-normally distributed random variables by equation (2-2).

$$\beta_{tot} = \sqrt{\beta_{DS}^{\ 2} + \beta_D^{\ 2} + \beta_C^{\ 2}} \qquad (2\text{-}2)$$

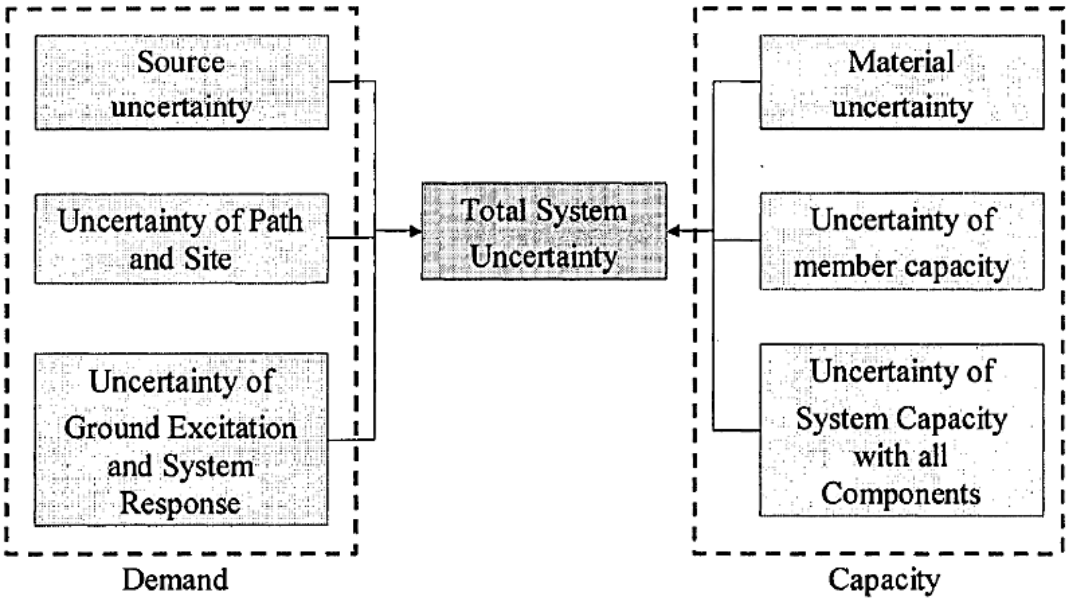

Figure 2-9: Uncertainty Sources for System Demand and Capacity

2.2.7 Estimation of Aleatory Uncertainty Parameter

There are several ways to estimate aleatory (record to record) uncertainty parameter values for a fragility function which depending upon the procedure used to obtain structural analysis data. Incremental dynamic analysis (IDA) is amongst dominate method used by research societies. Baker (2014) demonstrate the three different scale that can be implemented to estimate fragility parameter: Full Scale IDA, Truncated IDA and approximated IDA (SPO2IDA).

Incremental Dynamic Analysis

Incremental dynamic analysis involves performing a series of nonlinear dynamic analyses of a structural model for multiple records by scaling each record to several levels of intensity that are suitably selected to uncover the full range of the model's behavior: from elastic to yielding and nonlinear inelastic, finally leading to global dynamic instability.

(Vamvatsikos 2002). Fragility function parameters can be estimated from this data by taking logarithms of each ground motion's Intensity measurement (IM) value associated with onset of damage limit state, and computing their mean and standard deviation. IM is assumed to be lognormally distributed, in which its mean can be considered as median of IM (Baker 2014).

$$\ln \bar{\theta} = \frac{1}{n}\sum_{i=1}^{n} \ln IM_i \tag{2-3}$$

$$\bar{\beta} = \sqrt{\frac{1}{n-1}\sum_{i=1}^{n}\left(\ln\left(\frac{IM_i}{\bar{\theta}}\right)\right)^2} \tag{2-4}$$

Where n is number of ground motion considered,

IM_i is the Intensity measurement value associated with damage limit state for ith ground motion,

$\ln \bar{\theta}$ *and* $\bar{\beta}$ are mean and standard deviation

Truncated Incremental Dynamic Analysis

IDA is perform ony up to certain level of IM_{max}, above which no further analysis is performed. After performing IDA, Maximum likelihood methods will be used to compute fragility parameter by performing maximaization of likelihood function dicipted in Equation (6-3)

$$\left\{\bar{\theta},\bar{\beta}\right\} = \arg\max_{\theta,\beta} \sum_{i=1}^{m}\left\{\ln \Phi\left(\frac{\ln IM_i/\theta}{\beta}\right)\right\} + (n-m)\ln\left(1-\Phi\left(\frac{\ln IM_{\max}/\theta}{\beta}\right)\right) \tag{2-5}$$

Where n is number of ground motion data considered in the analysis, m is number of ground motion that cause collapse at IM levels less than IM_{max} *and* $\phi()$ denotes the standard normal distribution probability density function.

Static Pushover to Incremental Dynamic Analysis (SPO2IDA)

Deriving fragility parameter based on dynamic analysis involves intensive nonlinear modelling and multiple analysis. Hence, developing efficient approximate method is inevitable. SPO2IDA is one of approximate alternative available, which was developed by Vamvatsikos and Cornell (2005). SPO2IDA extracts IDA curves of SDOF and MDOF system from there capacity curve generated by pushover analysis as shown in Figure 2-10.

SPO2IDA tool could treat more complex SPO curves via quadrilinear approximation which compiles an elastic, a hardening, a negative-stiffness segment plus residual plateau that terminated with strength drop to zero. SPO2IDA tools[3] approximately predicts 16%, 50% and 84% fractile IDA curves

The prediction is based on the study of numerous SDOF systems having a wide range of periods, moderately pinching hysteresis and 5% viscous damping. Moreover, it is grounded on series of mathematical fitting equation provided by author using *R-μ-T (force reduction factor - ductility – period)* relationship of SPO curve. Furthermore, SPO2IDA offers direct estimates of the dispersion associated with record-to-record aleatory randomness of structural. The Force reduction factor *R* is defined as the ratio $S_a(T_1,5\%)/S_a^{yield}(T_1,5\%)$, is the $S_a(T_1,5\%)$ value to cause first yield whereas ductility μ is the oscillator's displacement δ, normalized by the yield displacement δ^{yield}.

SPO2IDA approximate seismic behavior of the first mode dominate MDOF system through SDOF having structure's fundamental period whose backbone curve closely matches capacity curve of MDOF. Although this methodology seems simple, it owns two main challenges: Defining of SPO curve and identification of Elastic Stiffness of MDOF.

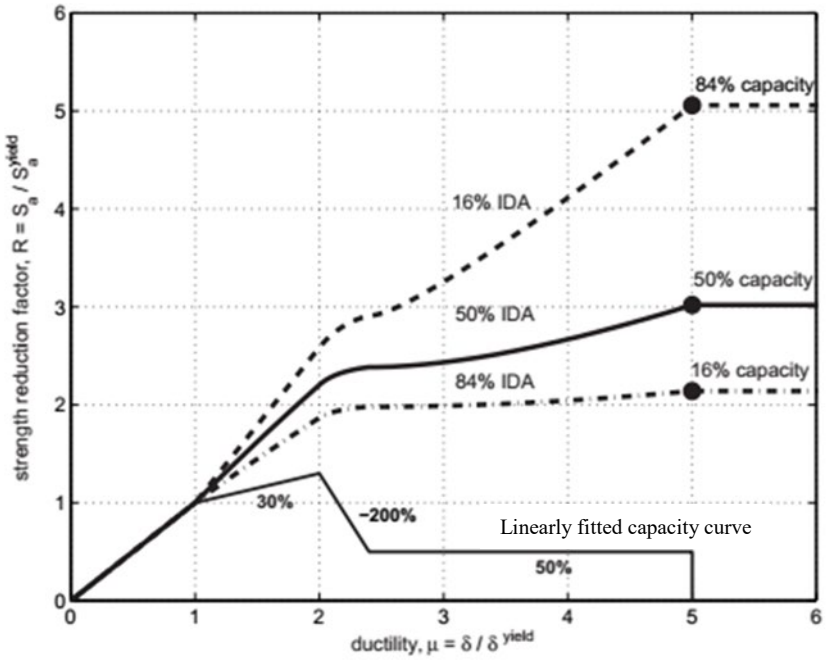

Figure 2-10: Conversion of capacity curve to IDA curve (Vamvatsikos and Cornell 2005)

[3] Matlab Program which is freely available at (http://users.ntua.gr/divamva/software.html) to convert pushover curve to their 16%, 50% and 84% fractile IDA curves.

Pushover analysis of MDOF does not yield a unique capacity hence, backbone Curve of Equivalent single degree of freedom (ESDOF) must be selected to mimic the worst- case of pushover analysis which can correctly approximated dynamic behavior of MDOF system (Vamvatsikos and Cornell 2005).

Unlike of SPO2IDA of SDOF system, SPO2IDA for MDOF system cannot exactly estimate yielding displacement and yielding base shear. In the case of SDOF, yielding displacement and base shear are common for all fractile. This is invalid for MDOF due to higher mode effects and redistribution of stress. Some records may cause early yielding, other cause late yielding at varying level of IM and DM. Vamvatsikos and Cornell (2005) suggest four methods to compute elastic stiffness of MDOF by assuming that SPO accuracy captures yielding DM. This assumption reduces the problem to single variable, finding of IM variable for their respective IDA curves. The following four alternative linear dynamic analysis are suggested based on their level of accuracy and computational intensiveness:

1. Select a suite records and perform time history analysis or response spectrum to determine peak DM values. Directly estimate the 16%, 50% and 84% of sample elastic stiffness, by computing elastic stiffness of each ground motion.
2. Select a suite records to generate their 16%, 50% and 84% spectra and perform response spectrum analysis to compute elastic stiffness of structure based on their elastic spectra.
3. Perform response spectrum analysis of structure based on elastic spectra given by building code and compute mean elastic stiffness. Mean Elastic stiffness will be taken to all IDA via assumption, no variability exists between elastic stiffness of other fractile.
4. Approximate the median IDR and RDR elastic stiffness by dividing any elastic capacity level of base shear by the effective first mode mass times the corresponding elastic IDR or RDR values respectively. Elastic stiffness of the remaining spectra is taken as the same as that of median.

Once IDA curves of each fractile are generated then fragility parameter; mean and dispersion are computed by the following equations.

$$\overline{\theta} = \ln\left(Sa_{f,50\%}^{LS}\right) \tag{2-6}$$

$$\overline{\beta} = \frac{1}{2}\ln\left(Sa^{LS}_{f,84\%} \Big/ Sa^{LS}_{f,16\%}\right) \tag{2-7}$$

The terms $Sa^{LS}_{f,x\%}$ represent the x% fractile spectra acceleration which the structural intensity causing exceedance of each limit state LS.

2.2.8 Estimation of Epistemic Uncertainties Parameter

Various researches propose different modeling uncertainty dispersion values in their investigations while HAZUS-MH5 recommends 0.4 for all damage states and SYNER-G doses not infer any values. Moreover, (Bradley 2010) and (Liel et al. 2009) provides a comprehensive review of available methodology to determine modeling uncertainty parameters. Wen et al. (2004) indicates that the level of modeling uncertainty is relatively insignificant and recommends 0.3 modeling uncertainty values. On the contrary, FEMA P695 (2009) provides the modeling uncertainty values ranges between 0.1 to 0.5 which is dependent on the level of model idealization and expected accuracy. For medium level accuracy and modeling, FEMA P695 recommends modeling uncertainty values 0.35 which is consistent with Haselton and Deierlein (2008) finding. Besides this, ignoring modeling uncertainty in performance assessment can induce to 20% shift in median collapse response fragility (Liel et al. 2009).

2.2.9 Previous Studies on Fragility Analysis

Due to the increasing seismic vulnerability of the communities, several earthquake loss assessment and performance evaluation studies have been carried out for different regions around the world. The following paragraphs summarized recent list of research works related to seismic fragility analysis.

Dumova-Jovanoska (2000) presented fragility curves and damage probability matrices using analytical methods for RC buildings designed according to the Macedonian design code. Two sets of buildings were analyzed; six storey frame buildings and sixteen story frame-wall buildings. Nonlinear time-history analysis was performed for 240 set of synthetic time histories and the response of the structure to the earthquake excitation was defined according to modified Park and Ang (1985) damage model using five damage states to express the condition of damage.

Akkar et al. (2005) studied fragility functions are determined for low- and mid-rise ordinary concrete buildings. 32 sample buildings representing the general characteristics

of two to five-story existing substandard reinforced concrete buildings in Turkey were used. A hybrid approach was employed where building capacities were obtained from field data and their dynamic responses are calculated by response history analyses. The inelastic dynamic structural characteristics of the buildings investigated are represented by a family of equivalent single-degree-of-freedom systems and their seismic deformation demands are calculated under 82 ground-motion records. Fragility functions were dictated separately for two- to five-story concrete buildings as the probabilities of exceeding the specified displacement-based damage limit states, where seismic intensities are expressed in Peak ground velocity PGV terms. Damage threshold level were nominated based on global drifts; light damage, modern damage, and severe damage states. The Produced fragility curves were compared to previous studies and with damage distribution of 6478 two- to five story buildings in Düzce observed after the 1999 Düzce earthquake. The study indicates number of stories has a significant effect on the probability of exceeding the moderate and the severe damage limit states. The author concluded dynamic response displacements are significantly better correlated with PGV than PGA across the structural period range from 0.2 to 1.0 second.

Ramamoorthy et al. (2006) constructed fragility curves to assess the seismic vulnerability of a hypothetical two-story reinforced concrete frame building designed only for gravity loads. Fragility curves were also developed for the same building modestly retrofitted by means of column strengthening. A Bayesian methodology was used to construct probabilistic demand models to predict the maximum inter-story drifts, given the spectral acceleration at the fundamental period of the building. The data for the models are obtained using two-dimensional inelastic time history analyses of the building for a suite of synthetic ground motions, developed for the Memphis region. In the absence of probabilistic capacity models for gravity load designed structures, capacity limit states are considered based on FEMA 356 guidelines and deterministic nonlinear pushover analyses. The results quantify the vulnerability of low-rise reinforced concrete frame buildings and show the effectiveness of seismic retrofitting in reducing the probability of failure. Important contribution of this studies is usage of lower bound data and use of bilinear demand model that can properly account the higher mode effect. The study shows seismic performance of gravity design buildings can be significantly improved by using simple and modest retrofitting strategies.

Ellingwood et al. (2007) evaluated the seismic fragility of typical low-to-mid-rise steel and reinforced concrete buildings in the Central and Eastern United State (CEUS). Four frames were selected to be representative of construction in the CEUS: two steel and two RC, which were designed for gravity and wind effects. Nonlinear time history analyses were performed using different sets of synthetic ground motions to assess the seismic demand on the frames and maximum inter-story drift angle (max) was selected as the demand variable. The studies indicates maximum inter-story drift limits at the CP level embedded in FEMA 273/356 and in HAZUS are overly conservative for building frames.

Hueste and Bai (2007) evaluated effectiveness of retrofitting strategies by estimating the reduction in the probability of exceeding a certain limit state, as compared to the un-retrofitted structure. A five-story, reinforced concrete office building designed based on the code requirements used in the Central US region during the early 1980s was selected as a case study building. The case study building has a moment frame system not specially detailed for ductile behavior. The floor system was composed of a flat slab and perimeter moment resisting frames with spandrel beams. Three retrofit techniques were evaluated: addition of shear walls, addition of RC column jackets, and confinement of the column plastic hinge regions using externally bonded steel plates. FEMA 356 global drift limits was used as damage measurement moreover, punching shear prediction model was used to establish an upper bound drift limit. Fragility curves were developed using nonlinear time history analysis with 20 synthetic ground motion data for each retrofitting techniques. The fragility curves derived in study were also compared to those for RC structures found in the literature.

Ji et al. (2007) presented analytical framework and sample application for the seismic fragility assessment of reinforced-concrete high-rise buildings. Simple lumped-parameter model representative of the complex high-rise building system. The parameters for this model were selected using genetic algorithms. The development of a simple lumped-parameter model is presented for an existing high-rise structure with dual core walls and a reinforced concrete frame.

Erberik (2008) also assessed seismic fragility of 28 reinforced concrete buildings extracted from a building database of approximately 500 buildings in Duzce, Turkey. Number of stories of the selected buildings ranges between two and six. Building damages were relegated in four level: none, light, moderate and severe or collapsed. Estimated damage

distributions seem to be comparable with the actual damage data. The influence of sampling techniques, sample size, type of hysteresis model and limit state definitions on the fragility curves was investigated. The results revealed that the uncertainty in capacity and degradation characteristics have a significant influence whereas the other investigated parameters do not seem to have an important role on the final fragility functions of building stacks.

Kappos and Panagopoulos (2010) appraised vulnerability of 54 common reinforce concrete building in Greek. Building were assorted in to eight class based on basis material, structural system, height and age and the existence or otherwise of brick masonry infills. The R/ C building models were analyzed for a total of 16 carefully selected accelerograms (half of them from actual Greek records, the other half synthetic) that are representative of different ground conditions. Vulnerability curves for several damage states were derived using hybrid approach which combines statistical data with appropriately processed results from nonlinear dynamic or static analyses that permit interpolation and (under certain conditions) extrapolation of statistical data to PGAs and/or spectral displacements for which no data is available. The study also offered techniques to improve the quality of results by applying a weighting technique to both the analytical and the statistical input data buildings.

Papailia (2011) developed of fragility functions for generic archetypal Reinforced Concrete (RC) frame, wall, and wall-frame buildings. The author carried out influence of story variation, material properties, frame stiffness and bay length on seismic performance of buildings. The study was conducted by considering chord rotation as damage measurement and PGA as intensity measurement.

Jeong et al. (2012) studied seismic performance of twelve medium-rise RC buildings designed to Eurocode 8, were evaluated by analytically-derived fragility relationships using sixty natural records. The selected buildings have the same overall plan dimensions. The fragilities and damage state probabilities were used to investigate the impact of design criteria and structural systems on safety margins and to establish a perspective on seismic performance of well-designed mid-rise RC buildings. The study states seismic performance of frames with elevation irregularities is not deficient to the performance of their regular counterparts provided that the buildings are designed by a modern seismic code.

Tsionis and Fardis (2014) produced fragility curves for the reinforced concrete buildings and bridges in the city of Thessaloniki, for use in the systemic seismic vulnerability and risk analysis of the urban area. Fragility curves were constructed for two damage states: yielding and ultimate. Chord rotation at the end of the member used to evaluate damage and PGA is used as intensity measure. In the study, the RC buildings are classified on the basis of the structural system (infilled frames, frames with open ground story and dual buildings), level of seismic design ("low", "medium" and "high") and height (low-rise, mid-rise and high-rise buildings). Fragility curves were developed for prototype regular buildings designed for low and medium level seismic code. In order to compute seismic capacity of model building Static pushover analysis under a unidirectional set of lateral forces with an inverted triangular pattern was conducted.

Saruddin and Nazri (2015) in their conference paper, studied seismic performance of Moment resisting steel frame (MRSF) and Moment resisting concrete frame (MRCF). Two sets of prototype buildings models were analyzed; three- and six-story frame, designed as per Eurocode. Incremental dynamic analysis was conducted under seven sets of ground motion records, and scaling peak ground acceleration increased every 0.05 g until it achieved 0.6 g. Fragility curves were used to provide improved prediction in damage to structure and based on CP level, both three- and six-story frames, MRSF has better performance than MRCF.

Abdelnaby (2016) investigated of the seismic fragility relationships of reinforced concrete (RC) frame systems prone to mainshock-aftershocks sequences. Fragility curves were derived for the following four scenarios: mainshock only, mainshock-aftershocks sequence, aftershocks only with no consideration to previous damage induced due to mainshock, and aftershocks only considering damage caused by the mainshock for two damage limit state. Three story RC frame, 2-bay (longitudinal) by 4-bay (transverse) designed to three design concepts (gravity, direct, and capacity design approach) was examined. Nonlinear dynamic response history analyses were conducted using 240 real earthquake sequences from March 11, 2011 Tohoku earthquakes. For damage control limit state vulnerability of the seismically designed frames (based on either capacity or direct design methods) under mainshocks only and mainshock-aftershocks sequence are almost the same whereas, for gravity designed frame, vulnerability of the mainshock-aftershocks sequence is higher compared to the vulnerability only considering mainshocks. The study

reveals multiple earthquakes have significant effects on the vulnerability relationships of Reinforced concrete frames.

Astriana et al. (2017) studied seismic performance of five story moment resisting frame and frame -wall systems designed according to Indonesian code. Capacity spectrum method stated in ATC-40 was utilized to evaluate performance of buildings. The study used five damage states based on HAZUS-MH MR5 and ATC-40. Seismic uncertainty parameters were adopted from HAZUS. Fragility curves were developed for intensity 0.2g to 0.6g at 0.05g interval using log-normal distribution.

The weakness of different fragility analysis approach was observed in the previously listed studies. The limitations include subjectivity in expert opinion, time-demanding in analytical and particularity in the empirical approach. With all its limitation, analytical fragility is the most dominant approaches employed in the research community and a simplified structural model which resembles the real structure behavior can further reduce the time demand resulted from extensive nonlinear analysis. However, the previous studies do not provide a simplified analytical approach to investigate the fragility of structure. This paper aspires to find a simplified analytical solution which minimizes time demand required under previous analytical fragility analyses and integrable to existing commercial structural analysis software.

CHAPTER 3: DESCRIPTION AND MODELING OF CASE STUDY BUILDING

3.1 Description of Case Study Building

Presently, Addis Ababa is challenged with housing shortage due to the continually increasing population growth and immigration from different corners of the country. The City government has launched the Addis Ababa Integrated Housing Development Program (AAIHDP) to alleviate housing shortage. (UN-HABITAT, 2011). The program comprises of four different schemes based on percent of advance payment modalities such as 10/90, 20/80, 40/60 and housing associations.

The selected case study building is a 2B+G+12 with three floors of solid slab and remaining floor are ribbed slab system. The ribbed slab composed of precast concrete rib joist, top concrete and HCB filling blocks. The layout of rib joist is displayed in Figure 3-3 and corresponding ribbed slab section is depicted is Figure 3-4. The building is located at Meri Loqe 40/60 condominium in Addis Ababa. The building was primarily chosen for study because it has repetition and expected to continue for coming housing projects. It also is habitation for larger community which invest and queue up for longer years to get it. The Meri site composed of 14 identical block of case study building; those blocks incorporate 1843 house unit. Nevertheless, the building is also adopted at different site in Addis Ababa with story range of seven to eighteen with a total of 364 blocks accompanying by 35,325 housing units[4]. All building types have two similar main twin towers separated by expansion joint and accessed through common lift shaft, and stair case.

Particularly in the case study building, the size of expansion joint between main tower and stair is 200mm, 20mm in between tower and ramp as indicated in Figure 3-2. The ramp is used as access for vehicles to get in to their parking spot located at the two basement floors. Though, the building was separated by expansion joints, they share mat foundation that was constructed as a single unit.

[4] **https://addisbiz.com/blog/245-40-60-condominium-sites-locations-number-of-blocks-how-many-houses-completion-date-and-current-status [access date: 22-Dec-2018]**

The two basement floors have story height of 3.0m and the remaining all upper stories have story height of 3.2m. The two basement floors are assigned for car parking, from ground floor up to second floor are designed for commercial purpose and the remaining floor are allocated to residential (Apartment).

Figure 3-1: Typical Floor Plan from 2nd to 12th floor

The lateral load resisting system of the building is characterized by combination of shear wall and frame in both orthogonal directions. The main twin towers are made of three

shear walls and twenty-three column per each floor as indicated in Figure 3-3. The shear walls are 250mm thick that are reinforced with Φ12 c/c 150mm longitudinally and Φ10 c/c 150mm as stirrup all the way through base to top roof level of the building. The layout of the columns is indicated in the Figure 3-2 and their section properties are tabulated in Table 3-1. All Floor beams are dimensioned 250mm width and 500mm in depth with a broader range of flexural and shear reinforcement.

Table 3-1: Column reinforcement details.

Column ID	Size (mm)	Story Range	Longitudinal reinforcement
C1	600 X 500	B2 - 12th	16Φ16
C2	600 X 500	B2 - 5th	18Φ16
	600 X 400	6th - 12th	12Φ16
C3	600 X 400	B2 - 12th	12Φ16
C4	600 X 600	B2 - 2nd	16Φ24
	600 X 400	3rd - 7th	16Φ20
	600 X 400	8th - 12th	12Φ16
C5	600 X 600	B2 - 2nd	20Φ16
	600 X 400	3rd - 12th	16Φ16
C6	600 X 600	B2 – 2nd	20Φ16
	600 X 500	3rd - 12th	16Φ16
C7	700 X 700	B2 - 2nd	20Φ20
	600 X 600	3rd	20Φ20
	600 X 500	4th - 12th	16Φ16
C8	700 X 700	B2	16Φ20
	600 X 600	B1 - 2nd	16Φ20
	600 X 500	3rd -12th	16Φ16
C9	700 X 700	B2 - 1st	16Φ24 + 8Φ20
	600 X 500	2nd - 4th	20Φ20
	600 X 500	5th - 12th	16Φ16
The shear reinforcements in all columns are 4legΦ10 with spacing of 100mm at one meter below and above floor level and 200mm at mid height of column in both orthogonal directions.			

Material grade:

The structural working drawing states, C-25 concrete grade for floor beams and slabs while, C-30 for foundation, column and shear wall. Furthermore, G-60(fy_{min}[5]=400Mpa)

[5] fy_{min} :minimum yield strength of reinforcement bar

reinforcement grade is specified for diameter 12 and above reinforcement bars, G-40 (fy_{min}=300Mpa) for the remaining reinforcement bars.

Due to their Architectural and Structural similarities of twin tower, the study considers single main tower1 as its structural model building. The study is also bounded to evaluate performance of main towers and it does not consider parking ramp and common stair case tower. Although, these parts of the building were interconnected by mat foundation at their base, the study assumes their superstructures' response are independent.

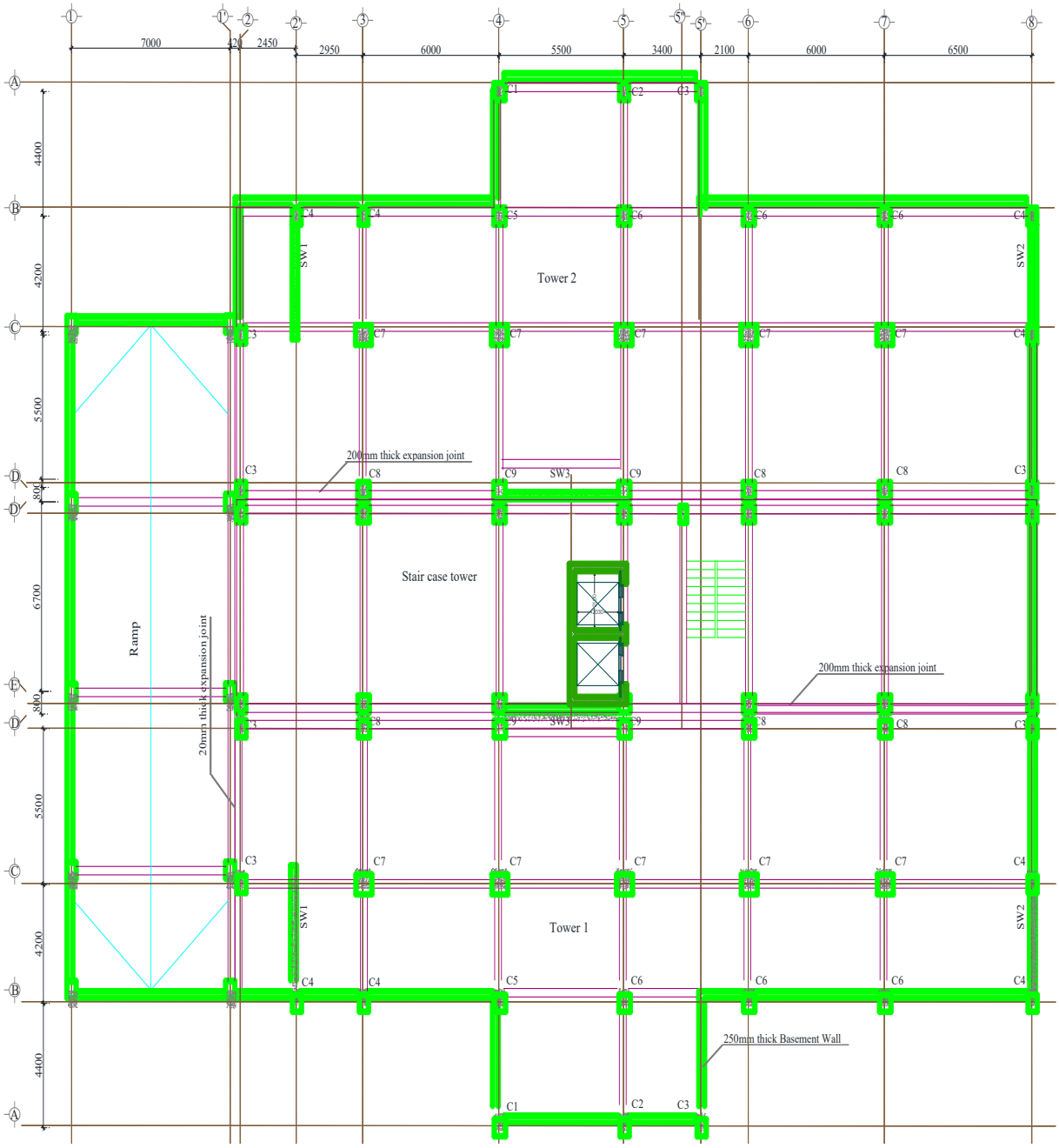

Figure 3-2: Structural layout of the building with its expansion joint at basement floor 2

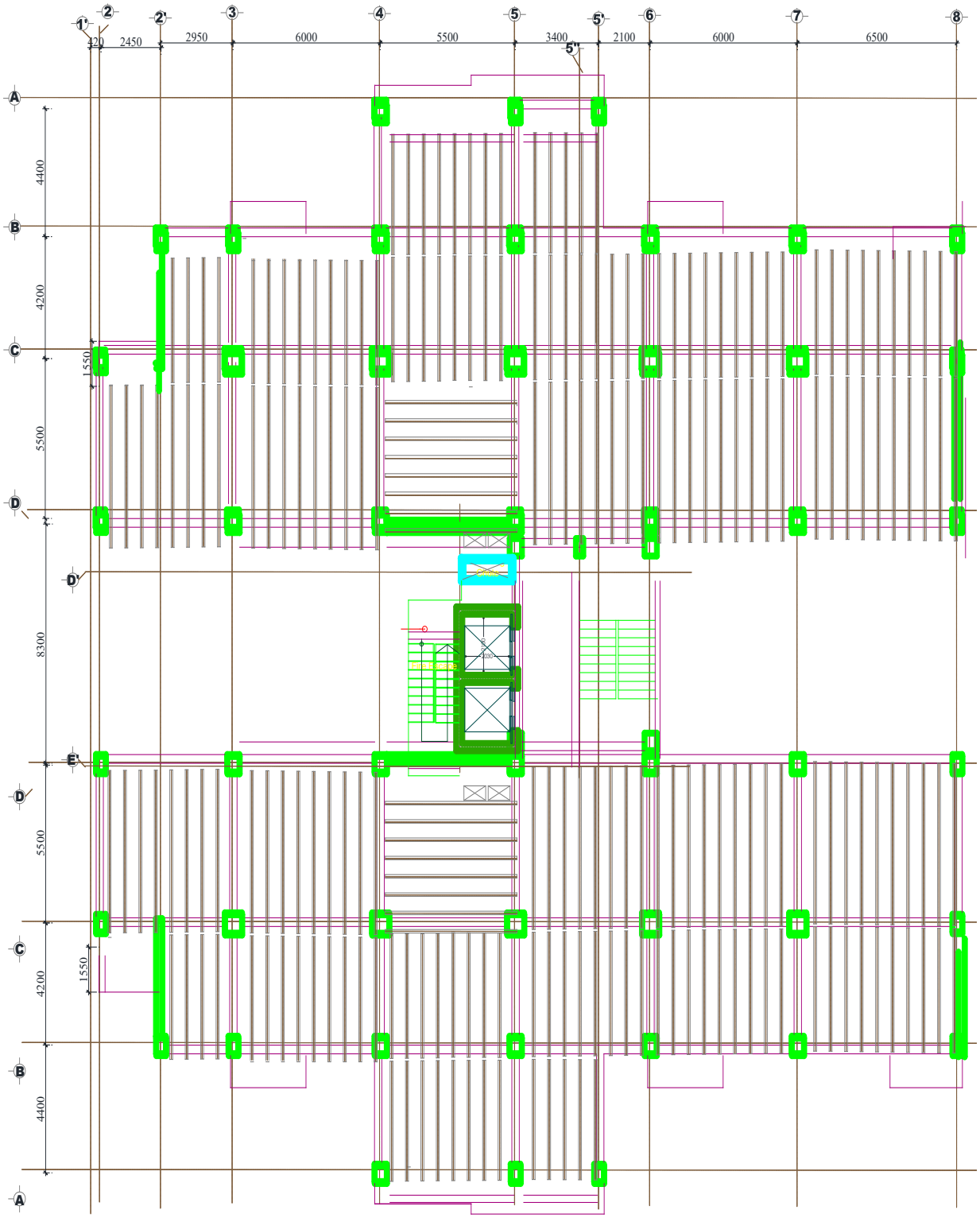

Figure 3-3: Typical floor structural system and rib layout from 2nd to 12th floor

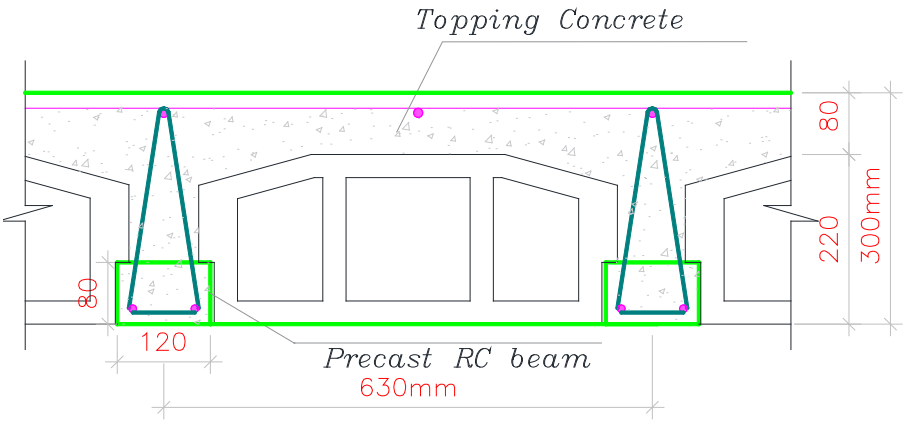

Figure 3-4 Typical Ribbed Slab Section

3.2 Modeling of the Case Study Building for Pushover Analysis

This section of the study discusses the methodology adopted to model the case study building to evaluate its performance level and generate capacity curves. The building was modelled in SAP 2000V21 (unlicensed) finite element software as shown in Figure 3-5. The frame element is modelled as a line element with linearly elastic properties with concentrated or distributed nonlinearity at nodal points. The material nonlinearity of the building as considers as concentrated plasticity for beam and fiber hinge for columns element.

Material inelasticity of beam is represented by assigning concentrated plastic hinge at the end of the member where flexural yielding is expected to occur. In order to tune the flexural hinges of beams, moment-curvature analysis of each beam section has been conducted. Various studies indicates transvers reinforcement of beams significantly enhance its flexural ductility, without significant reduction in ultimate moment capacity (Park and Paulay 1975). To utilize this merit of transvers reinforcement Kent and Park confinement model is implemented. Moment-curvature analysis program was developed in MATLAB® and detail of the script with material constitute model is given on Appendix E. Furthermore, the moment-curvature curve is converted to a quadrilinear moment rotation curve of FEMA356 to create a user-defined hinge in SAP2000 and the conversion was conducted by computing equivalent hinge length as shown Figure 3-7 A number of literature recommend different equation to compute plastic hinge length of frame element, Paulay and Priestley (1992) suggest plastic hinge length with adequate accuracy can be

approximated as 0.5h where h, is depth of section and ATC-40 also states that the plastic hinge length, 0.5h where h is the section depth in the direction of loading, is an acceptable value that usually gives conservative results.

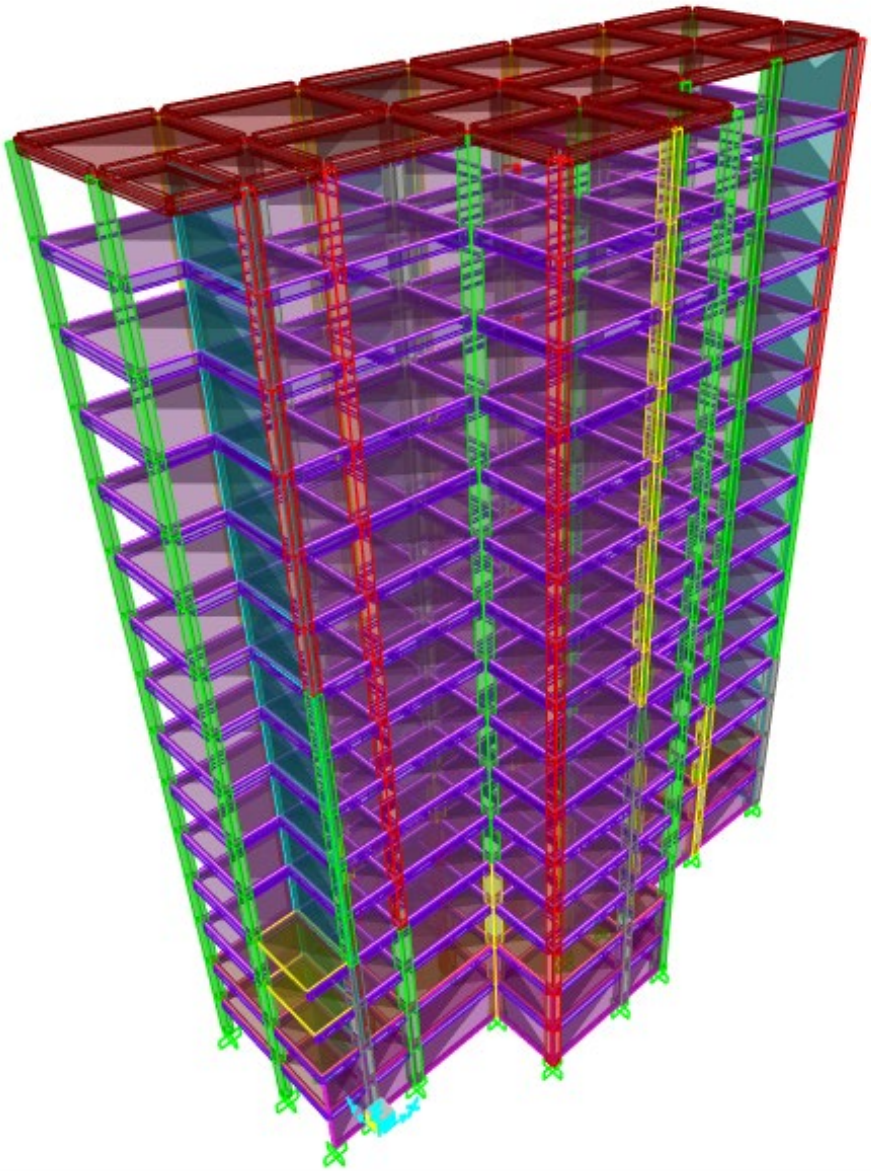

Figure 3-5: 3D modeling of the building in SAP2000

In this study, user-defined plastic hinges, which are obtained from Moment-curvature relation, are assigned to beam elements. Plastic hinge length is taken as half of the section depth. After generation of quadrilinear moment-rotation curve of beam section as per FEMA 356 and the three acceptance criteria: IO, LS and CP [6]has been defined as 10%,

[6] IO-Immediate Occupancy
LS- Life Safety
CP- Collapse Prevention

65% and 90% of plastic capacity respectively. For building with low concrete strength and/or insufficient amount of transverse reinforcement, shear failures of members should be taken into consideration. Accordingly, shear hinges are account for beams and columns. Moreover, Due to brittle failure of concrete in shear, no ductility is considered for this type of hinges. Shear hinge properties are defined such that when the shear force in the member reaches its strength, member fails immediately.

A sample beam whose section properties is depicted in Table 3-2 illustrates methods used to its model flexural and shear hinge. The moment curvature analysis of the beam for negative moment is shown in Figure 3-6 while its linearly fitting on user defined moment hinge is presented in Figure 3-7. Moreover, the force-controlled shear hinge of the beam is depicted in Figure 3.8

Table 3-2: Section properties of sample beam

Beam Size (mm)	Flexural reinforcement (mm^2)		Shear Reinforcement	Shear capacity (kN)
	Negative	Positive		
250X500	1366.59	710	2leg Ø10 at 200mm	280

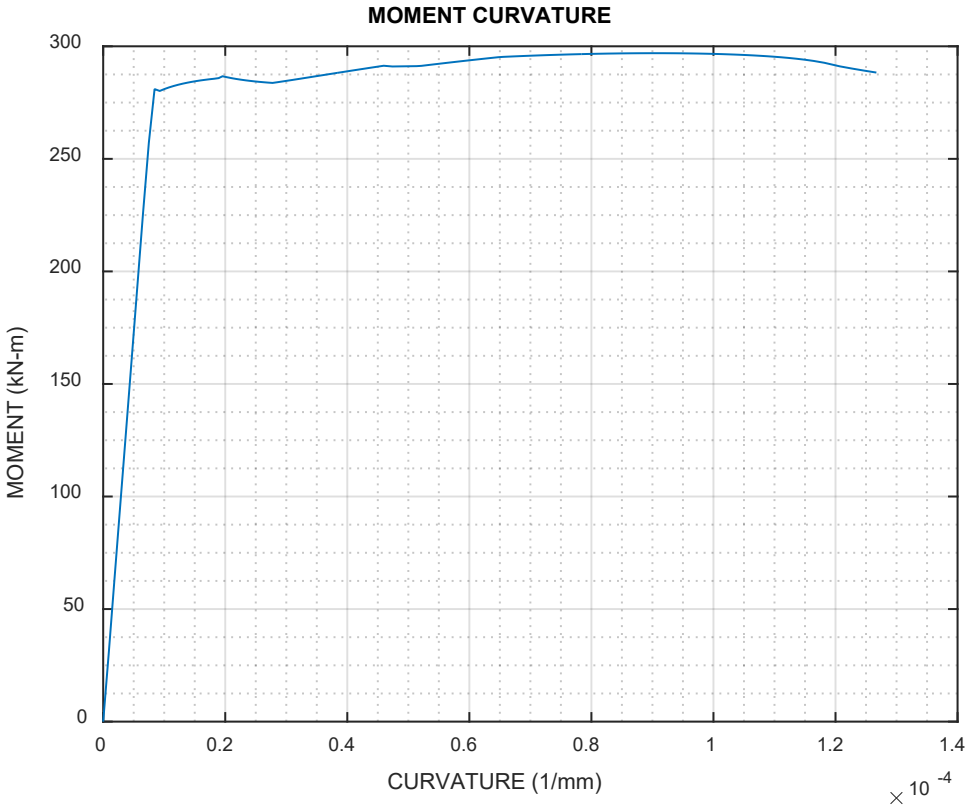

Figure 3-6: Moment-Curvature curve of sample beam

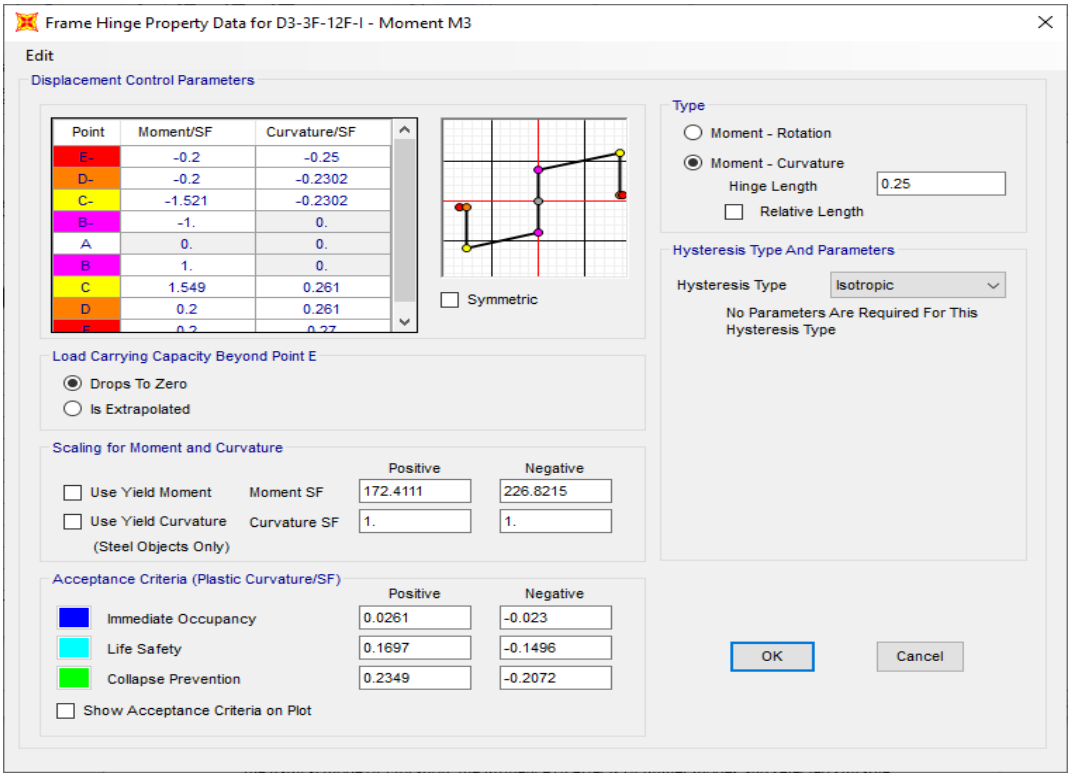

Figure 3-7: Use-defined flexural hinge for sample beam in SAP2000

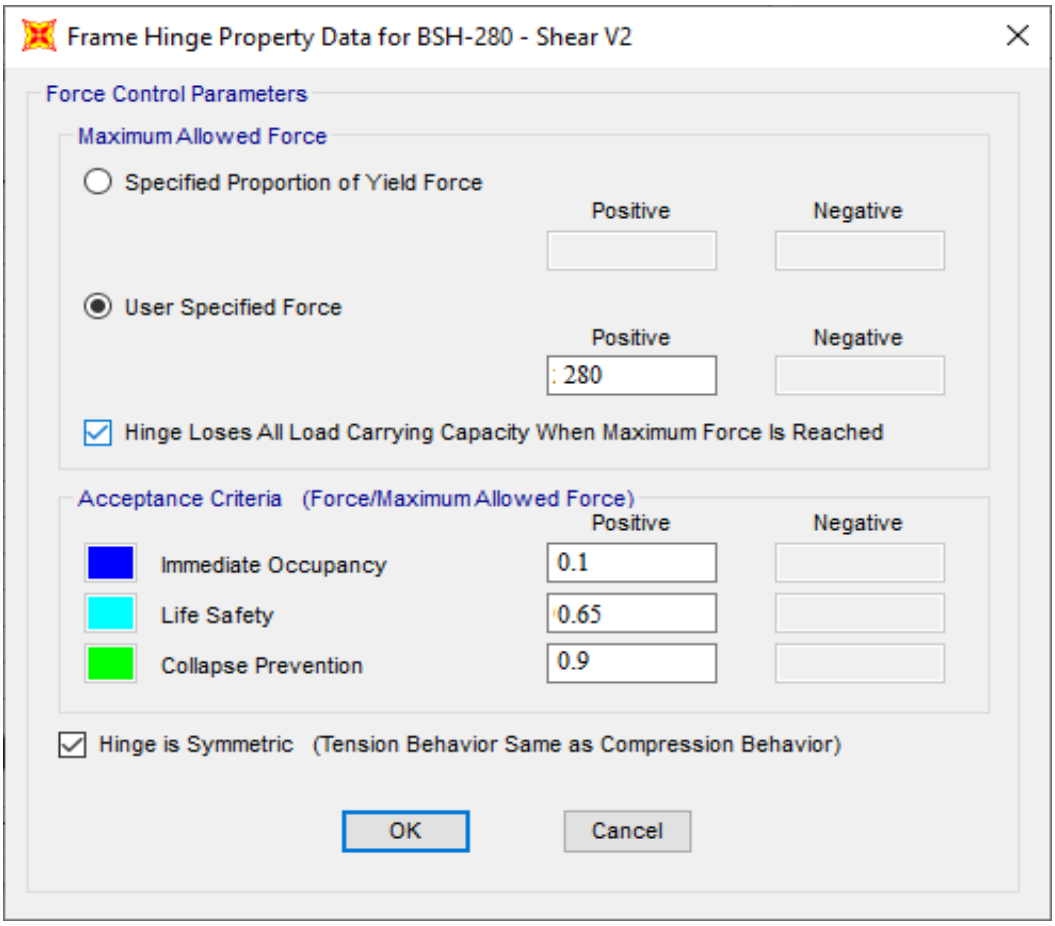

Figure 3-8: Use-defined Shear hinge for sample beam in SAP2000

Nonlinearity of column element created by using inbuilt P-M2-M3 fiber hinge model. Material properties of each element are assigned as per their prescribed relationship; Mander et al. (1998) model was used to combine the confining role of transvers reinforcement. SAP2000 fiber hinges model has limitation regarding identifying status of hinges and strain on constitutive material is monitored. Hence, the user needs to identify the status of hinge by checking against its section capacity. In addition to material inelasticity, geometric nonlinearity is also incorporated by using second order analysis: P-delta analysis tool provided in the software.

Before applying nonlinear pushover analysis, modal analysis was conducted to investigate the natural mode of vibration, the influence of effects of higher modes and selected suitable load pattern for pushover analysis. Cracking of element is introduced to the structure by using effective stiffness provided in FEMA 356 § 6.4.1.2. For reinforced concrete buildings with low concrete strength and/or low shear reinforcement, shear failure could be the dominate mode of failure. Hence, to consider this condition shear hinge was introduced the nonlinear model as a force-controlled hinge for beams and columns. Furthermore, shear hinge properties are defined such that when the shear force in the member reaches its strength member fails immediately, no ductility is considered for shear hinges.

Member shear capacity are computed as per ES EN 1992-1:2015 recommendation. Furthermore, NIST (2017) suggest for well detailed beams and columns that are flexurally dominated, Effective shear stiffness is taken as 40% of uncrack sections. However, the existing beam and column of the case study building are not well detailed seismic detailing, hence the shear hinges were introduced instead of reducing shear stiffness of the member to count their shear failure. In addition, flexural stiffness is taken 50% of uncrack stiffness for beam, column and shear wall. Floor diaphragms are assigned to each floor with FEMA 356 § 3.2.4 provision. Rigid floor diaphragm is assigned to floor with solid slab and flexible floor diaphragms is assigned to floor with ribbed slab. The inertial mass of the model was assigned as per the ES EN 1998-1:2015 requirement. Aforementioned, the case study building has two basement floor which accounts 5% of total seismic weight of the whole structure. The ground floor and below two basement floor elements are assumed to experience relatively small displacements, and do not significantly contribute to the modal response of the building. Hence, the modal analysis is conducted by taking only mass above the ground floor. The basic modal properties of the building are

summarized in Table 3-3. The effective masses indicate that the first mode is predominantly translational in the Y direction, the second mode is translational in the X direction and the third mode is predominantly torsional.

Table 3-3: Modal periods and participating mass ratios with respect to mass of superstructure

Mode	*Period*	*% Effective Mass**		
	(Sec)	X	Y	Torsion
1	2.284	1.88	67.48	4
2	2.17	65.74 [67.71]	3.08 [70.56]	3.48 [7.48]
3	1.667	5.23 [72.84]	1.82 [72.38]	63.9 [71.38]
4	0.575	1.41 [74.25]	13.77 [86.15]	1.27 [72.65]
5	0.526	13.54 [87.78]	2.65 [88.79]	0.82 [73.47]
6	0.363	1.95 [89.73]	0.75 [89.80]	16.3 [89.76]
7	0.277	0.07 [89.80]	5.03 [94.09]	0.03 [89.79]
8	0.247	4.29 [94.09]	0.13 [94.71]	0.94 [90.73]
9	0.202	0.04 [94.13]	1.5 [96.21]	0.00 [90.73]

**Accumulated modal mass is in the parentheses.*

Result of pushover analysis considerable dependent on material specification and selected lateral load distribution. Studies in FEMA -440 have shown that multiple load pattern has little improvement on accuracy of pushover analysis and single pattern based on first mode shape is recommended. This suggestion is conclusion in case first mode dominate structure. Whereas, ES EN 1998-1:2015 suggest to use at least two load distribution: Uniform load pattern and SRSS load pattern.

Meanwhile the building is not first mode dominate building, using single first mode load pattern is insufficient. Therefore, two load patterns are adopted: first mode load pattern and SRSS load pattern including all mode that has effective mass participation ratio greater than 5%. Table 3-4 displays normalized load pattern used in pushover analysis in two orthogonal direction.

Table 3-4: Normalized load shape used in pushover analysis

STORY	*STORY MASS (ton)*	*Center of Mass (m)*		*Normalized First Mode*		*Normalized SRSS*	
		X_{COM}	Y_{COM}	PUSH X	PUSH Y	PUSH X	PUSH Y
First	632.95	18.03	8.16	0.037	0.043	0.135	0.140
Second	624.4	17.69	8.16	0.088	0.093	0.267	0.276
Third	710.37	17.55	8.27	0.152	0.157	0.402	0.416
Fourth	709.14	17.55	8.27	0.228	0.231	0.512	0.534
Fifth	708.91	17.55	8.28	0.312	0.314	0.582	0.611
Sixth	708.67	17.55	8.28	0.400	0.402	0.604	0.637
Seventh	708.67	17.55	8.28	0.491	0.493	0.581	0.613
Eighth	708.67	17.55	8.28	0.582	0.584	0.533	0.558
Ninth	708.67	17.55	8.28	0.672	0.673	0.502	0.514
Tenth	708.67	17.55	8.28	0.760	0.760	0.538	0.546
Eleventh	708.67	17.55	8.28	0.844	0.845	0.657	0.676
Twelfth	708.67	17.55	8.28	0.925	0.925	0.828	0.851
Roof	375.44	17.24	8.24	1.000	1.000	1.000	1.000
SUM	**8721.9**						

The study is intended to assess global performance of building under seismic excitation and the performance point of the building are represented in capacity curve is identified as intersection point between capacity curve and demand curve and display capacity curve of the building in the two orthogonal direction. The performance point of the building under each load pattern is determined by CSM of FEMA 440 with available inside inbuilt program in SAP 2000 and sample of the procedure is shown in Figure 3-11. The performance points of case study building under different ground motion intensity are given in Table 3-5 and Table 3-6. Moreover, SYNER-G seismic performance evaluation standard uses inter-story drift and roof drift as damage measurement parameter. Hence, the capacity curves are further developed by considering maximum inter-story drift as controlling parameter.

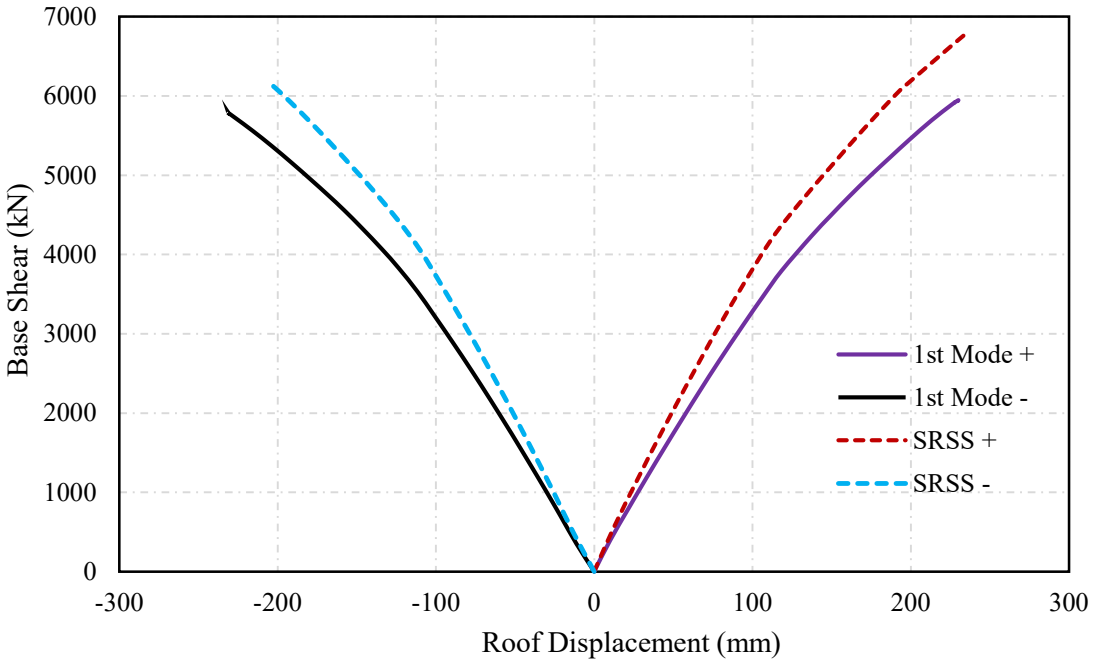

Figure 3-9: Capacity curve in longitudinal(X) direction

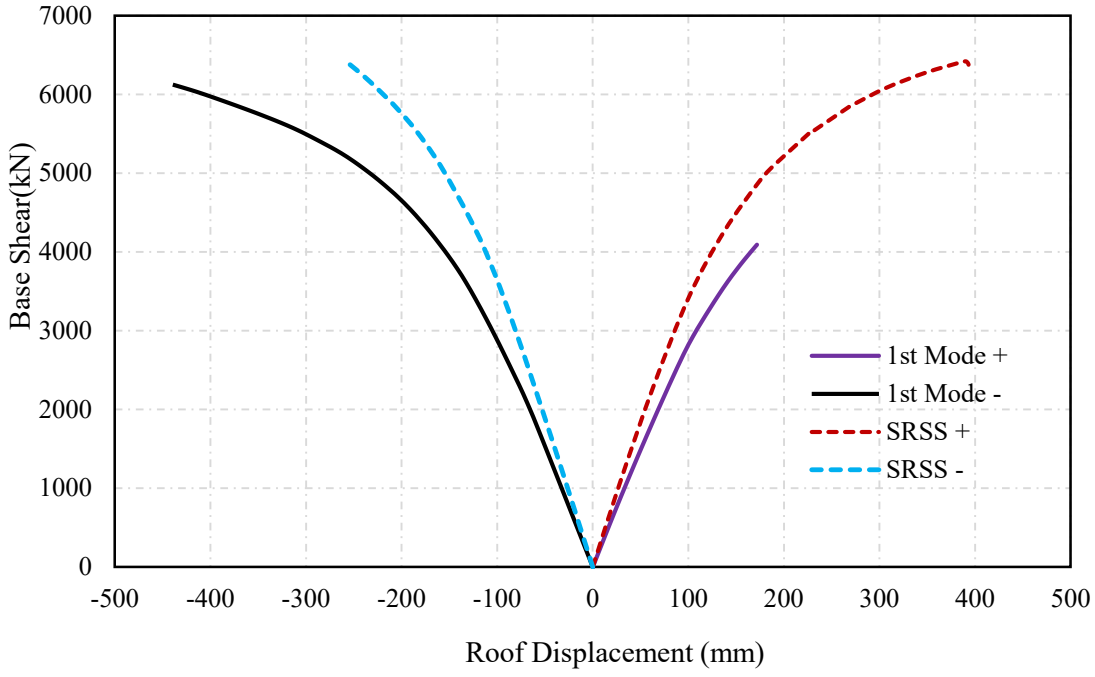

Figure 3-10: Capacity curve in transvers(Y) direction

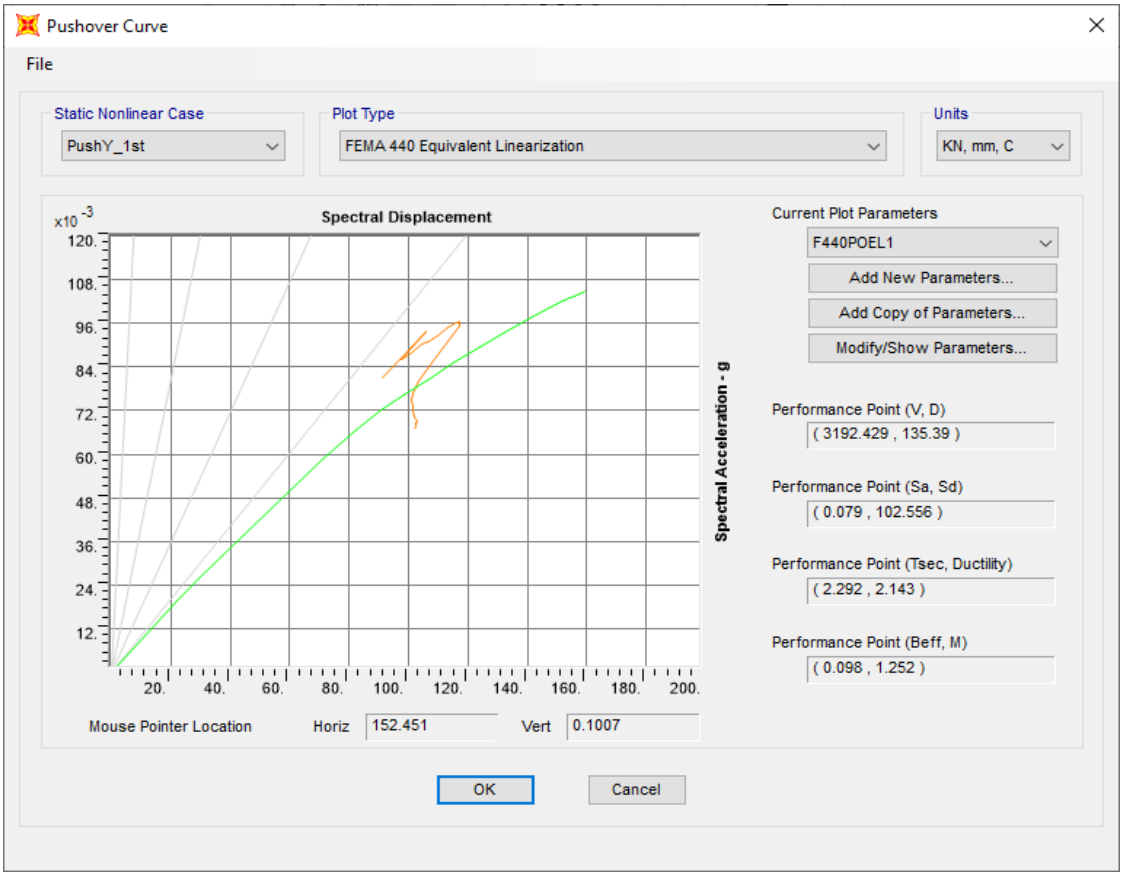

Figure 3-11: Performance point of the building under first mode load pattern in Y direction.

Table 3-5: Performance point of the building in X direction

Load Case PUSH X	**Demand: [0.15] PGA**		**Demand: [0.1] PGA**		**Demand: [0.05] PGA**	
	V_b (kN)	Δ_{Roof} (mm)	V_b (kN)	Δ_{Roof} (mm)	V_b (kN)	Δ_{Roof} (mm)
1st mode +[7]	NA[8]	NA	5,290.69	190.46	3,377.77	103.39
1st mode -	NA	NA	5,038.85	184.41	3,196.14	99.87
SRSS +	6,349.84	209.13	4,799.89	136.19	2,938.46	74.52
SRSS -	NA	NA	4,700.27	135.06	2,781.48	72.53

Table 3-6: Performance point of the building in Y direction

Load Case PUSH Y	**Demand: [0.15] PGA**		**Demand: [0.1] PGA**		**Demand: [0.05] PGA**	
	V_b (kN)	Δ_{Roof} (mm)	V_b (kN)	Δ_{Roof} (mm)	V_b (kN)	Δ_{Roof} (mm)
1st mode +	4099.21	190.04	3192.43	135.39	1897.42	82.21
1st mode -	4045.86	139.405	3005.89	87.78	1725.26	38.82
SRSS +	5478.65	241.19	4418.67	163.99	2899.41	100.79
SRSS -	5790.89	185.06	4630.02	120.25	2909.24	60.7

[7] The + and – sign indicates the load application direction in for positive and negative sense respectively
[8] The performance point is not available which means the building does not sustain the loading or the incoming demand load exceed the capacity of the building.

The capacity curve of the building in the two opposite direction for a single loading was observed in the capacity cure plotted Figure 3-9 and Figure 3-10. The difference are mainly resulted from variation of the top and bottom flexural reinforcement of beams. Those variation will result different beam flexural capacity in for positive and negative moments. The difference was quiet visible for capacity curves extracted form nonlinear analysis without shear hinge.

3.3 Drift Limit and Performance Level Evaluation

Parallel to modal analysis 3D elastic response spectrum analysis is conducted to evaluate the drift and stability of the building under 0.1g PGA demand. Elastic seismic spectrum curve is utilized to define the demand for response spectrum analysis, the seismic mass of the building is defined similarly as the modal analysis. The subsequent result of elastic response spectrum analysis is indicated in Figure 3-12. ES EN 1998:2015 § 4.4.3.2 specifies maximum Inter-story drift limit to be 1% for buildings having a non-structural element of brittle material attached to the structure. Furthermore, ES EN 1998:2015§ 4.4.2.2 provision also limits the maximum story sensitivity coefficient to be below 0.3 if not the structure will be unstable with second-order effect. The maximum story sensitivity coefficient and Inter-story drift are 0.05 and 0.38% respectively which are with the limit.

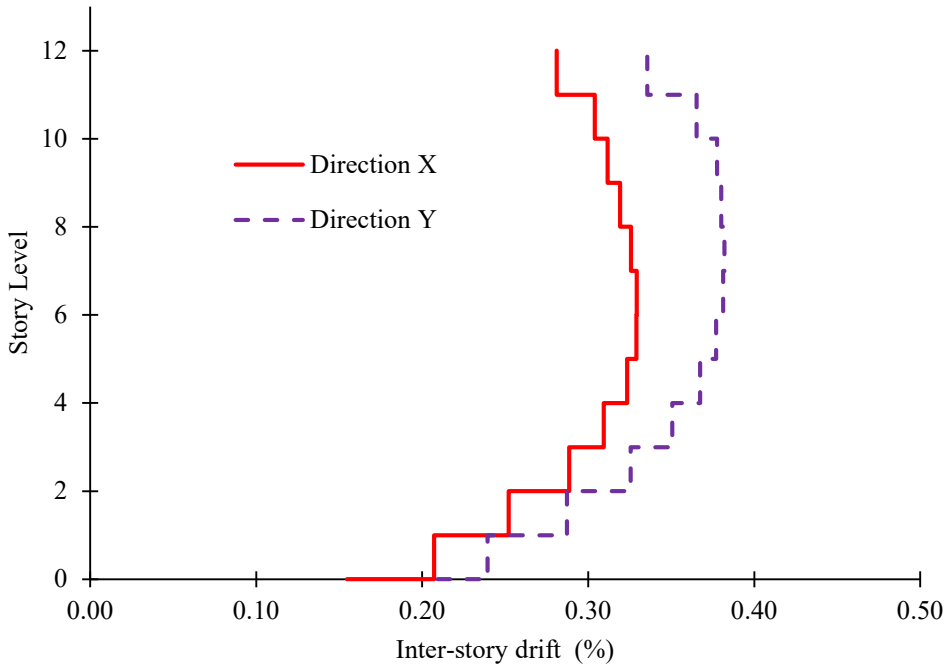

Figure 3-12: Elastic Inter-story drift of the building in 0.1g PGA demand

The global performance level of the building is evaluated based on FEMA 356 provision which limits roof drift 0.5%, 1% and 2% for IO, LS and CP level respectively. The values were selected from the performance level stated for a shear wall building. The maximum roof drift ratio of the case study was 0.49% under 0.1g PGA[9] which near to IO threshold. Hence the building satisfies IO performance level as per FEMA 356. In the country Performance point of the building under 0.15g PGA was not available which means the building is unable to sustain incoming demand.

[9] The demand is described in peak ground acceleration for demand spectrum curve provided in the new code ES EN 1998-1:2015

CHAPTER 4: SELECTION AND MATCHING OF GROUND MOTIONS

The evaluation of the structural response through dynamic analysis includes characterization of the seismic input that represent both the hazard and the near-surface geology at the site. Ground motion excitation that can be used in seismic time history analysis are typically of three types(Bommer and Acevedo 2004; Cimellaro et al. 2011):

(1) Select real accelerograms from past strong motion databases;

(2) Simulate synthetic ground motions from theoretical seismological models of seismic fault rupture;

(3) Simulate artificial accelerograms using stochastic or random vibration theory methods to match the target response spectra.

Over a region where no ample record of earthquake exists, either adopt real records of other areas or generate synthetic records is inevitable. The increasing availability of strong-motion accelerograms, and the relative ease with which they can be bought in contrast to synthetic or artificial records, makes the use of real records an ever extra alluring alternative for defining the enter to dynamic analyses of structures. However, due to the large variability in records representing a scenario, several points arise regarding the criteria for appropriate selection and manipulation of such records. Though seismic code has poor guide line in selection of real record, the experts on filed urges the selection of ground motion record from other site needs at least basis on similarity geological and tectonic behavior (Iervolino et al. 2008). The local and regional geological and tectonic conditions mainly define the similarity of the site of interest and those sites where actual strong ground motions were previously recorded. The selection and suiting of strong ground motion for need to considerer the following parameters: such as the magnitude of an earthquake, the distance of the site from the causative fault, fault mechanism, geology of the travel path of seismic waves from the source to the site and the local soil conditions at the site usually expressed in shear wave velocity within 30m (Kalkan and Chopra 2010). List of available strong ground motion data banks and their respective web address are cited in Bommer and Acevedo (2004).

Even though Ethiopian is located on East Africa were larger tectonic movement is undergoing no strong ground motion record were found but Gouin (1979) collects some

of earthquake events with their intensity. Studies on seismic risk and hazard assessment of the region argues that the evaluation can be resolved from strong ground motion attention relationship of the Western United States suggesting the subsequent points (Kebede and Eck 1997, Ayele 2017):

1. Both California and the Horn of Africa have substantial parts of their surface areas as plate boundaries running all along their lengths; and
2. The hypo-central depths of earthquakes are in both regions constrained to the crust.

As a result of those points, this study was drawn to utilize input ground motions recorded from PEER[10] Strong ground motion database of Western United States is adopted with selection criteria are described in the subsequent sections.

4.1 Parameter for Selecting Real Records

4.1.1 Earthquake Magnitude

Magnitude of earthquake has significant impact on structural response so considering earthquake magnitude for selection record become inevitable. Geographically Addis Ababa is located at margin of Main rift system, which makes the site to face several earthquakes shaking in its history. 4.1 magnitude earthquake was observed with epicenter, 22km from the city in 1979 and another destructive Kara Kore earthquake was observed in 1961 which has 6.8 magnitude at 200 km away from the city (Gouin 1979; Mammo 2005). Studies seismic hazard analysis of the city and the region indicates that the city is warned that earthquake of about the same size as those of the 1906 and 1961 earthquakes could occur at about 27 km from the city(Kebede and Eck 1997). This study considers earthquake records that has moment magnitude 4.5 to 7 which also is indicated in seismic hazard analysis of the region by Kebede and Eck (1997).

4.1.2 Source-Site Distance

PEER ground motion database requests the definition of two distance measures parameters: Rupture distance and Joyner-Boore distance. Rupture distance, R_{rup}, being defined as the closest distance from a site to the rupture plane and Joyner-Boore distance, R_{JB}, determined as the closest distance from a site to the vertical projection of a fault plane

[10] The Pacific Earthquake Engineering Research (PEER) database is well-developed ground motion database in existence which has collected, processed and archived ground motion data for more than 20 years to date. This well-designed and implemented online utility is freely available to the users at (http://peer.berkeley.edu/peer_ground_motion_database)

on the Earth's surface. Graphical illustration of those distance parameter is demonstrated in Figure 4-1. Due to lack of sufficient data on fault type, the two distance parameter was computed by considering conservative estimation of 10km average depth as per Ayele (2017) assumption. The active tectonic fault of the region, Wonji fault belt is nearly situated at 70-100 km from Addis Ababa. Hereafter, considering R_{JB} and R_{rup} up to 140km will be good estimation of the parameters.

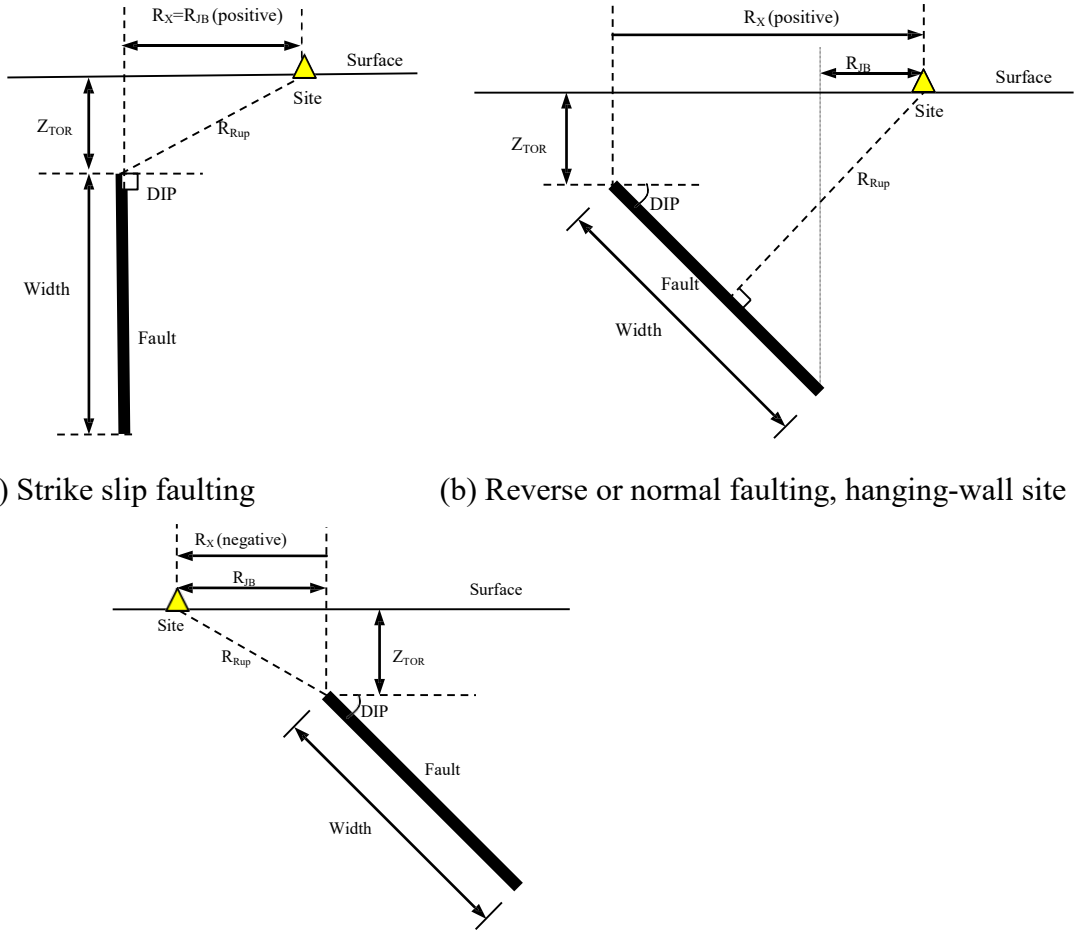

(a) Strike slip faulting

(b) Reverse or normal faulting, hanging-wall site

(c) Reverse or normal faulting, foot-wall site

Figure 4-1: Definition of Fault Geometry and Distance Measures on PEER database

4.1.3 Faulting Mechanism

Another input parameter in the filtering process is the fault mechanism type that defines the region of interest. Surface geology research shows that the Main Ethiopian Rift(MER) is dominated by normal fault(Kebede and Eck 1997; Resource 2018) contrarily, Korme et al. (2003) indicates part of central part of MER, Wonji fault belt floor is characterized by strike-slip fault. As a result, earthquake records with normal fault and strike slip mechanism are considered as entrant record.

4.1.4 Soil characteristic of the site

The average shear wave speed of top 30 meters of the location of intrigued is once more another crucial sifting basis. This shear wave speed ought to be the speed comparing to the reference location condition which is the location condition underneath the location profiles being analyzed in ground response analysis. Ground type 'C' as per ES EN 1998:2015 with V_{30} ranging 180-360m/s is assumed in filtering process.

4.1.5 Definition of Target Response Spectrum

Selection of ground motion records is usually followed by suiting it to response spectrum of the site hence, having target spectrum that represent hazard level of the site becomes crucial. On the other word, matching involves reducing of deviation of response spectra from target one which means using target spectrum as selection criteria will reduce computation time. The revise building code ES EN 1998:2015 specifies two type of response spectrum based on surface wave magnitude of earthquake at the site. Type 1 response spectrum curve was specified for site which has surface wave magnitude less than 5 while 'Type2' -response spectrum is provide for areas with surface magnitude wave greater than 5. Majority of earthquake in the country and Addis Ababa are originated from fault rapture of Main Ethiopian rift system which is generally characterized by surface magnitude of 5.5 to 6.5 (Gouin 1979; Kebede and Eck 1997). Consequently, 'Type 1' response spectrum curve was selected as target spectrum curve of site. Mathematical expressions of 'Type 1' response spectrum curve is available in section 3.2.2.2 of the code.

4.2 Response Spectrum Matching

Response-spectrum matching is a process in which a real recorded earthquake ground motion is modified in some manner such that its response spectrum matches a desired target spectrum across a range of periods and on desired damping values. Two procedures of matching accelerogram have been proposed; frequency-domain and time-domain techniques. The frequency -domain approaches involves adjusting Fourier amplitude spectra of the real record to have close match. However, adjusting Fourier amplitude corrupts the velocity and displacement spectrum time series and can results in motions with unrealistic high energy. While time- domain matching adjust time history by adding wavelet to acceleration time series. The wavelet transform basically consists of using modulating functions, selectively located in time to modify the spectrum of the signal, where and when it is needed in order to match the target spectrum(Iervolino et al. 2008).

Wavelet adjustment of recorded accelerograms has the same advantages as the Fourier adjustment methods but leads to a more focused correction in the time domain thus introducing less energy into the ground motion and preserves the non-stationary characteristics of the original ground motion. Hence it removes drift of velocity and displacement time-series(Hancock et al. 2006)

A typical code or guideline provision would require scaling of the two horizontal components of each ground motion (called a data set) such that the average square root of the sum of the squares (SRSS) of the 5% damped response spectra of the data set used does not fall below a times the 5% damped response spectrum for periods between T_0 and T_n and For conventional buildings, T_0 and T_n are usually assigned values such as $0.2T_1$ and $1.5T_1$ where T_1 is the fundamental period of the structure. While ES EN 1998:2015 proposes T_n to be twice of fundamental period.

This study utilized SeismoMatch software version 2020 to match selected records to target spectral. SeismoMatch adjusts earthquake accelerograms to match a specific target response spectrum, using the wavelets that created to match earthquake records. The matching was conducted in two stages by allowing tolerance of 0.3[11]: in the first round, fitting was conducted over short period 0.2 to 1sec, then over all spectral match sustained within $0.2T_1$ to 4sec. The proceeding section provides lists of selected earthquake records selected from PEER database and which also converges in the course of matching. Moreover, response spectrum curves for selected and match records are shown in Figure 4-2 and Figure 4-3, while detail of their selected time histories is given in Table 4-1.

Table 4-1: Selected Earthquake records from PEER NGA-West2 database

Earthquake Name[12]	**Year**	**Magnitude**	**R_{jb} (km)**	**R_{rup} (km)**	**Horizontal Component ID**
Borrego	*1942*	6.5	56.88	56.88	RSN9_BORREGO_B-ELC090
Victoria_ Mexico	1980	6.33	39.1	39.3	RSN268_VICT_SHP280
Big Bear-01	1992	6.46	44.48	44.65	RSN907_BIGBEAR_H4P090/180
Big Bear-02	1992	6.46	107.18	107.26	RSN918_BIGBEAR_NBI360
Big Bear-03	1992	6.46	113.58	114.31	RSN920_BIGBEAR_NSS180
Big Bear-04	1992	6.46	34.98	35.2	RSN931_BIGBEAR_HOS180

[11] It is lower limited provided by software under academic and trail license.
[12] Except the last two Earthquakes which have normal fault mechanism, the remaining Earthquakes have strike slip mechanism.

Northwest China-04	*1997*	*5.8*	*35.6*	*40*	RSN1755_NWCHINA4_XIK270
Taiwan Smart1(33)	*1985*	*5.8*	*41.34*	*41.55*	RSN3609_SMART1.33_33I03EW

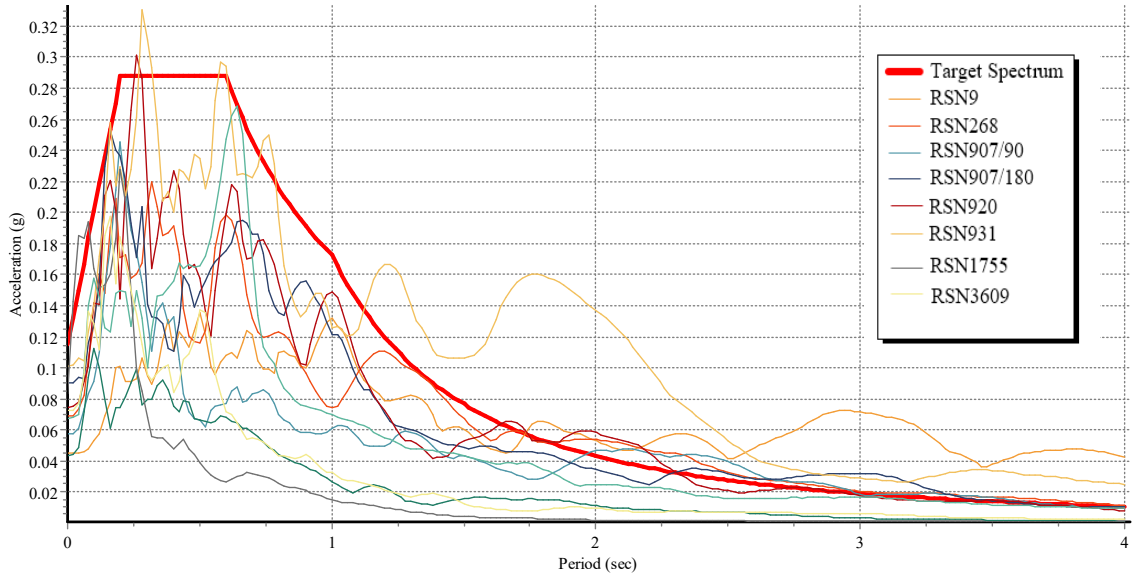

Figure 4-2: Response Spectrum of unscaled selected records

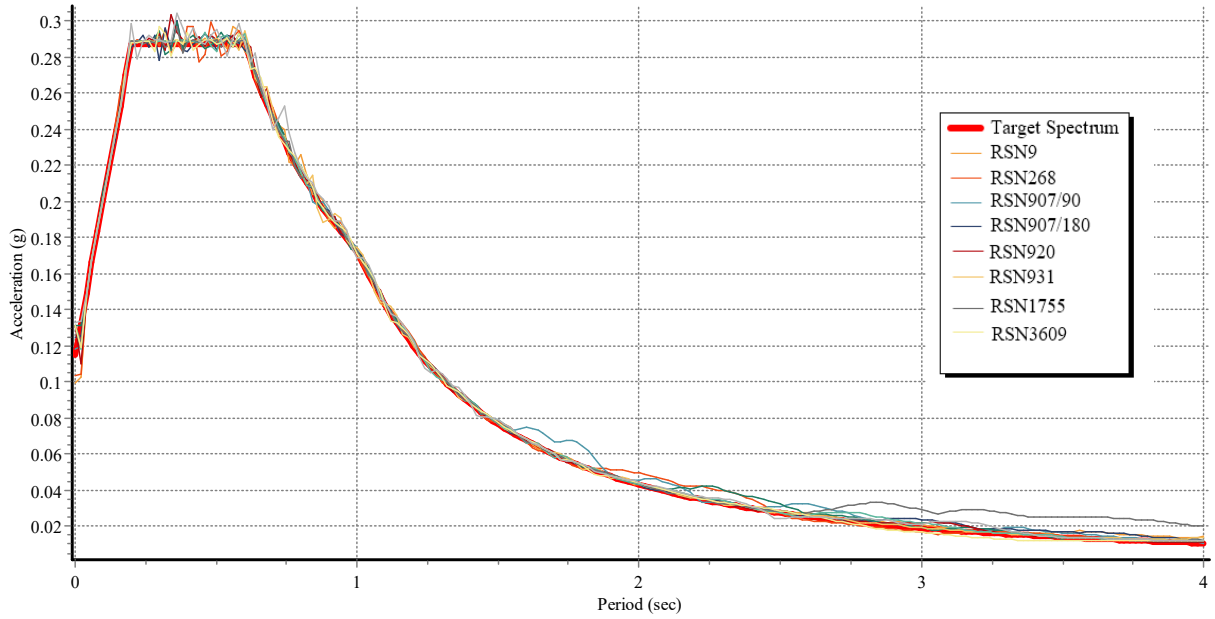

Figure 4-3: Response spectrum of selected matched records.

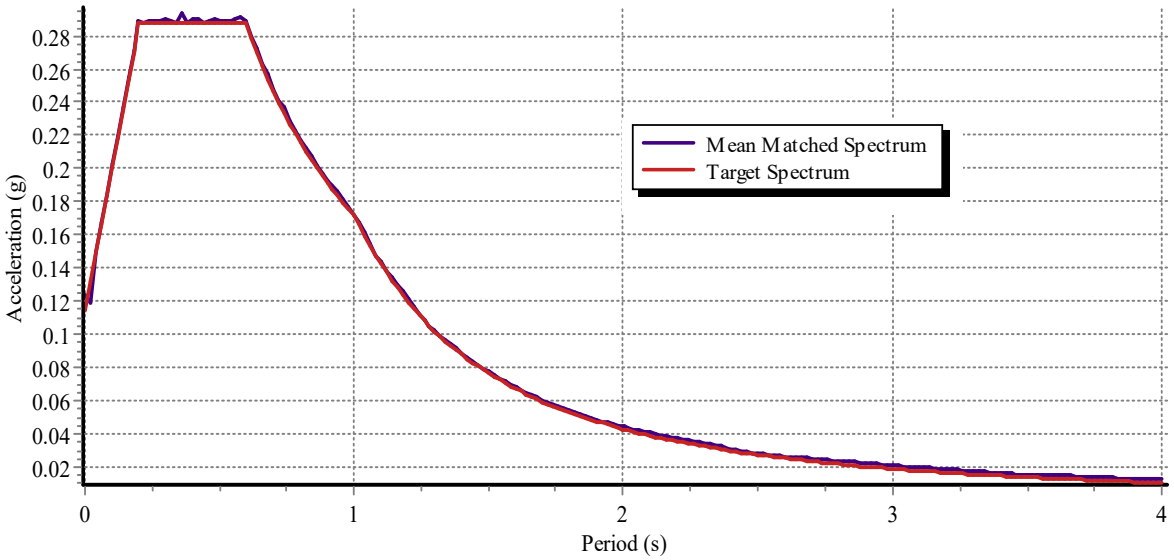

Figure 4-4: Mean of matched spectrum and target spectrum

Time history analysis of the building is conducted those records and elastic stiffness of the building is determined under linear regression using base shear versus top roof displacement data. Figure 4-5 indicates typical graphical representation of structural response and elastic stiffness under each record are collected to compute mean and standard deviation of response.

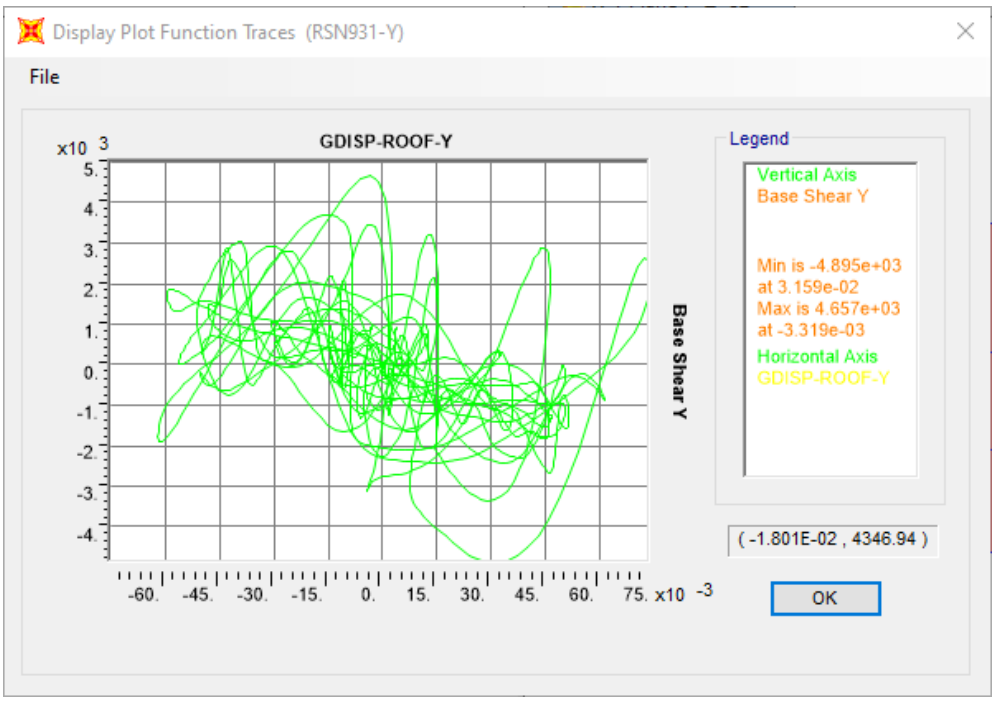

Figure 4-5 : Roof displacement vs base shear under RSN 931 (Big Bear-04) Earthquake.

Assuming the response follow normal distribution, the 50%, 84% and 16% fractile elastic stiffness can be computed by adding and subtraction standard deviation from the mean

respectively (Wilcox 2009). Table 4-2 portrays elastic stiffness of the building under each record and their statistical results.

Table 4-2: Statically computation of elastic stiffness of the building under selected records.

Earthquake record	Elastic stiffness	
	Kx[13]	Ky
RSN 9	29.6911	26.0471
RSN 268	30.0595	25.4816
RSN 907/90	28.7972	24.6455
RSN 907/180	30.1576	25.5892
RSN 920	30.4963	23.9874
RSN 931	29.424	26.5756
RSN 1755	32.0004	29.3075
RSN 3609	33.1774	28.8145
Mean	*30.4754*	*26.3061*
Standard deviation	*1.3434*	*1.7595*
K50[14]	***30.4754***	***26.3061***
K16	***29.1320***	***24.5465***
K84	***31.8188***	***28.0656***

[13] X and Y represent elastic stuffiness in each orthogonal direction in kN/mm
[14] The number after 'K' points percentage fractile of elastic stiffness.

CHAPTER 5: CONSTRUCTION OF SEISMIC FRAGILITY CURVES

An approximate version of IDA, Static Pushover Analysis to Incremental dynamic analysis (SPO2IDA) is selected to compute uncertainty parameters to generate fragility curves of the case study building. SPO2IDA will render 16%, 50% and 84% fractile IDA curves that are extracted from building capacity curve. In doing so, computational and time demand required by extensive nonlinear analysis will be substantially reduced. Aforementioned in section 2.2, the transition of the capacity curve to its IDA curves depend on the algorithm developed by Vamvatsikos and Cornell (2005). SPO2IDA also requires the following input parameters: fundamental mode of vibration, pinching weight and capacity curve parameters. The capacity curve parameters include slopes of the linearized fitted capacity curve. The procedures look simple but it also has two basic challenges: a selection of capacity curve which represent the worst failure model and quantification capacity curve parameter under limits imposed by the program. Luca et al. (2012) capacity curve fitting model also offers an option to consider the limiting value of SPO2IDA during its fitting optimization. The subsequent section in-detail describes the method used to generate the fragility curvefor the case studt building and finally discuss the obtained results.

5.1 Selection of capacity curve

The capacity curve which mimics the worst damage in the building is picked out to generate fragility function The capacity curves are selected among the eight capacity curve result of the two-load pattern used for pushover analysis indicated in Figure 3-9 and Figure 3-10. FEMA-356 suggests capacity curve should be selected from the result of load pattern which provides a larger performance point (FEMA 2005). In line with this recommendation capacity curves which result in greater performance point is selected as the worst capacity curve. Next, the worst capacity curve is approximated to Elastic Hardening model (EH) by using Luca et al. (2012) Model. Luca et al. (2012) investigate the error introduced when fitting the capacity curve using EC8 and FEMA 356 recommendation as compared to the NDP result and propose an alternative solution which minimizes the induced error. The proposed method is like FEMA 356 fitting rule, except the elastic stiffness is defined so that the intersection between the capacity curve and the fitted elastic segment is at 10% of the maximum base shear. The deformation corresponding to ultimate shear capacity is considered as ultimate deformation and post

hardening stiffness is computed by approximating the areas under the curve and approximated lines. The Matlab® script of the proposed method is also freely available at (http://users.ntua.gr /divamva/software.html).

5.2 Generations of IDA curves by using SPO2IDA

The IDA curves are generated for the selected capacity curve by using SPO2IDA which was in detail discussed in section 2.2. The IDA curves are produced for two damage states: Roof drift ration (θ_{roof}) and maximum Inter-story drift (θ_{max}). The elastic stiffness of the resulted IDA Curve is further modified at its elastic stiffness that was extracted from statistic results of Time history Analysis of the building subjected to selected accelerograms shown in Table 4-2.

Further calibration is conducted to enhance the accuracy of computed dispersion values as per technical recommendation. This can be performed by having recommended uncertainty value for the typical limit state, usually at inception collapse damage and the error is assumed to propagate along the IDA curves without affecting its monotonicity. With this assumption, linear interpolation is adopted to calibrate record to record variability against the dispersion of collapse prevention damage state provide by FEMA P695 § 6.4.1 which suggests aleatory at near collapse damage should not less than 0.4. The adjustment in the IDA curve provides a further gap between 16% and 84% fractile IDA. Finally, R-μ scale of IDA are converted to their $Sa_{(T1)}$ – drift scale by multiplying respective axis by their drift at yielding and spectra acceleration at yielding. The subsequent Figure 5-1 and 5-2 provide IDA curves in the transverse (Y) direction and all IDA Curves also are provided in Appendix C.

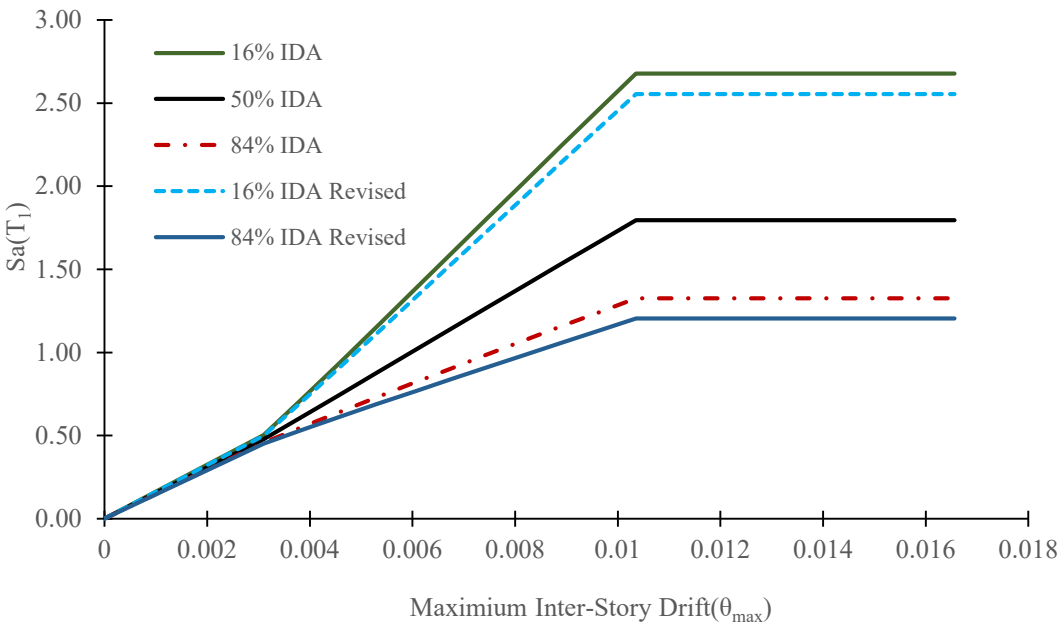

Figure 5-1: IDA Curves in Y direction under IDR damage states

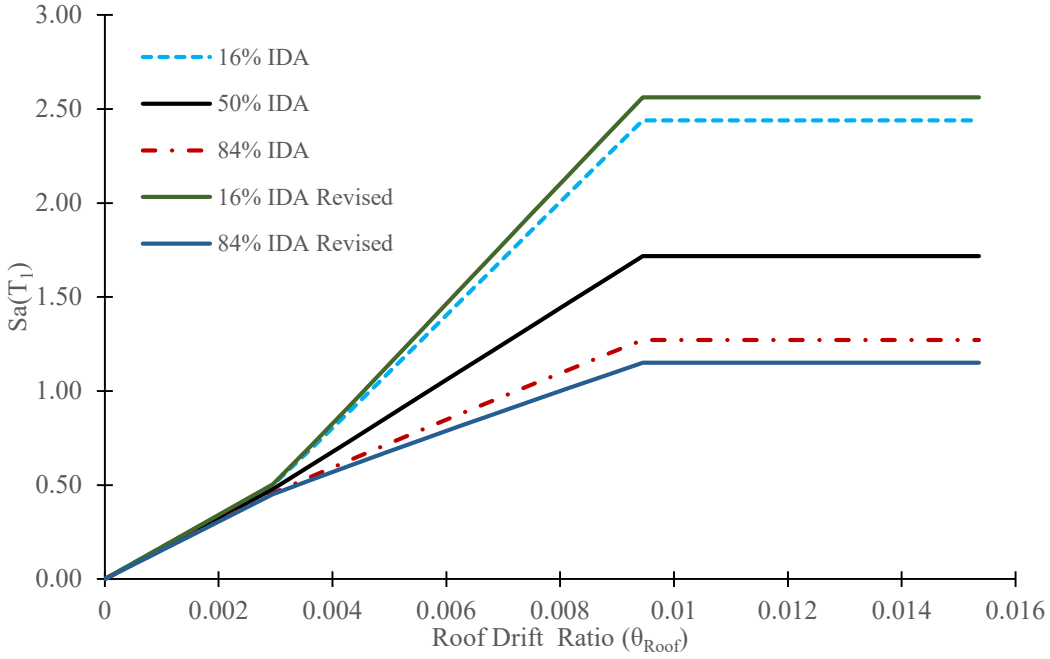

Figure 5-2: IDA Curves in Y direction under RDR damage states

Lastly, the compute record to record variability induced in the building is combined to modelling uncertainty to yield total uncertainty dispersion values. This study adopted FEMA P695 recommendation to incorporate modelling uncertainty in the formation of damage fragility curves which also resembles the result of recent studies.

5.3 Damage state definition

Both SYNER-G and HAZUS-MH technical manual consider inter-story drift to define their respective damage state threshold, which is a vital damage measurement to capture local failures. SYNER-G damage thresholds are dependent on ultimate and yield displacement of the structure which also makes suitable to consider roof drift as damage measurement. While HAZUS-MH defines the limits as a fixed inter-story drift for the selected building typology and seismic design level. The study use Roof drift and inter-story drift as damages measurement where their thresholds are defined with SYNER-G indicated on Table 5-1 and Table 5-2

Table 5-1: Damage state definition as per SYNER-G

Damage state	Drift limit
DS1 No damage	$\Delta < 0.7\Delta_y$
DS2 Slight	$0.7\Delta_y < \Delta < 0.7\Delta_y + 0.05\Delta_{uy}$
DS3 Moderate	$0.7\Delta_y + 0.05\Delta_{uy} < \Delta < 0.7\Delta_y + 0.2\Delta_{uy}$
DS4 Extensive	$0.7\Delta_y + 0.20\Delta_{uy} < \Delta < 0.7\Delta_y + 0.5\Delta_{uy}$
DS5 Very heavy	$0.7\Delta_y + 0.5\Delta_{uy} < \Delta < 0.7\Delta_y + \Delta_{uy}$
With $\Delta_{uy} = 0.9\Delta_u - 0.7\Delta_y$; Δ_y: Yielding drift and Δ_u: Ultimate drift	

Table 5-2: Computed damage threshold limit and fragility parameter

Standards	Damage State	Damage Threshold Drift limit (%)	Uncertainty Parameters		
			β_{RTR}	β_M	β_{Tot}
SYNER-G (θ_{max})	D1: No damage	0.1610	0.054	0.350	0.354
	D2: Slight	0.1825	0.061	0.350	0.355
	D3: Moderate	0.2470	0.105	0.350	0.365
	D4: Extensive	0.3760	0.260	0.350	0.436
	D5: Very heavy	0.5909	0.378	0.350	0.515
SYNER-G (θ_{Roof})	D1: No damage	0.1238	0.054	0.350	0.354
	D2: Slight	0.1425	0.062	0.350	0.355
	D3: Moderate	0.1985	0.126	0.350	0.372
	D4: Extensive	0.3104	0.286	0.350	0.452
	D5: Very heavy	0.4971	0.384	0.350	0.520

Once the median threshold and total uncertainty parameter are estimated, the subsequent fragility curve is generated with cumulative lognormal distribution function provided in section 2.2. The fragility curves are produced for the two orthogonal directions and worst is selected from among the two curves by comparing their damage probability of damage states. Figure 5-3 displays the fragility curve of the case study building while Appendix B provides all generated fragility curves.

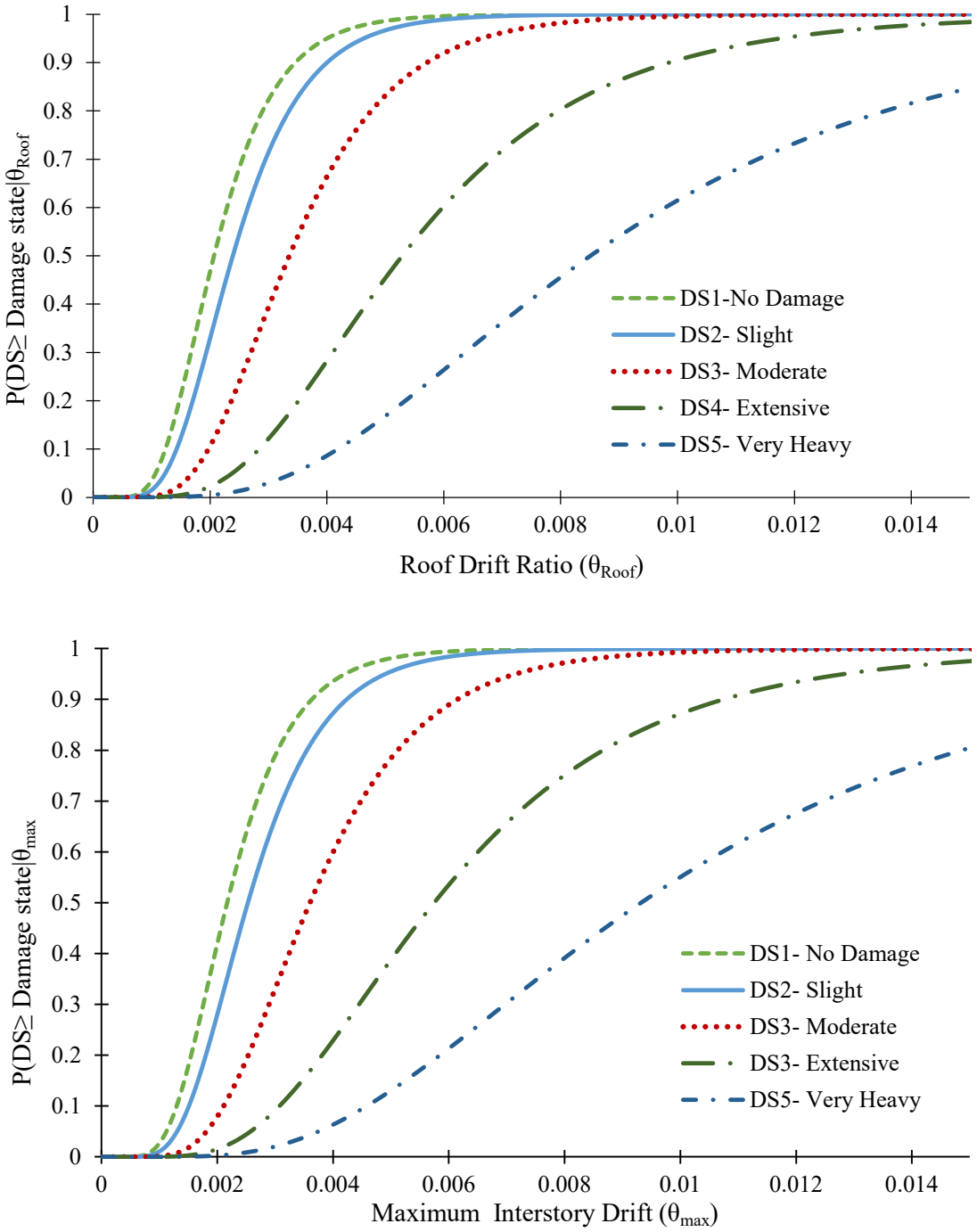

Figure 5-3: Fragility curve of the building SYNER-G in Y direction

After constructing of fragility curve, probability of being in or exceeded at each limit stated are identified by reading performance level drift of the building obtain from pushover analysis to its corresponding ordinate on fragility curve. Accordingly, the largest damage probability of the case study building that are associated with performance point are extracted and the results are revealed in the following chart.

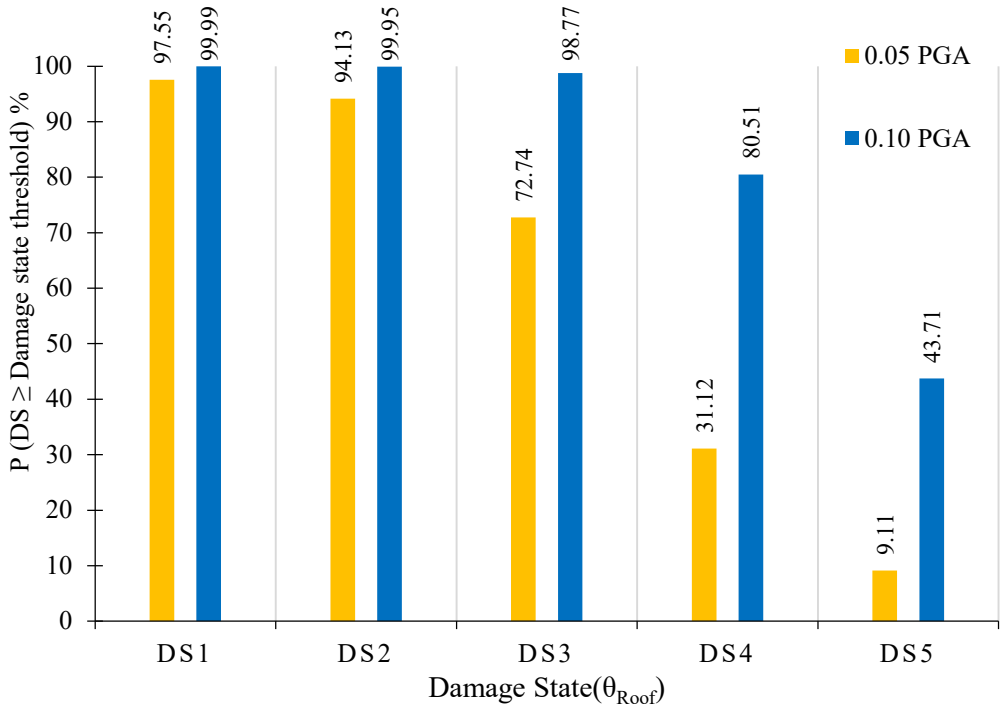

Figure 5-4: Building's probability of damage as per SYNER-G with RDR damage measurement

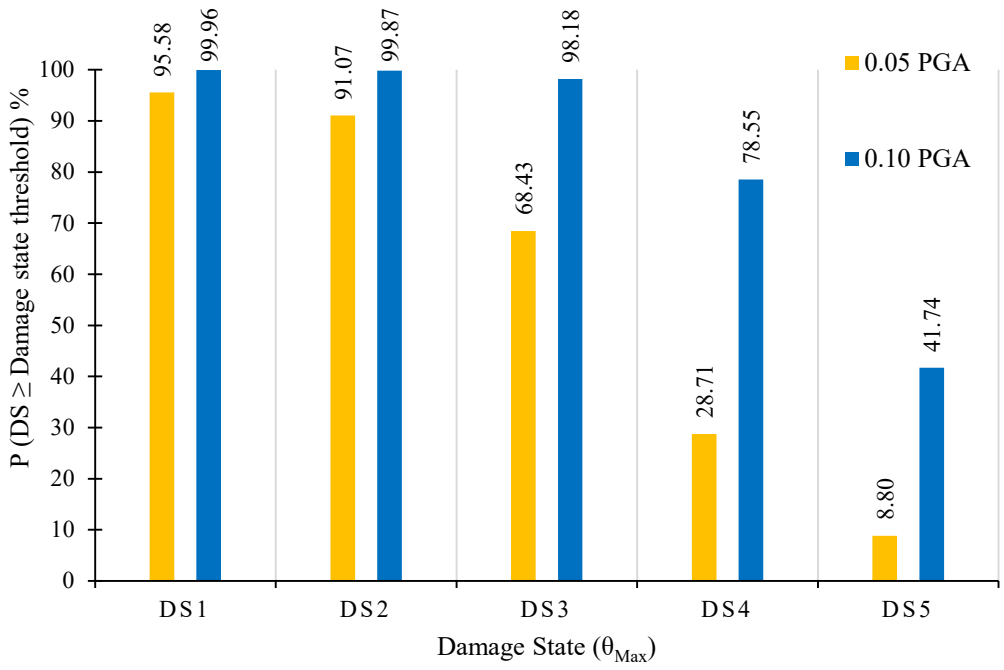

Figure 5-5: Building's probability of damage as per SYNER-G with IDR damage measurement

The result of the analysis generally shows that fragility of the building due to the change in peak ground acceleration has increased. The increment is substantial as the damage gets to near collapse state while it is not significant at earlier damage states especially at DS1-no damage state. Since, the damage threshold limit corresponding to DS1 is within the elastic range, it is expected to have little impact on unless the demand induces a base greater than elastic base shear resistance of the structure.

Defining the least acceptable fragility values is not a simple task, involve assessing risk induce in physical damage, cost of replacement and other relevant parameters like the importance of the building, insurance policy and investment cost. Hence, existing building performance assessment standard usually lift it for the engineer's decision. On the other hand, FEMA P695 specifies that the accepted probability of exceeding to failure damage state must be below 10%. Though, implementing FEMA P695 requirement in an area that has poor construction practices and lack of good risk management practices may underestimate the incoming risk. Due to lack of available list allowable damage fragility limit value as a nation, this study adopted FEMA P695 requirement as reference performance evaluation bases. The building fails to satisfy FEMA P695 damage probability limit for 0.1g PGA while the building lies on the bounder point when its failure is evaluated under 0.05g PGA.

CHAPTER 6: CONCLUSION AND RECOMMENDATION

6.1 Conclusions

1. The change in Peak Ground Acceleration in the new code ES EN 1998:2015 significant affect the performance of similar building which has been designed as per previous building code. The problem will be detrimental if the building did not properly detail following the seismic requirement and lacks good construction practices. The relative change in probability damage for 0.05g PGA and 0.1g PGA demand was evaluated by considering their probability damage ratio under each damage states which show up to four times increment.
2. The fragility of the building is evaluated for based on FEMA P695 requirement against collapse damage state and fails to satisfy the limit for 0.1g PGA while the building lies on the boundary point for 0.05g PGA. Beside, building satisfies immediate occupancy (IO) performance level requirement of FEMA 356 when subjected to 0.1g PGA demand.
3. The computation effort and time demand required to generate fragility curve substantially reduced by using the provided approximated method.

6.2 Recommendations

1. The frame verification indicates that the effect shear reinforcement must be considered in performance assessment of building and determination of frames ductility.
2. The performance of the building should be supported by further filed inspection to capture any existing physical damage and validate working drawing.
3. Further study should be done by considering bond-slip in addition to shear and flexural hinge to address all possible type of failure.
4. The performance of the existing buildings should be meticulously investigated and appropriated mitigation method should be implemented to minimize induces risk.
5. Further fragility analysis should be conducted in the national to decide the least allowable probability of damage value.

REFERENCE

Abdelnaby, A. E. (2016). "Fragility Curves for Rc Frames Subjected to Tohoku Mainshock-Aftershocks Sequences." *Journal of Earthquake Engineering*.

Akkar, S., Sucuog˘lu, H., and Yakut, A. (2005). "Displacement-Based Fragility Functions for Low- and Mid-Rise Ordinary Concrete Buildings." *Earthquake Spectra*, 21(4), 901–927.

Astriana, L., Sangadij, S., Purwanto, E., and Kristiawan, S. A. (2017). "Assessign Seismic Performance of Moment Resisting Frame and Frame-Shear Wall System Using Seismic Fagility Curve." *Procedia Engineering* 171, 1069 – 1076.

ATC (1996). " Seismic Evaluation and Retrofit of Concrete Buildings." *ATC-40 Report*, Applied Technology Council, Redwood City, California.

Ayele, A. (2017). "Probabilistic Seismic Hazard Analysis for Ethiopia and the Neighboring Region." *Journal of African Earth Sciences*, 134, 257-264.

Baker, J. W. (2014). "Efficient Analytical Fragility Function Fitting Using Dynamic Structural Analysis." *TECHNICAL NOTE 473*, S. University, ed.

Bommer, J. J., and Acevedo, A. B. (2004). "The Use of Real Earthquake Accelerograms as Input to Dynamic Analysis." *Journal of Earthquake Engineering*, 8(sup001), 43-91.

Bradley, B. A. (2010). "Epistemic Uncertainties in Component Fraglity Functions." *Earthquake Spectra*, 26(1), 41-62.

Cimellaro, G. P., Reinhorn, M., D'Ambrisi, A., and Stefano, M. D. (2011). "Fragility Analysis and Seismic Record Selection." *Journal of Structural Engineering*, 137(3).

Dumova-Jovanoska, E. (2000). "Fragility Curves for Reinforced Concrete Structures in Skopje (Macedonia) Region." *Soil Dynamics and Earthquake Engineering* 19, 455-466.

Ellingwood, B. R., Celik, O. C., and Kinali, a. K. (2007). "Fragility Assessment of Building Structural Systems in Mid-America." *Earthquake engineering and structural dynamics*, 36, 1935–1952.

Elnashai, A. S., and Sarno, L. D. (2008). *Fundamentals of Earthquake Engineering*, John Wiley & Sons, Ltd, United Kingdom.

Erberik, M. A. (2008). "Fragility-Based Assessment of Typical Mid-Rise and Low-Rise Rc Buildings in Turkey." *Engineering Structures* 30, 1360–1374.

Erberik, M. A. (2015). "Seismic Fragility Analysis." *Encyclopedia of Earthquake Engineering*.

FEMA (2005). *Fema 440 -Improvement of Nonlinear Static Seismic Analysis Procedures*, Federal Emergency Management Agency, Washington, D.C.

FEMA (2009). *Fema P695- Quantification of Building Seismic Performance Factors*, Federal Emergency Management Agency, Washington, D.C.

Gouin, P. (1979). *Earthquake History of Ethiopian and Horn of Africa*, International Development Research Centre, Ottawa.

Hancock, J., Watson-Lamprey, J., Abrahamson, N. A., Bommer, J. J., Markatis, A., Mccoy, E., and Mendis, R. (2006). "An Improved Method of Matching Response Spectra of Recorded Earthquake Ground Motion Using Wavelets." *Journal of Earthquake Engineering*, 10(1).

Haselton, C. B., and Deierlein, G. G. (2008). "Assessing Seismic Collapse Safety of Modern Reinforced Concrete Moment-Frame Buildings." Pacific Earthquake Engineering Research Center.

Hueste, M. B. D., and Bai, J.-W. (2007). "Seismic Retrofit of a Reinforced Concrete Flat-Slab Structure: Part Ii — Seismic Fragility Analysis." *Engineering Structures* 29, 1178–1188.

Iervolino, I., Maddaloni, G., and Cosenza, E. (2008). "Eurocode 8 Compliant Real Record Sets for Seismic Analysis of Structures." *Journal of Earthquake Engineering*, 12(1), 54-90.

Jeong, S.-H., Mwafy, A. M., and Elnashai, A. S. (2012). "Probabilistic Seismic Performance Assessment of Code-Compliant Multi-Story Rc Buildings." *Engineering Structures*, 34, 527-537.

Ji, J., Elnashai, A. S., and Kuchma, D. A. (2007). "An Analytical Framework for Seismic Fragility Analysis of Rc High-Rise Buildings." *Engineering Structures* 29, 3197–3209.

Kappos, A. J., and Panagopoulos, G. (2010). "Fragility Curves for Reinforced Concrete Buildings in Greece." *Structure and Infrastructure Engineering*, 6(1-2), 39-53.

Kebede, F., and Eck, T. v. (1997). "Probabilistic Seismic Hazard Assessment for the Horn of Africa Based on Seismotectonic Regionalisation." *Tectonophysics* 270 221-237.

Korme, T., Acocella, V., and Abebe, B. (2003). "The Role of Pre-Existing Structures in the Origin, Propagation and Architecture of Faults in the Main Ethiopian Rift." *Gondwana Research*, 7(2).

Kostov, M., Kaneva, A., Vaseva, M., Stefanov, D., and Koleva, N. (2007). "An Advanced Approach to Earthquake Risk Scenarios of Sofia." *8th Pacific Conference on Earthquake Engineering*Singapore.

Krawinkler, H., and Seneviratna, G. (1998). "Pros and Cons of a Pushover Analysis of Seismic Performance Evaluation." *Engineering structures*, 20(4-6), 452-464.

Liel, A. B., Haselton, C. B., Deierlein, G. G., and Baker, J. W. (2009). "Incorporating Modeling Uncertainties in the Assessment of Seismic Collapse Risk of Buildings." *Structural Safety*, 31.

Luca, F. D., Vamvatsikos, D., and Iervolino, I. (2012). "Near-Optimal Piecewise Linear Fits of Static Pushover Capacity Curves for Equivalent Sdof Analysis." *Earthquake Engineering & Structural Dynamics*.

Mammo, T. (2005). "Site-Specific Ground Motion Simulation and Seismic Response Analysis at the Proposed Bridge Sites within the City of Addis Ababa, Ethiopia." *Engineering Geology*, 79.

Mander, J. B., Priestley, M. J. N., and Park, R. (1998). "Theoretical Stress-Strain Model for Confined Concrete." *Journal of Structural Engineering*, 114(8).

NIST (2013). *Nonlinear Analysis Research and Development Program for Performance-Based Seismic Engineering Gcr 14-917-27*, National Institute of Standards and Technology.

NIST (2017). *Guidelines for Nonlinear Structural Analysis for Design of Buildings Gcr 14-917-46v3*, National Institute of Standards and Technology.

Papailia, A. (2011). "Seismic Fragility Curves for Reinforced Concrete Buildings." Msc, University of Patras.

Park, R., and Paulay, T. (1975). *Reinforced Concrete Structures*, John Wiley and Sons, New York, New York.

Paulay, T., and Priestley, M. J. N. (1992). *Seismic Design of Reinforced Concrete and Masonry Buildings* Jhon Wiley & Sons, Inc.

PEER (2010). "Peer/Atc 72-1 Modeling and Acceptance Criteria for Seismic Design and Analysis of Tall Buildings." Pacific Earthquake Engineering Research Center, University of California, Berkeley, California.

Pinho, R. (2007). "Nonlinear Dynamic Analysis of Structures Subjected to Seismic Action." *Advanced Earthquake Engineering Analysis*, Springer, 63-89.

Pitilakis, K., Crowley, H., and Kaynia, A. M. (2014). "Syner-G: Typology Definition and Fragility Functions for Physical Elements at Seismic Risk." *Geotechnical, Geological and Earthquake Engineering*, A. Ansal, ed., Springer Science+Business Media Dordrecht New York.

Porter, K. (2017). *A Beginner's Guide to Fragility, Vulnerability, and Risk*, University of Colorado Boulder.

Ramamoorthy, S. K., Gardoni, P., and Bracci, J. M. (2006). "Probabilistic Demand Models and Fragility Curves for Reinforced Concrete Frames." *Journal of the Structural Engineering*, ASCE.132(10), 1563–1572.

Rao, G. V. R., Gopalakrishnan, N., Jaya, K. P., Muthumani, K., Reddy, G. R., and Parulekar, M. (2014). "Studies on Nonlinear Behavior of Shear Walls of Medium Aspect Ratio under Monotonic and Cyclic Loading." *Journal of Performance of Constructed Facilities*, 14.

Resource, I. o. G. a. E. (2018). "The Ethiopian Rift Valley Geologic Evolution." <http://ethiopianrift.igg.cnr.it/rift%20valley%20history.htm>. (December 8, 2018).

Saruddin, S. N. A., and Nazri, F. M. (2015). "Fragility Curves for Low- and Mid-Rise Buildings in Malaysia." *Procedia Engineering* 125, 873 – 878.

SYNER-G (2011). "Systematic Seismic Vulnerability and Risk Analysis for Buildings, Lifeline Networks and Infrastructures Safety Gain - D3.1 - Fragility Functios for Common Rc Buildig Types in Europe." *Seventh Framework Programme*.

Tsionis, G., and Fardis, M. N. (2014). "Seismic Fragility Curves for Reinforced Concrete Buildings and Bridges in Thessaloniki." *Second European conference on Earthquake Engineering*Istanbul.

Vamvatsikos, D. (2002). "Seismic Performance, Capacity and Reliability of Structures as Seen through Incremental Dynamic Analysis." PHD Dissertation, Stanford University, Stanford.

Vamvatsikos, D., and Cornell, C. A. (2005). "Direct Estimation of Seismic Demand and Capacity of Multidegree-of-Freedom Systems through Incremental Dynamic Analysis of Single Degree of Freedom Approximation." *Journal of Structural Engineering*, 131(4).

Vecchio, F. J., and Emara, M. B. (1992). "Shear Deformations in Reinforced Concrete Frames." *ACI Structural Journal*, 89(1).

Wen, Y. K., Ellingwood, B. R., and Bracci, J. (2004). "Vulnerability Function Framework for Consequence-Based Engineering." *Mid-America earthquake center*, University of Illinois at Urbana-Champaign, Illinois.

Wilcox, R. R. (2009). *Basic Statistics : Understanding Conventional Methods and Modern Insights*, Oxford University Press, Inc., New York.

APPENDIX A: SOFTWARE VERIFICATION

A.1 Frame Verification

In this section, two story with single bay reinforced concrete frame was used to verify the Pushover result of SAP 2000 V21 (unlicensed). The selected frame was experimental tested by Vecchio and Emara (1992). The frame was constructed with a center-to-center span of 3500 mm, a story height of 2000 mm and an overall height of 4600 mm as shown Figure A-1. All beams and columns were 300 mm wide and 400 mm deep, while the base was 800 mm wide and 400 mm deep. The frame was built integral with a large, heavily reinforced concrete base to create an essentially fixed foundation. The base was fixed to the lab floor using ten pairs of bolts, which were post-tensioned to prevent slip. All members were similarly reinforced with four No.20 deformed bar both at as top reinforcement, four No.20 deformed bar as bottom reinforcement and No.10 closed stirrups at 125mm spacing were use as shear reinforcement. Reinforcement anchorage was achieved by welding the ends of the reinforcement to stiff bearing plates. Material properties were determined from concrete cylinder tests and steel coupon tests, as depicted in Table.

The testing of the frame involved applying an axial load of 700 kN to each column, maintained constant throughout the test, while monotonically applying a lateral load to the Top story beam until the ultimate capacity of the frame was reached. The column loads were provided by two pairs of 450 kN capacity hydraulic jacks, applied through two transverse beams in the force-controlled mode. The lateral load was provided by a 1000 kN capacity actuator, mounted laterally against a reacting strong wall, in a displacement mode

Table A-1: Material Properties of Vecchio and Emara (1992)

Reinforcement								
Bar No	**A_s** (mm^2)	**dia** (mm)	**f_y** (MPa)	**f_u** (MPa)	**E_s** (MPa)	**E_{sh}** (MPa)	**ε_{sh}** ($x10^{-3}$)	**ε_{su}** ($x10^{-3}$)
No.20	300	19.5	418	596	192500	3100	9.5	66.9
No.10	100	11.3	454	640	192500*	3100*	9.5*	69.5

Concrete				
f'_c (MPa)	**ε_0** (x10-3)	**E_c** (MPa)	**G_c** (MPa)	**υ**
30	1.85	23674	9864*	0.2*

* estimated

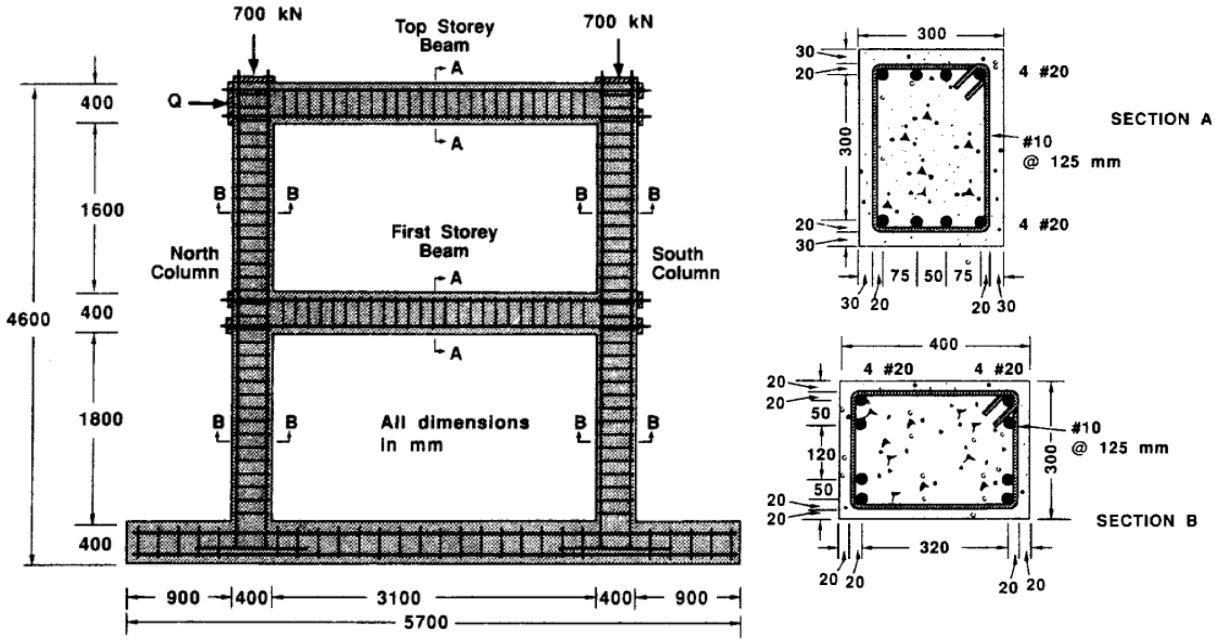

Figure A-1: Structural Details adopted from Vecchio and Emara (1992)

Nonlinear Analysis with SAP2000

Vencchio and Emara frame modeled in SAP 2000 V21 with as aforementioned material properties and geometric sections. End of Rigid end offsets with rigid end factors of 1.0, which correspond to a fully rigid connection, were used in order to account for the overlapping portions of the beam column connections as suggested by FEMA 356 (2000) Clause 6.5.2. The effective stiffness values recommended by FEMA 356 (2000) clause 6.4.1 and schematic representation of the SAP model is show in the Figure A-2.

Three different pushover analysis was conducted to investigate effect of plastic hinge modeling in nonlinear analysis of frame, there results was compared to experimental result. The four different hinge combination are: Auto hinges 15(both M3 and P-M3), User defined 16(UD) by Fiber hinge and Auto M3 with Fiber hinge17. Capacity curves of each analysis are shown the Figure A-3 and tabular compassion are depicted in Table A-2

[15] Auto hinges are software inbuilt hinges according to FEMA 356 Table 6.7 and 6.8.
[16] User defined (UD) hinge are implemented for the beam section using moment curvature analysis.
[17] Fiber Hinges are used only for Column members.

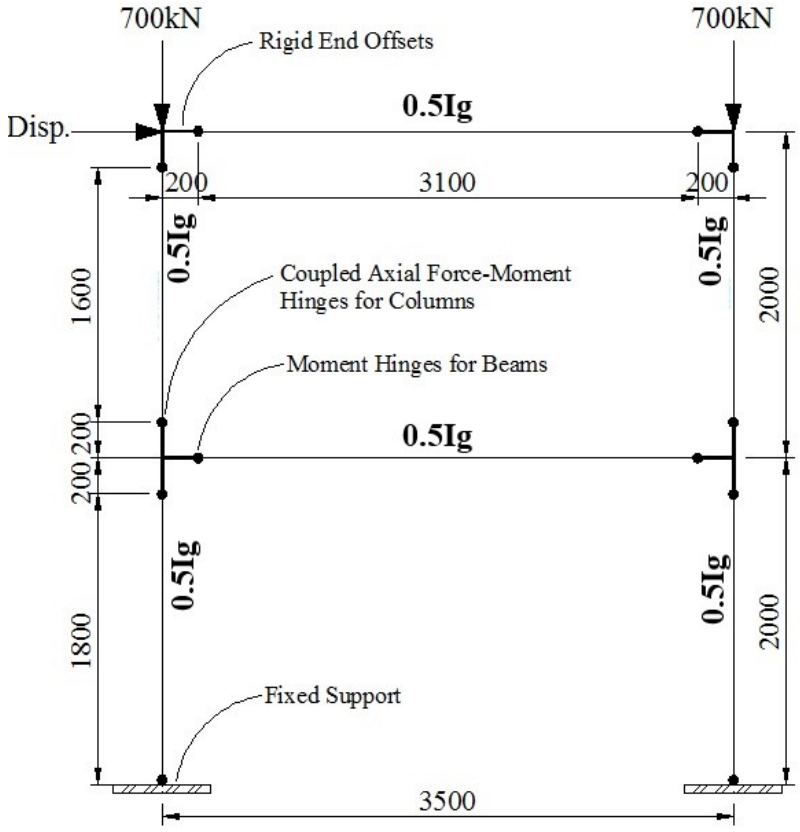

Figure A-2: SAP Model of Vecchio and Emara Frame.

Table A-2: Comparison of experimental and analytical response

Parameters at maximum drift level	Experimental	Hinge modeling types		
		Fiber hinge and Auto M3	Fiber hinge and UD M3	Auto hinges
Base shear(kN)	300.96	292.10 [2.94][18]	298.85 [0.7]	296.77[1.39]
Top story drift(mm)	151.41	102.78 [32.12]	174.5 [15.24]	99.64 [34.19]

The results indicates user defined and fiber hinge well capture the experimental result even if it has slight differ estimating in maximum load capacity. Moreover the experimental studies was interrupted due to shorting of actuator stock, the relative error in top story drift under fiber hinge and UD M3 model may be further reduced if the experiment was sustained until failure. Moreover, usage of Park and Pauly's confinement model from beam element enhance ductility of the frame, convey maximum deformation as closer as experimental studies.

[18] The values in the parenthesis indicate relative error in percentage with respect to experimental results

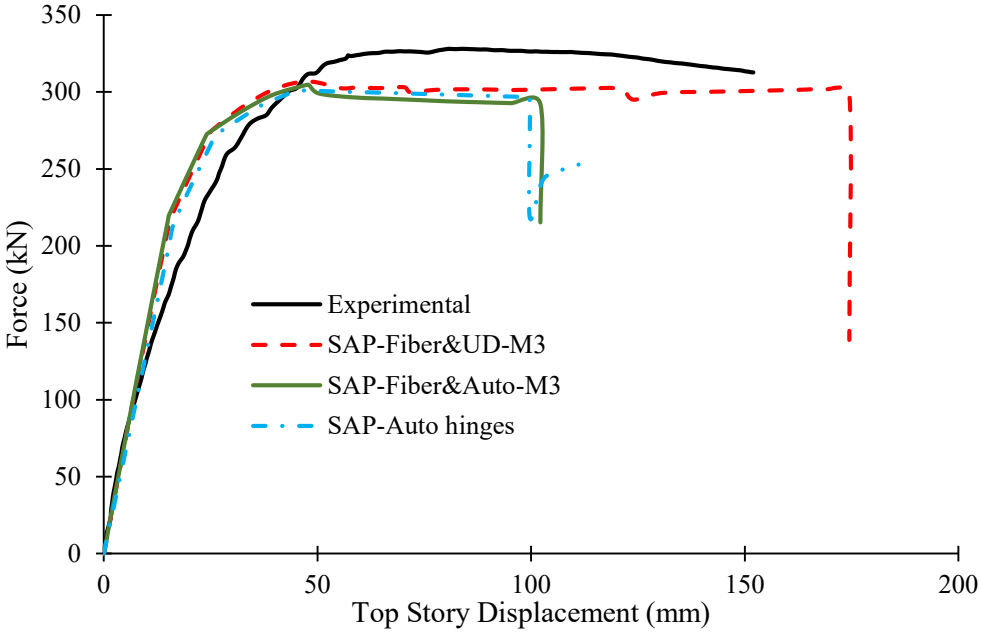

Figure A-3: Comparison of capacity curve of selected Frame.

A.2 Wall Verification

In this section, the selected nonlinear wall modeling technique will be evaluated against experimentally tested shear wall by Rao et al. (2014). The shear wall was 3 m in height, 1.56 m in width, and 200mm thick as indicated in Figure A-4. Shear wall was constructed from M30 grade concrete and Fe-415 steel reinforcement, a total of sixteen diameter 10 rebars are placed as longitudinal reinforcement in two layers with a non-uniform spacing in plan. At both ends of a shear wall, three rebar in each layer are kept with a spacing of 150 mm center-to-center (c/c) and the remaining rebars are spaced at 300 mm. The boundary element was created by provided four vertical rebars with special 8mm diameter confining reinforcement that are longitudinally spaced at 150mm. In addition to confining reinforcement at the boundary and C-clamps, 10mm diameter horizontal reinforcement with 300mm longitudinal spacing are used as stirrup. The test shear wall has a base raft of dimensions 2.5 × 2.5 × 0.4 m thick acting as the foundation. The base raft is provided with mild steel sleeves every 1 m so that the structure could be fixed using through-through high-strength bolts to the heavy-duty test floor and the raft foundation is rigidly anchored to the test floor. The shear wall is loaded axially with 160 kN, which creates a constant axial stress in the shear wall of 0.513 Mpa. The axial load is simulated with a monolithic top slab of plan dimensions 2.5 × 2.5 m with 0.5 m thickness and an additional 8.5-tone

concrete mass block. Monotonic loads are applied through a hydraulic jack at the top slab of the shear wall. The hydraulic jack is connected at one end to the reacting strong wall and the other end is connected to the top slab of the shear wall through a calibrated load cell and a heavy distributor beam.

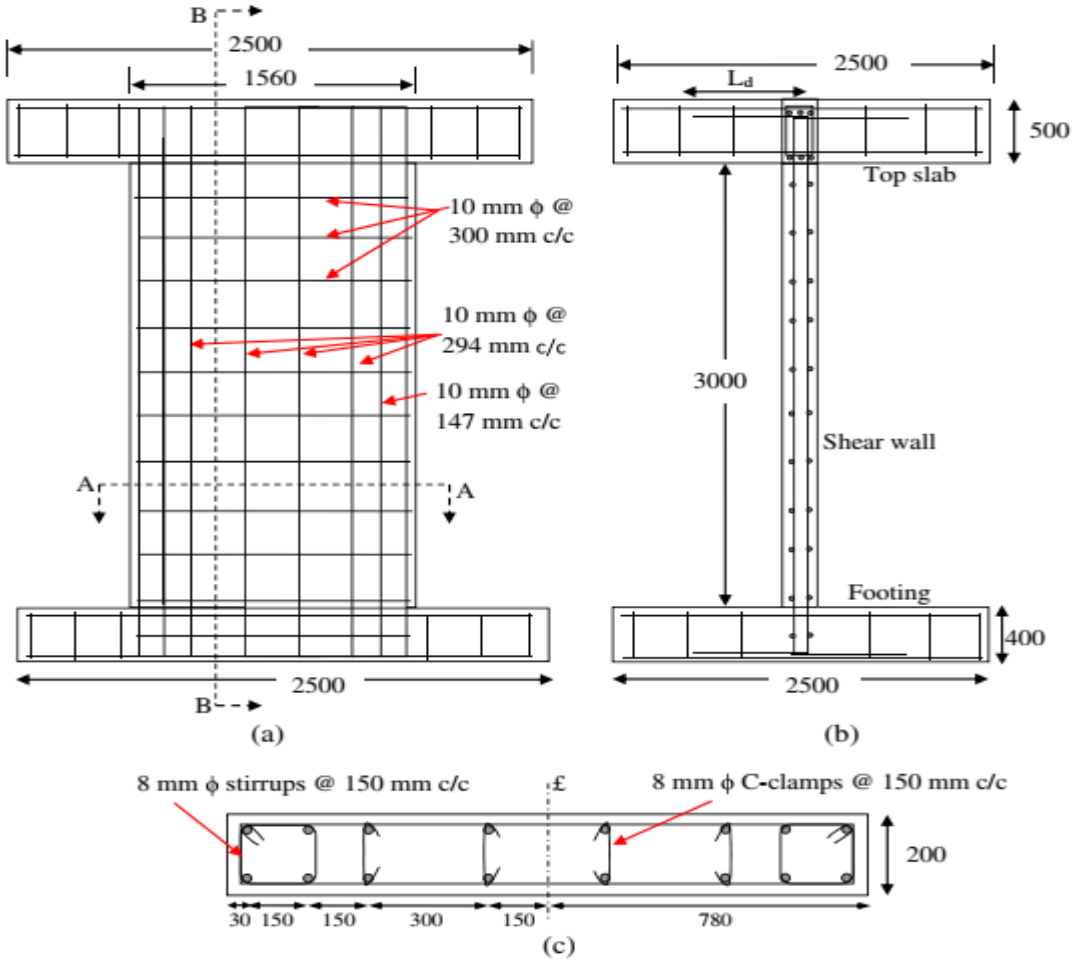

Figure A-4: Structural details of the shear wall: (a) elevation; (b) section B-B; (c) section A-A (all dimensions shown are in mm, drawn not to a scale)

Nonlinear Analysis with SAP2000

The selected shear was modeled in SAP2000 with multilayer shell element. Although the authors do not indicate detail stress-strain relationship of the constitute material, stress-strain relationship are adopted for M30 and Fe-415 from default Indian Standard database available in the software. The Shear wall was divided in to three section; two confined section to simulated boundary element and single middle unconfined section. The confinement effects was considered by Mander et al. (1998) confined concrete model.

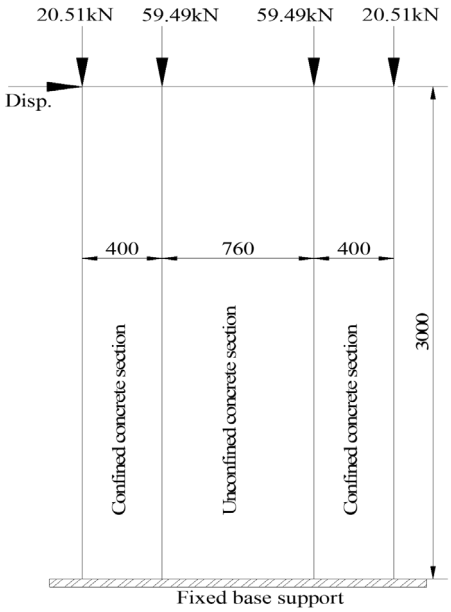

Figure A-5: Schematic representation of the SAP model

The applied constant axial load that is 160kN is divide into four nodal loads as per their tributary area and shown in Figure A-5. The effective section stiffness was considered 50% of the uncracked section flexural stiffness. In-plane flexural strength is consider to be nonlinear while shear strength is consider elastic throughout in pushover analysis. The resulted capacity curve is portrayed in Figure A-6 which gives a close match to the experimental observed capacity curve. The maximum displacement recorded from the experimental test was 65.12mm while the calculated is 64.5mm which is closer match. Furthermore, the base shear corresponsding to ultimate displacement under experimental and analytical result is 206.26kN and 201.75kN respectively.

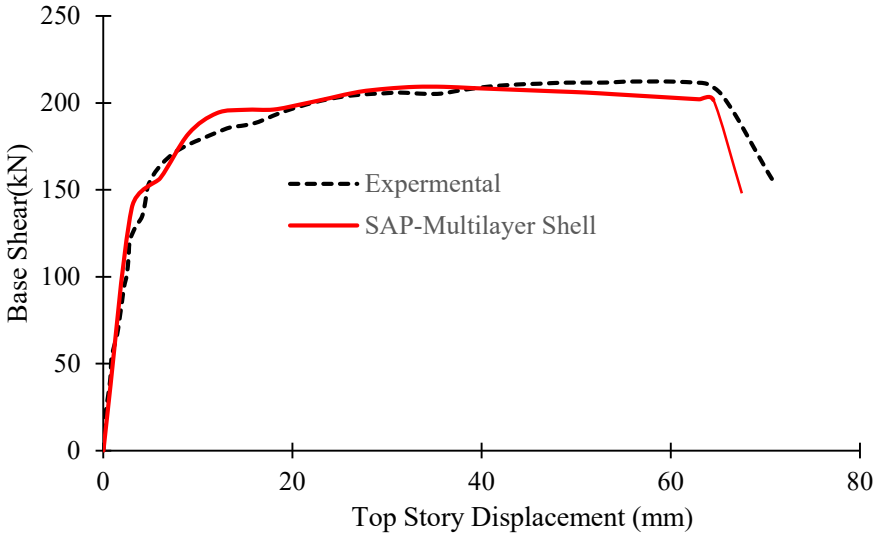

Figure A-6: Capacity curve of selected shear wall

APPENDIX B: FRAGILITY CURVES

This appended provides resulted fragility curve of the case study building along its two orthogonal directions.

B.1 Fragility curves of the case study building

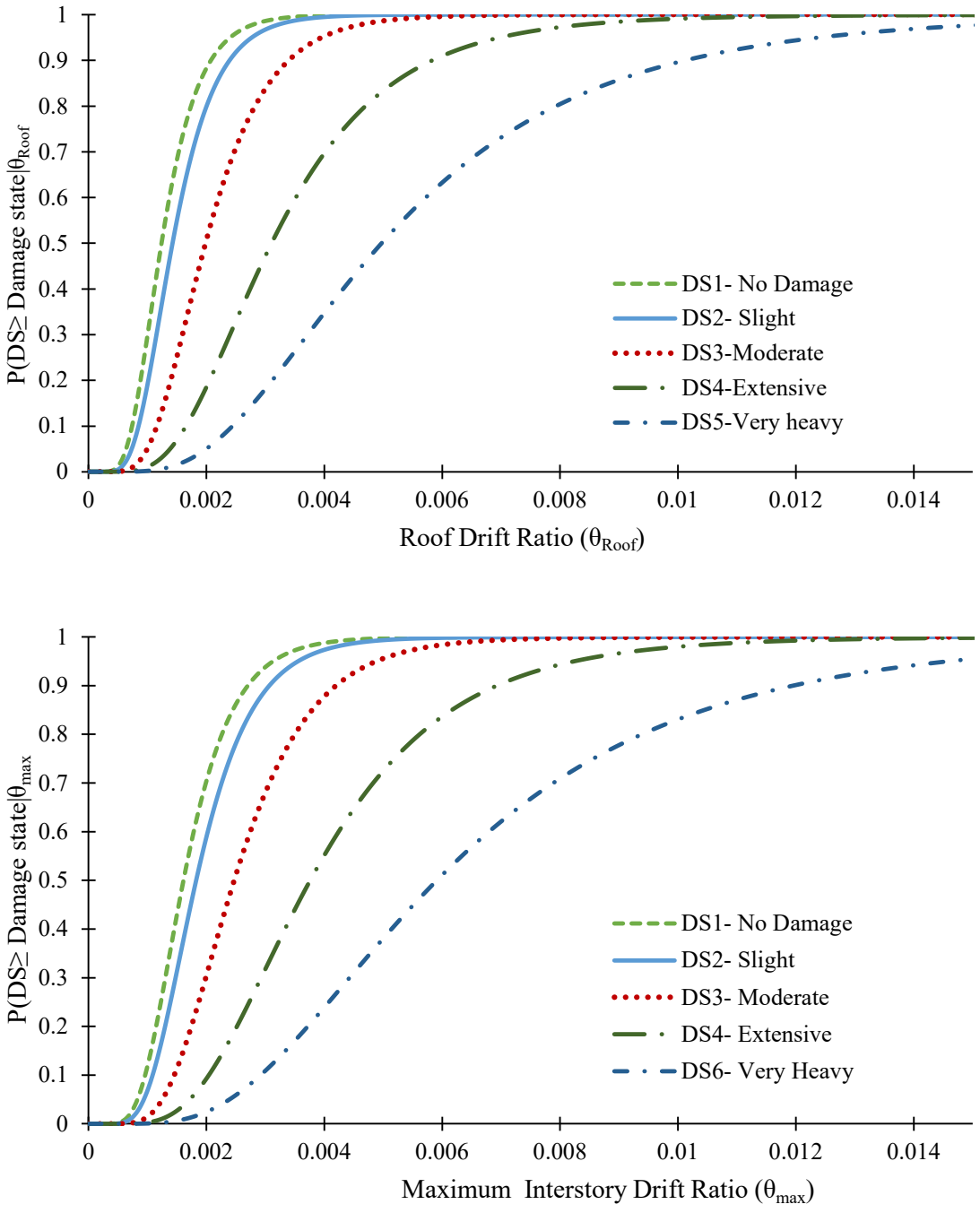

Figure B-1: Global-level building fragility curve in X direction

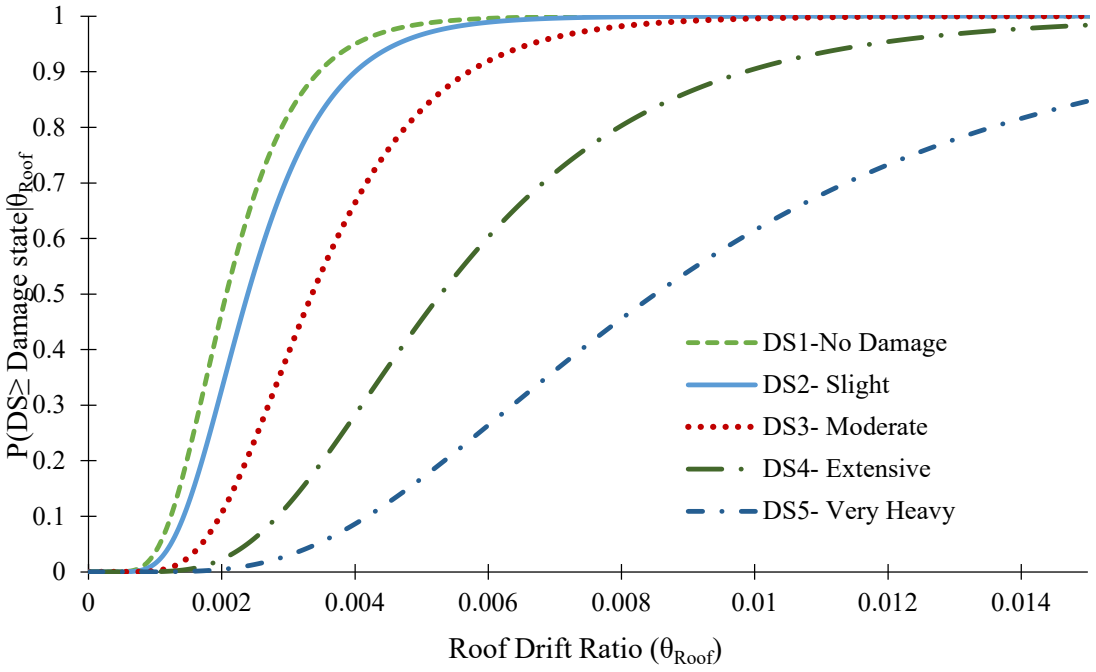

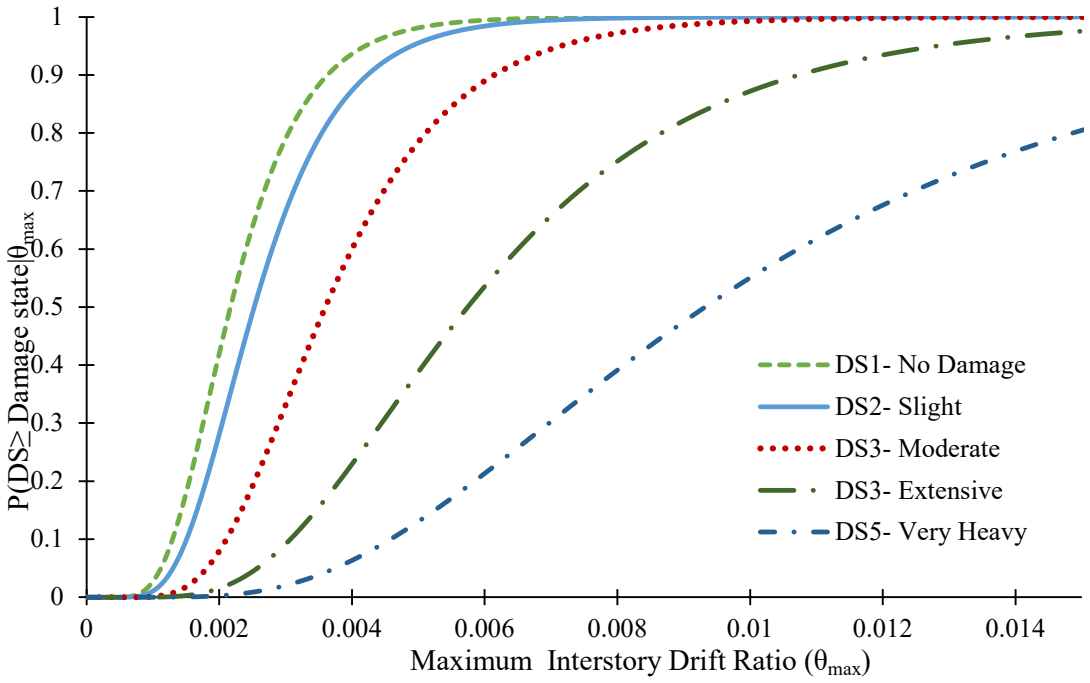

Figure B-2: Global-level building fragility curve in Y direction

APPENDIX C: SELECTED CAPACITY AND IDA CURVES

C.1 Selected worst capacity curves and their linearly fitted curve

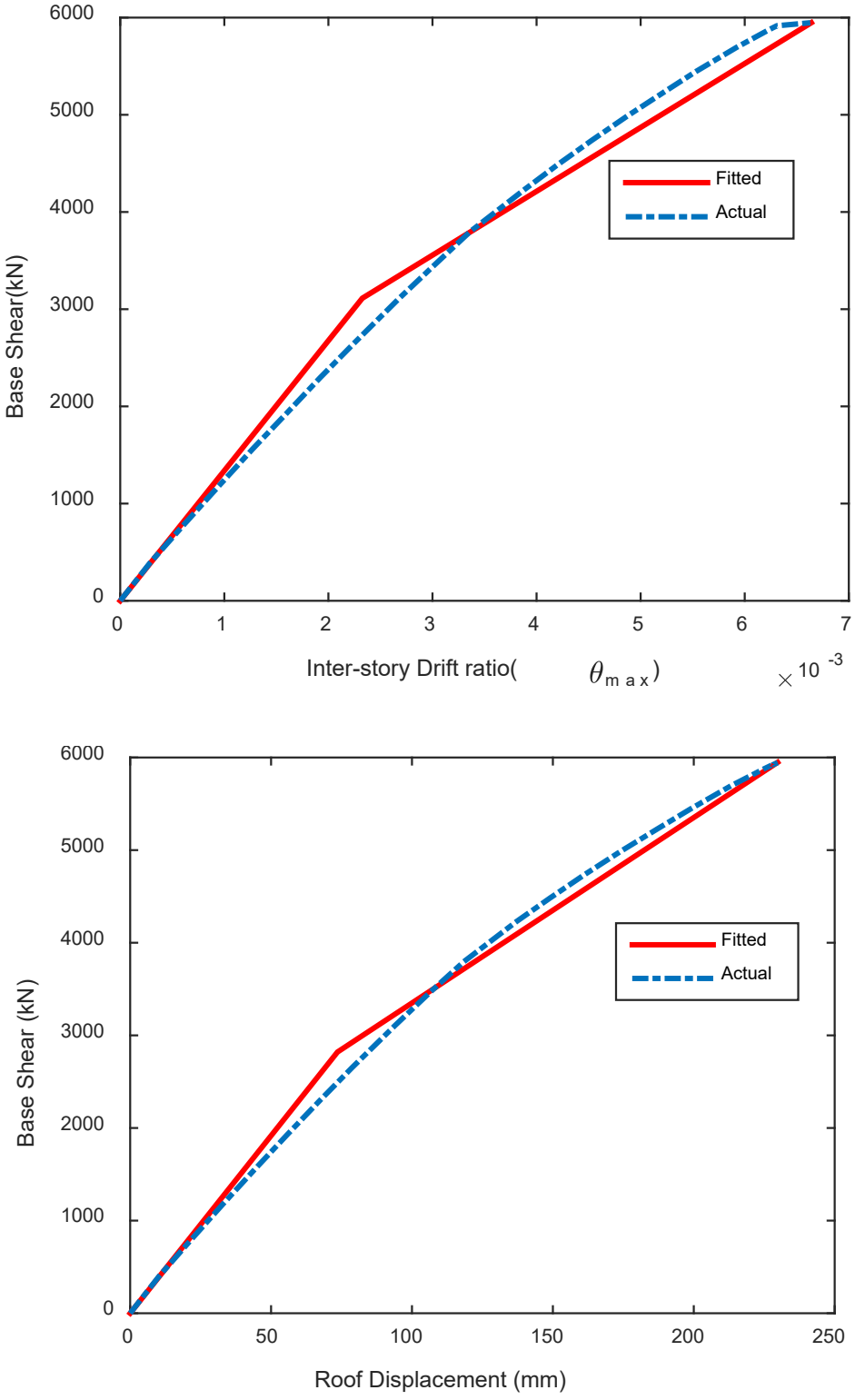

Figure C-1: Selected capacity curve in X directions

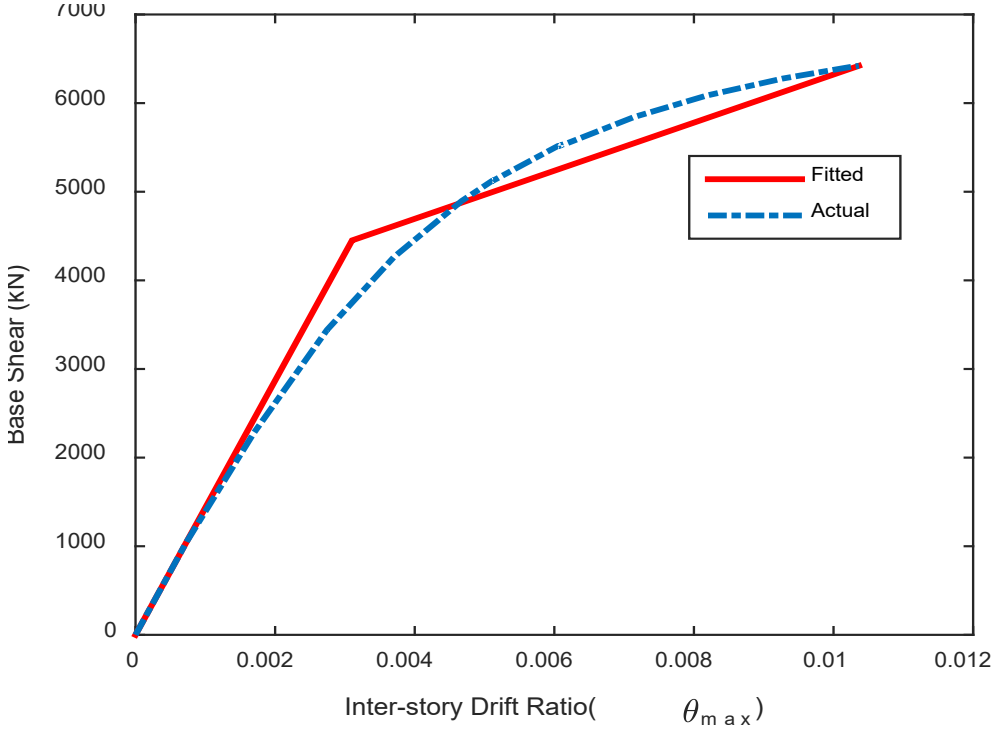

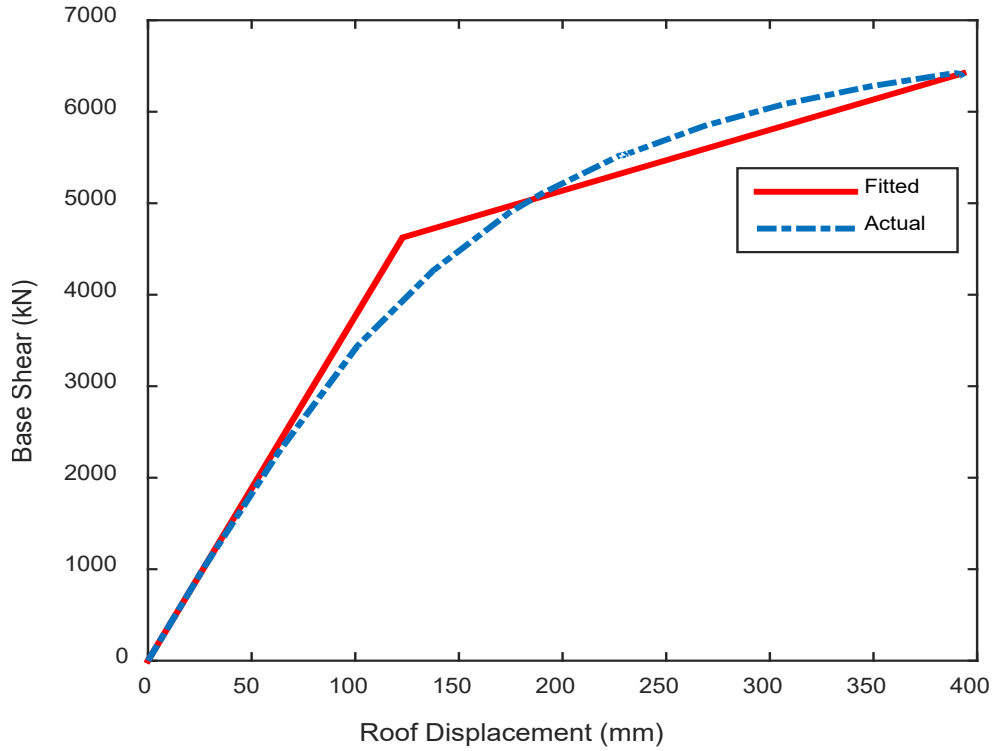

Figure C-2: Selected capacity curve in Y directions

C.1 IDA curves extracted from capacity curve

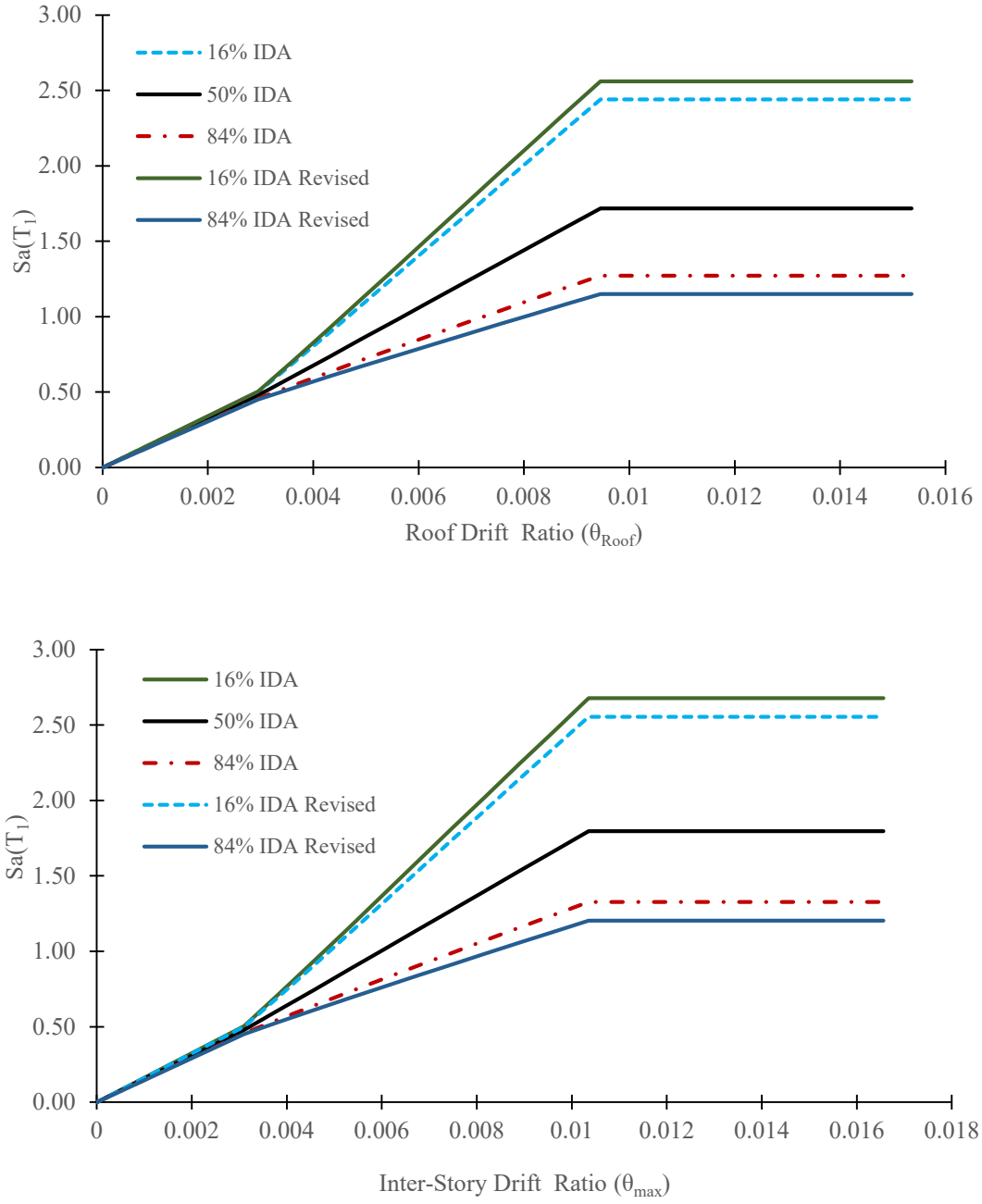

Figure C-3: IDA curves extracted from capacity curve in Y directions

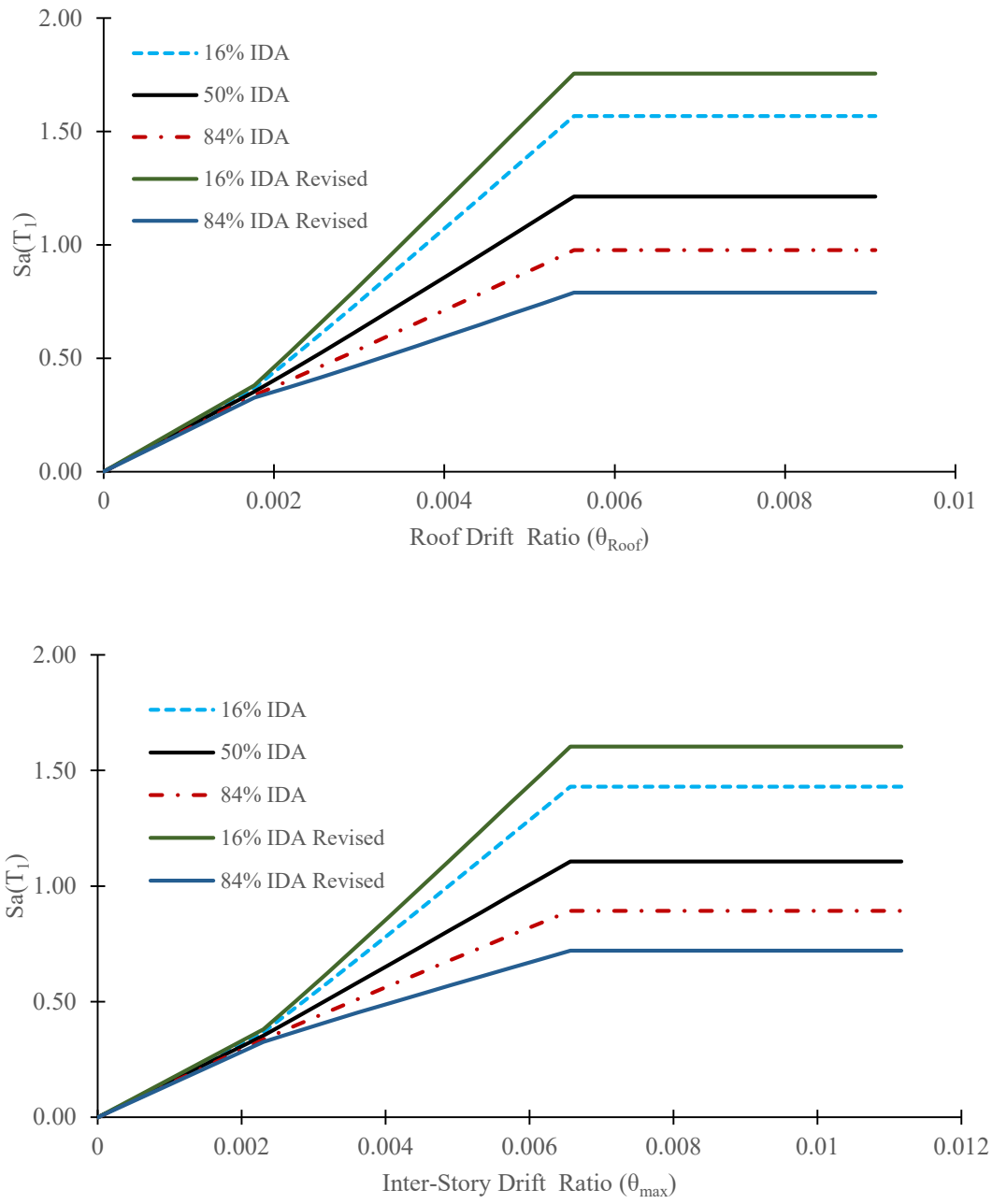

Figure C-4: IDA curves extracted from capacity curve in X directions.

APPENDIX D: SELECTED UNSCALED TIME HISTORIES

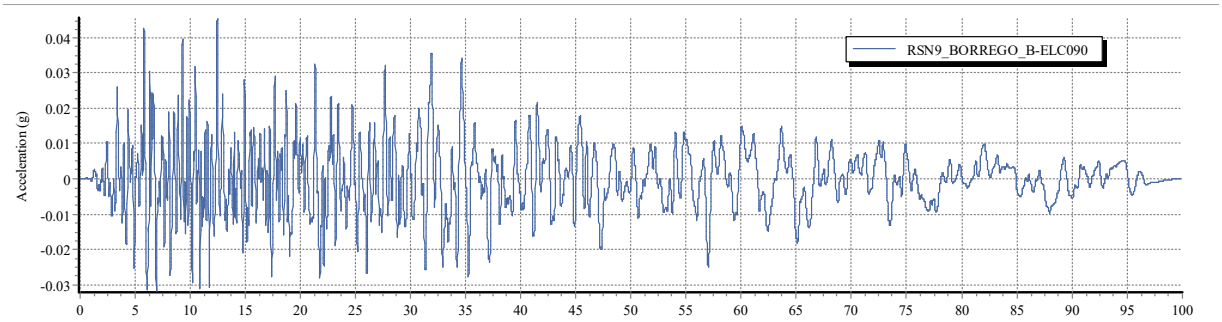

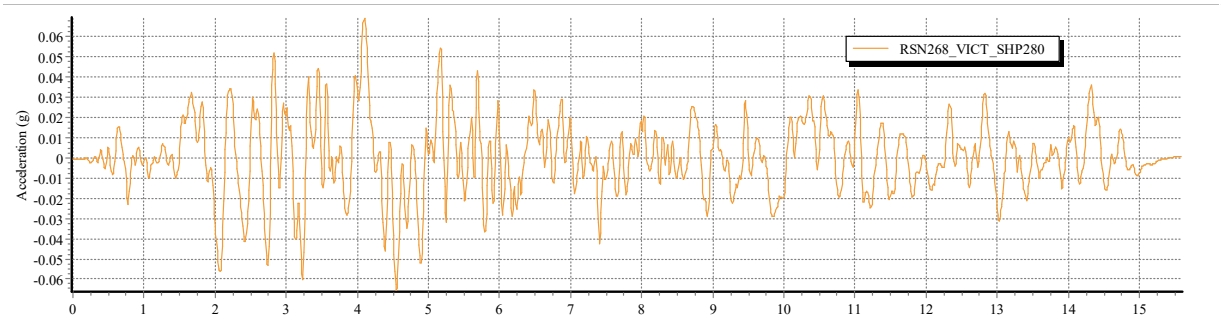

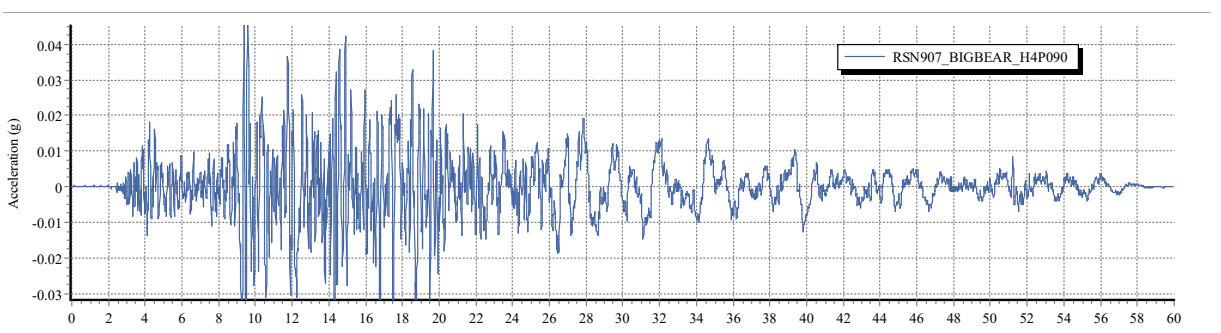

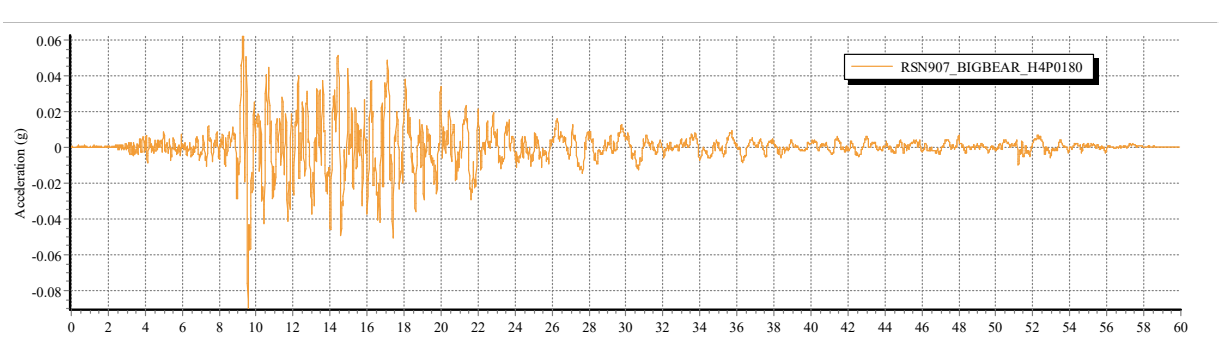

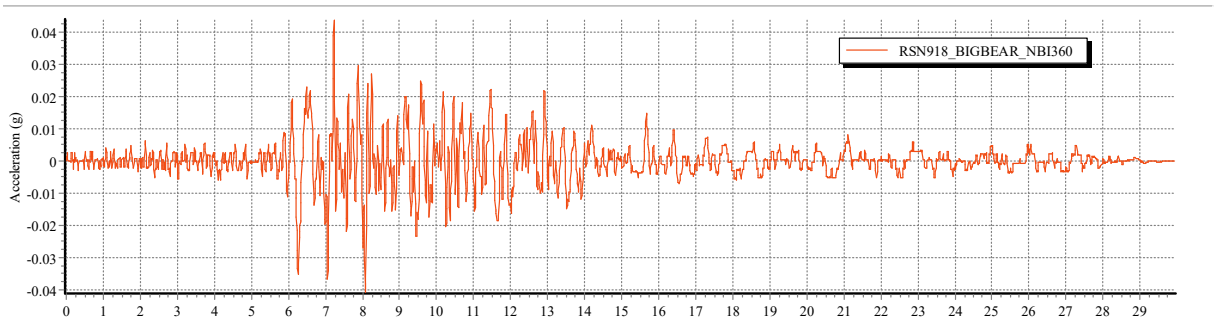

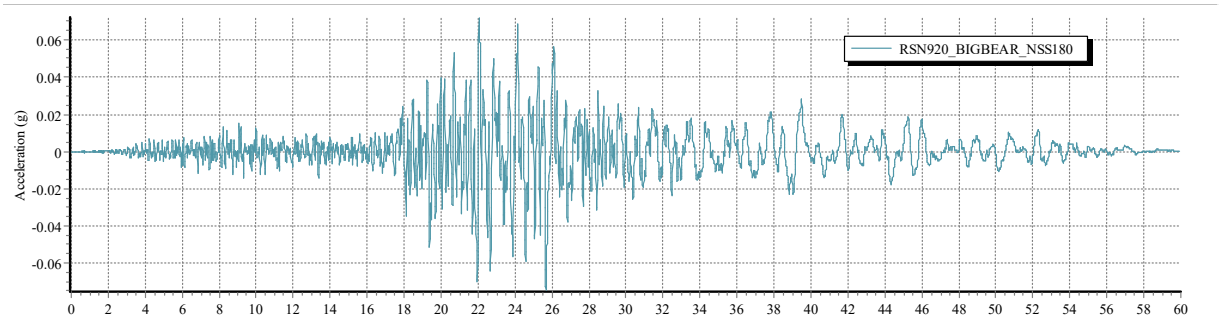
RSN920_BIGBEAR_NSS180
Acceleration (g)

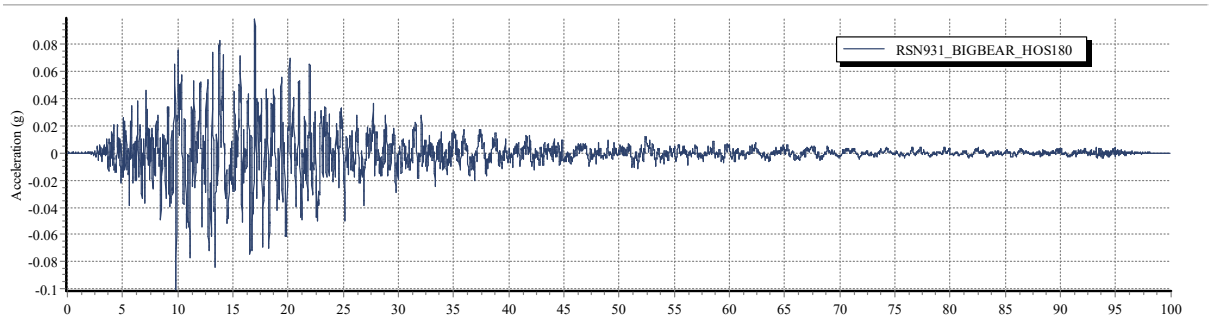
RSN931_BIGBEAR_HOS180
Acceleration (g)

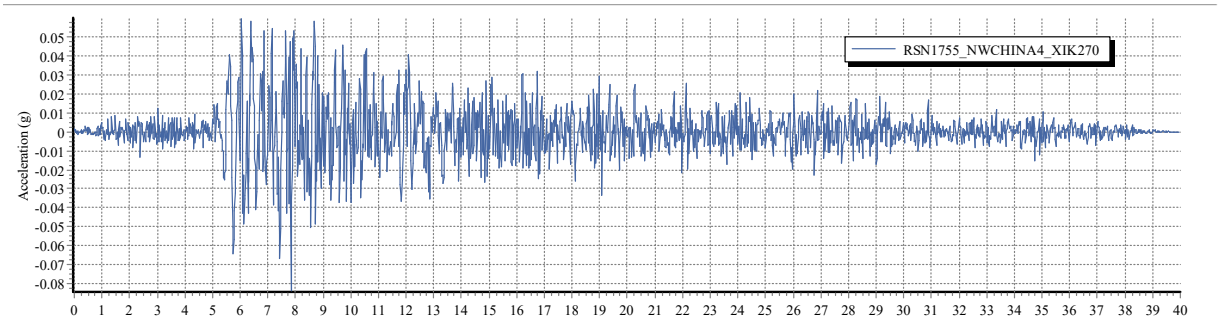
RSN1755_NWCHINA4_XIK270
Acceleration (g)

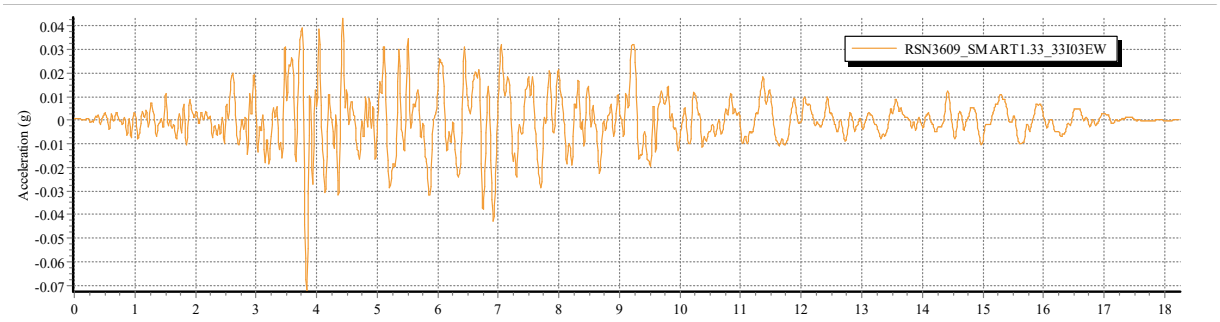
RSN3609_SMART1.33_33I03EW
Acceleration (g)

APPENDIX E: MATERIAL MODEL AND MATLAB PROGRAM FOR MOMENT- CURVATURE ANALYSIS

E.1 Constitute material model:

In order to determine material nonlinearity, providing material constitute model is mandatory and the model are expressed interims of stress-strain relationship. The building is composed of reinforced concrete material that has two component, concrete can reinforcement bar. Several models are available to mathematically expressed stress strain relationship equation. The study utilizes the following constitutive model detail of their mathematical expression are as follows:

E.1.1 Kent and Park's constitutive material model

Park and Paulay (1975) provide mathematical equation to relate stress and strain in order to determine stress-strain relationship model of reinforced concrete confined by rectangular hoops. The proposed model is graphically illustrated in figure below and their equations are posted in the next section.

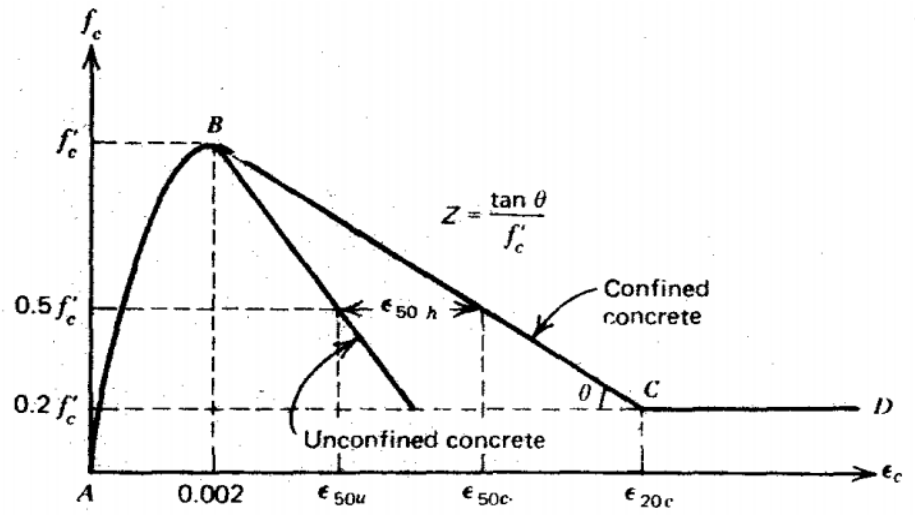

Figure E-1: Kent and Park's model for confined and unconfined concrete Park and Paulay (1995)

From AB: $\varepsilon_c \leq 0.002$

$$f_c = f_c^{'}\left[\frac{2\varepsilon_c}{0.002} - \left(\frac{2\varepsilon_c}{0.002}\right)^2\right] \quad \text{(E-1)}$$

Region BC: $0.002 < \varepsilon_c \leq \varepsilon_{20c}$

$$f_c = f_c^{'}\left[1 - Z(\varepsilon_c - 0.002)\right] \tag{E-2}$$

$$Z = \frac{0.5}{\varepsilon_{50u} + \varepsilon_{50h} - 0.002};\quad \varepsilon_{50u} = \frac{3 + 0.029 f_c^{'}}{145 f_c^{'} - 1000};\quad \varepsilon_{50h} = \frac{3}{4}\rho_s\sqrt{\frac{b^{"}}{s_h}} \tag{E-3}$$

Region CD: $\varepsilon_c > \varepsilon_{20c}$

$$f_c = 0.2 f_c^{'} \tag{E-4}$$

Park and Paulay (1975) also propose constitutive law of reinforcing steel as indicated in figure below and mathematically expressed by the following equation

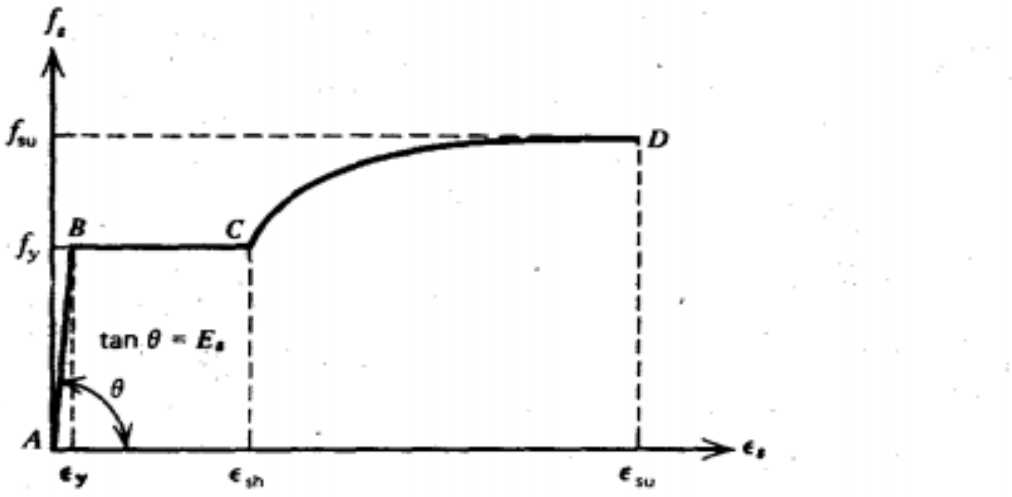

Figure E-2: Stress-strain relationship for reinforcing steel proposed by Park and Paulay (1995)

From AB: $\varepsilon_s \leq \varepsilon_y$

$$f_s = E\varepsilon_s \tag{E-5}$$

From BC: $\varepsilon_y < \varepsilon_s \leq \varepsilon_{sh}$

$$f_s = f_y = E\varepsilon_s \tag{E-6}$$

From CD: $\varepsilon_{sh} < \varepsilon_s \leq \varepsilon_{su}$

$$f_s = f_y\left[\frac{m(\varepsilon_s - \varepsilon_{sh}) + 2}{60(\varepsilon_s - \varepsilon_{sh}) + 2} + \frac{(\varepsilon_s - \varepsilon_{sh})(60 - m)}{2(30r + 1)^2}\right] \tag{E-7}$$

$$m = \frac{f_{su}}{f_y}\frac{(30r+1)^2 + 60r - 1}{15r^2} \quad \text{and} \quad r = \varepsilon_{su} - \varepsilon_{sh} \tag{E-8}$$

E.2 MATLAB program for the computational stress-block based moment-curvature analysis

```
%%  ------------Input the following data ------------ %%
clear all; clc;
h = input('Enter the height of the section (mm): ');
b = input('Enter the breadth of the section (mm): ');
clearcover = input('Enter the clearcover of the section (mm): ');
fc = input('Enter unconfined concrete strength (MPa): ');
fcc = input('Enter confined concrete strength (MPa): ');
Es  = 200000;   % (Mpa)
fy  = input('Enter yield strength of reinforcing steel (MPa): ');
fsu = input('Enter ultimate strength of steel (MPa): ');
esh = input('Enter strain hardening strain: ');
esu = input('Enter ultimate steel strain: ');
fyh = input('Enter yield strength of shear reinforcement bars(Mpa): ') ;
diastirrup = input('Enter diameter of stirrups (mm): ');
stirrupspacing = input('Enter stirrup spacing (mm): ');
stirrupperimeter = input ('Enter perimeter of stirrup (mm): ');
stirrupperimeter = 2*(h-2* clearcover + b-2* clearcover);
Ast1 = input ('Enter tension reinforcement area (mm2): ');
 Ast2 = input ('Enter compression reinforcement area (mm2): ');
 dAst1 = input ('Enter distance from extreme compression fiber to tension reinforcement (mm): ');
dAst2 = input ('Enter distance from extreme compression fiber to compression reinforcement (mm): ');
%%------------volumetric ration of shear reinforcement------------%%
rohshear = (stirrupperimeter *pi()*diastirrup^2/4)/ ((h-2* clearcover)*(b-2* clearcover )* stirrupspacing);
%%------------computation of steel reinforcement parameters------------%%
ey = fy / Es;
```

```
r = esu-esh;
m = (fsu/fy)*((30*r+1)^2 -60*r -1)/(15*r^2);
%% ------------Calculating concrete properties ------------%%
Ec = 5000*sqrt(fc);
espall = 0.004;
ecu  = 0.004+(1.4*rohshear*fyh*esu)/fcc;
e50h = 0.75*rohshear*sqrt((b-2*clearcover)/stirrupspacing);
e50u = (3+0.29*fcc)/(145*fcc-1000);
z    = 0.5/(e50h+e50u-0.002);
e20c = 0.002+0.8/z;
%% ------------Values for first iteration ------------%%
plotM(1)=0; PlotPhi(1)=0;deltaneutral=0;
neutralx(1) = 0.5*h +deltaneutral;
steelstrain1 = [];steelstrain2 =[]; confstrainext = []; unconfstrainext = [];
for i=2:300
   confstrainext(i)=(i-1)*ecu/299;
   %for the while loop to take place the first time
   j=2;
   deltaP = 70;
   while (abs(deltaP) > 50)
      unconfstrainext = (neutralx(j-1) * confstrainext(i)) / (neutralx(j-1)-clearcover );
      steelstrain1 = ((dAst1- neutralx(j-1))*confstrainext(i)) / (neutralx(j-1)-clearcover);
      steelstrain2 = ((neutralx(j-1)- dAst2 )* confstrainext(i)) / (neutralx(j-1)-clearcover);
      %% Stresses in steel
      if steelstrain1 <= ey
         steelstress1 = Es * steelstrain1 ;
      elseif steelstrain1 > ey && steelstrain1 <= esh;
         steelstress1 = Es*ey;
      elseif steelstrain1 > esh && steelstrain1 <= esu
```

```
        steelstress1 = fy*(((m*(steelstrain1-esh)+2)/(60*(steelstrain1-esh)+2)) +
((steelstrain1-esh)*(60-m))/(2*(30*r+1)^2));
    end
        if steelstrain2 <= ey
        steelstress2 = Es * steelstrain2;
    elseif steelstrain2 > ey && steelstrain2 <= esh;
        steelstress2 = Es*ey;
    elseif steelstrain2 > esh && steelstrain2 <= esu
        steelstress2 = fy*(((m*(steelstrain2-esh)+2)/(60*(steelstrain2-esh)+2)) +
((steelstrain2-esh)*(60-m))/(2*(30*r+1)^2));
    end
    steelforce1 = steelstress1*Ast1;
    steelforce2 = steelstress2*Ast2;
    %% Stress-block parameters for unconfined concrete Stress-block
    if abs(unconfstrainext)<= 0.002
        alphauc1 = 500*unconfstrainext*(1-(500*unconfstrainext/3));
        alphauc2 = 500*confstrainext(i)*(1-(500*confstrainext(i)/3));
        gammauc1 = (1-125*unconfstrainext)/(3-500*unconfstrainext);
        gammauc2 = (1-125*confstrainext(i))/(3-500*confstrainext(i));
        unconfconforce1 = alphauc1*fcc*b*neutralx(j-1);
        unconfconforce2 = alphauc2*fcc*(b-2*clearcover)*(neutralx(j-1)-clearcover);
        unconfconforce = unconfconforce1-unconfconforce2;
        unconfconmoment = unconfconforce1*gammauc1*neutralx(j-1) -
unconfconforce2*(gammauc2*(neutralx(j-1)-clearcover) + clearcover);
       elseif abs(unconfstrainext)<= espall && abs(unconfstrainext)> 0.002
        alphauc1 = (1/750 - ((0.5/(e50u-0.002))*((unconfstrainext^2-0.002^2)/2 +
(0.002-2*e50u)*(unconfstrainext-0.002))))/unconfstrainext;
        alphauc2 = (1/750 - ((0.5/(e50u-0.002))*((confstrainext(i)^2-0.002^2)/2 + (0.002-
2*e50u)*(confstrainext(i)-0.002))))/confstrainext(i);
        %alphauc2 = ((confstrainext^2-0.002^2) + (confstrainext -0.002)*(0.002 -
2*e50u))/(confstrainext*(0.002-e50u));
```

```
        gammauc1 = 1-(0.002*(2/3-0.002/4)-(0.5/(e50u-0.002)*((unconfstrainext^3 -
0.002^3)/3 +(0.001-e50u)*(unconfstrainext^2-0.002^2))))/(0.004/3-((0.5/(e50u-
0.002))*((unconfstrainext^2 -0.002^2)/2 +(0.002-2*e50u)*(unconfstrainext-0.002))));

        gammauc2 = 1-(0.002*(2/3-0.002/4)-(0.5/(e50u-0.002)*((confstrainext(i)^3 -
0.002^3)/3 +(0.001-e50u)*(confstrainext(i)^2-0.002^2))))/(0.004/3-((0.5/(e50u-
0.002))*((confstrainext(i)^2 -0.002^2)/2 +(0.002-2*e50u)*(confstrainext(i)-0.002))));

        unconfconforce1 = alphauc1*fcc*b*neutralx(j-1);

        unconfconforce2 = alphauc2*fcc*(b-2*clearcover)*(neutralx(j-1)-clearcover);

        unconfconforce = unconfconforce1-unconfconforce2 ;

        unconfconmoment = unconfconforce1*gammauc1*neutralx(j-1) -
unconfconforce2*(gammauc2*(neutralx(j-1)-clearcover) + clearcover);

    elseif abs(unconfstrainext)> espall

        NXDspall = (neutralx(j-1)/unconfstrainext)*espall;

        alphauc1 = (1/750 - ((0.5/(e50u-0.002))*((espall^2-0.002^2)/2 + (0.002-
2*e50u)*(espall-0.002))))/espall;

        alphauc2 = alphauc1;

        gammauc1 = 1-(0.002*(2/3-0.002/4)-(0.5/(e50u-0.002)*((espall^3 -0.002^3)/3
+(0.001-e50u)*(espall^2-0.002^2))))/(0.004/3-((0.5/(e50u-0.002))*((espall^2 -
0.002^2)/2 +(0.002-2*e50u)*(espall-0.002))));

        %gammauc2 = 1-(0.002*(2/3-0.002/4)-(0.5/(e50u-0.002)*((espall^3 -0.002^3)/3
+(0.001-e50u)*(espall^2-0.002^2))))/(0.004/3-((0.5/(e50u-0.002))*((espall^2 -
0.002^2)/2 +(0.002-2*e50u)*(espall-0.002))));

        gammauc2 = gammauc1;

        % neglectiong contribution of top cover

        unconfconforce1 = alphauc1*fcc*b*(NXDspall);

        unconfconforce2 = alphauc2*fcc*(b-2*clearcover)*(NXDspall);

        unconfconmoment = unconfconforce1*(neutralx(j-1)-((1-
gammauc1)*NXDspall)) - unconfconforce2*(neutralx(j-1)-((1-gammauc2)*NXDspall));

        unconfconforce = unconfconforce1-unconfconforce2;

    end

    %% Stress-block parameters for confined concrete

       if abs(confstrainext(i))<= 0.002

        alphacc = 500*confstrainext(i)*(1-(500*confstrainext(i)/3));
```

```
        gammacc = (1-125*confstrainext(i))/(3-500*confstrainext(i));
    elseif abs(confstrainext(i))>0.002 && abs(confstrainext(i))<=e20c
        alphacc = (1/confstrainext(i))*(1/750+ (confstrainext(i)-0.002)-
0.5*z*(confstrainext(i)^2-0.002^2)+ z*(0.002*confstrainext(i)-0.002^2));
        gammacc = 1-(((-0.002^2/12) + 0.5*confstrainext(i)^2 -
(z/3)*(confstrainext(i)^3-0.002^3)+0.001*z*(confstrainext(i)^2-
0.002^2))/(confstrainext(i)*((1/750) + (confstrainext(i)-0.002)*(1+0.002*z) -
0.5*z*(confstrainext(i)^2-0.002^2))));
        elseif abs(confstrainext(i))<=ecu
        alphacc = (7/7500+0.32/z + 0.2*confstrainext(i))/confstrainext(i);
        gammacc = 1-(((19*0.002^2/60)+(32/375)*(1/z^2)+0.00064/z+
0.1*confstrainext(i)^2)/(confstrainext(i)*((7/7500+0.32/z + 0.2*confstrainext(i)))));
    end
    confconforce = (alphacc*fcc*(b-2*clearcover)*(neutralx(j-1)-clearcover));
    P(j) = (steelforce1-(confconforce + unconfconforce + steelforce2))/1000;
    deltaP = P(j);
    if deltaP > 50
        deltaneutral = 0.01;
    elseif deltaP < -50
        deltaneutral= 0.01;
    else
        deltaneutral=0;
    end
    neutralx(j) = neutralx(j-1) + deltaneutral;
    j=j+1;
  end
% -------------------------Plot matrix form of strains-----------------------------------%
unconfstrainext = (neutralx(j-2) * confstrainext) / (neutralx(j-2)-clearcover );
steelstrain1 = ((dAst1- neutralx(j-2))*confstrainext) / (neutralx(j-2)-clearcover);
steelstrain2 = ((neutralx(j-2)- dAst2 )* confstrainext) / (neutralx(j-2)-clearcover);
```

```
plotM(i) = (steelforce1*dAst1 - (steelforce2*dAst2 +
confconforce*gammacc*neutralx(j-1) + unconfconmoment))/1000000;    %kN.m

plotPhi(i) = confstrainext(i)*(1/(neutralx(j-1)-clearcover)) %(1/mm)

tempneutralx = neutralx(j-1);

neutralx = []; P = [];

neutralx(1) = tempneutralx;

end

%% Moment Curvature Plot

plot(plotPhi, plotM)

title('MOMENT CURVATURE');

xlabel('CURVATURE (1/mm)')

ylabel('MOMENT (kN-m)')

grid on

grid minor
```